Year : 2010

Visual functions in the healthy and schizophrenic brain: from stimulus control to illusory perceptions using electrical neuroimaging

Knebel Jean-François

UNIL | Université de Lausanne
Faculté de biologie et de médecine

Département des Neurosciences Cliniques et Département de Radiologie

VISUAL FUNCTIONS IN THE HEALTHY AND SCHIZOPHRENIC BRAIN: FROM STIMULUS CONTROL TO ILLUSORY PERCEPTIONS USING ELECTRICAL NEUROIMAGING

Thèse de doctorat en Neurosciences

Présentée à la

Faculté de Biologie et de Médecine
de l'Université de Lausanne

par

Jean-François Knebel

Physicien diplômé de l'Ecole Polytechnique Fédérale de Lausanne, Suisse

Jury

Prof. Reto Meuli, Président
P.D. Dr. Micah Murray, Directeur
P.D. Dr Thomas König, Expert
Prof. Christoph Michel, Expert

Lausanne 2010

Programme doctoral interuniversitaire en Neurosciences des Universités de Lausanne et Genève

UNIL | Université de Lausanne

UNIVERSITÉ DE GENÈVE

UNIL | Université de Lausanne
Faculté de biologie et de médecine

LEMANIC NEURO SCIENCE DOCTORAL SCHOOL

Programme doctoral interuniversitaire en Neurosciences des Universités de Lausanne et Genève

Imprimatur

Vu le rapport présenté par le jury d'examen, composé de

Président	Monsieur	Prof.	Reto **Meuli**
Directeur de thèse	Monsieur	Dr	Micah **Murray**
Co-directeur de thèse			
Experts	Monsieur	Prof.	Thomas **Koenig**
	Monsieur	Prof.	Christoph **Michel**

le Conseil de Faculté autorise l'impression de la thèse de

Monsieur Jean-François Knebel

Master of Science de Ecole Polytechnique de Lausanne

intitulée

Visual functions in the healthy and schizophrenic brain: from stimulus control to illusory perceptions using electrical neuroimaging

Lausanne, le 28 janvier 2011

pour Le Doyen
de la Faculté de Biologie et de Médecine

Prof. Reto Meuli

ACKNOWLEDGEMENTS

Before entering in the presentation for my thesis work I would like to thank all the people that helped me during these four years in the "Département de neuroscience Clinique "and "Département de radiologie" of the CHUV. I will start with my thesis director PD Dr. Micah M. Murray for his patience, pedagogic aptitude, high quality of knowledge transmission, and scientific passion. I would also like to thank my research colleagues, Nathalie Bourquin, Dr. Sonia Herbette, Dr. Ulrike Toepel, Dr. Laura De Santis, Holger Sperdin, Claudia Lietti, Dr. Mélanie Aeschlimann Rosanna De Meo, Antonia Thelen, Athina Tzovara, Dr. Marzia De Lucia, Dr. Céline Cappe, Dr. Eric Tardif, Dr. Lucas Spierer, Fosco Bernasconi, Aurélie Manuel, Ayse At, Professor Stephanie Clarke, and Raphaël Meylan. They all helped me with their advice, ideas, and friendship to overcome the unavoidable problem that a thesis could be. A special thanks to Dr. Mélanie Aeschlimann thanks to whom I discovered neuroscience and this scientific team. I would like to thank all the clinical team of the "neuropsychology et logopédie" for their support and their advice on patients. I would like to thank Antonia Thelen for her English corrections. I would also thank all my friends who supported me all of the time. I would thank my family for their unconditional support during this work and especially Céline who supported me during the last day of this thesis. Finally, I would thank "mc fly" my working computer that follow me all the time during my thesis without bugs and crashes. I hope, I have not forgotten anyone, if I have, I apologize.

ABSTRACT (ENGLISH)

This thesis focuses on the visual system in healthy subjects and schizophrenic patients. To address this research, advanced methods of analysis of electroencephalographic (EEG) data were used and developed. This manuscript is comprised of three scientific articles. The first article showed a novel method to control the physical features of visual stimuli (luminance and spatial frequencies). The second article showed, using electrical neuroimaging of EEG, a deficit in spatial processing associated with the dorsal pathway in chronic schizophrenic patients. This deficit was elicited by an absent modulation of the P1 component in terms of response strength and topography as well as source estimations. This deficit was orthogonal to the preserved ability to process Kanizsa-type illusory contours. Finally, the third article resolved ongoing debates concerning the neural mechanism mediating illusory contour sensitivity by using electrical neuroimaging to show that the first differentiation of illusory contour presence vs. absence is localized within the lateral occipital complex. This effect was subsequent to modulations due to the orientation of misaligned grating stimuli. Collectively, these results support a model where effects in V1/V2 are mediated by "top-down" modulation from the LOC.

To understand these three articles, the Introduction of this thesis presents the major concepts used in these articles. Additionally, a section is devoted to time-frequency analysis methods not presented in the articles themselves. The Introduction is divided in four parts. The first part presents three aspects of the visual system: cellular, regional, and its functional interactions. The second part presents an overview of schizophrenia and its sensory-cognitive deficits. The third part presents an overview of illusory contour processing and the three models examined in the third article. Finally, advanced analysis methods for EEG are presented, including time-frequency methodology.

The Introduction is followed by a synopsis of the main results in the articles as well as those obtained from the time-frequency analyses.

Finally, the Discussion chapter is divided along three axes. The first axis discusses the time frequency analysis and proposes a novel statistical approach that is independent of the reference. The second axis contextualizes the first article and discusses the quality of the stimulus control and direction for further improvements. Finally, both neurophysiologic articles are contextualized by proposing future experiments and hypotheses that may serve to improve our understanding of schizophrenia on the one hand and visual functions more generally.

ABSTRACT (FRENCH)

Ce travail de thèse basé sur le système visuel chez les sujets sains et chez les patients schizophrènes, s'articule autour de trois articles scientifiques publiés ou en cours de publication. Ces articles traitent des sujets suivants : le premier article présente une nouvelle méthode de traitement des composantes physiques des stimuli (luminance et fréquence spatiale). Le second article montre, à l'aide d'analyses de données EEG, un déficit de la voie magnocellulaire dans le traitement visuel des illusions chez les patients schizophrènes. Ceci est démontré par l'absence de modulation de la composante P1 chez les patients schizophrènes contrairement aux sujets sains. Cette absence est induite par des stimuli de type illusion Kanizsa de différentes excentricités. Finalement, le troisième article, également à l'aide de méthodes de neuroimagerie électrique (EEG), montre que le traitement des contours illusoires se trouve dans le complexe latéro-occipital (LOC), à l'aide d'illusion « misaligned gratings ». De plus il révèle que les activités démontrées précédemment dans les aires visuelles primaires sont dues à des inférences « top-down ».

Afin de permettre la compréhension de ces trois articles, l'introduction de ce manuscrit présente les concepts essentiels. De plus des méthodes d'analyses de temps-fréquence sont présentées. L'introduction est divisée en quatre parties : la première présente le système visuel depuis les cellules retino-corticales aux deux voix du traitement de l'information en passant par les régions composant le système visuel. La deuxième partie présente la schizophrénie par son diagnostic, ces déficits de bas niveau de traitement des stimuli visuel et ces déficits cognitifs. La troisième partie présente le traitement des contours illusoires et les trois modèles utilisés dans le dernier article. Finalement, les méthodes de traitement des données EEG seront explicitées, y compris les méthodes de temps-fréquences.

Les résultats des trois articles sont présentés dans le chapitre éponyme (du même nom). De plus ce chapitre comprendra les résultats obtenus à l'aide des méthodes de temps-fréquence

Finalement, la discussion sera orientée selon trois axes : les méthodes de temps-fréquence ainsi qu'une proposition de traitement de ces données par une méthode statistique indépendante de la référence. La discussion du premier article en montrera la qualité du traitement de ces stimuli. La discussion des deux articles neurophysiologiques, proposera de nouvelles d'expériences afin d'affiner les résultats actuels sur les déficits des schizophrènes. Ceci pourrait permettre d'établir un marqueur biologique fiable de la schizophrénie.

TABLE OF CONTENTS

LIST OF FIGURES

LIST OF EQUATIONS

CHAPTER 1 INTRODUCTION

This work is based on three scientific articles (Chapter 6). These articles focused on distinct topics. The first article developed a method for controlling physical attributes of groups of visual or auditory stimuli. In the case of visual stimuli, this control was performed on luminance and spatial frequency. The second article focused on early visual impairments in schizophrenia, particularly with regard to spatial information. Finally, the third article addressed a debate between three models of illusory contour processing in healthy subjects. The second and the third articles applied electrical neuroimaging analyses of event-related potentials, in large part because of the high temporal resolution this method affords. The common topic across these articles is the visual system and especially its early stages of processing.

To contextualize these three articles, the Introduction of the thesis explains the main concepts presented in these articles. This has been done in a simple and pedagogical way aiming at transmitting basic knowledge to the next PhD student who will continue this work.

The Introduction is organized in four sections. The first section focuses on visual processing of information. This will be done according to 3 aspects: cellular subtypes, regional specialization, and dynamic and functional interactions. The second section focuses on schizophrenia. This section comprises a definition of schizophrenia and their high- and low- level visual processing deficits. The third section overviews the current understanding of illusory contour processing at its competing models. Finally, the forth section focuses on electrical neuroimaging analysis methods. In this section a new method, which is not used in the articles, will be presented. This method relies on a time-frequency transformation and its statistical analysis.

1.1 Organization of the Visual System

Vision is a powerful sense. We are instantly able to dissociate and recognize objects in a complex scene. This segmentation, which seems simple, is in fact a complex process. Evidence of this complexity is clear in the failure of computer vision to reproduce human psychophysical capabilities. One such ability is the reconstruction of absent contours and the segmentation of images. Figure 2 shows an illusory contour developed by Gaetano Kanizsa (Kanizsa, 1976), where the border of an illusory triangle can be seen (further details on the visual processes supporting this perception are provided in 1.2).

In neuroscience, the visual system is one of the most studied sensory modalities. As it is relatively simple to obtain and to control physical features of visual stimuli, it makes them

particularly salient for research. To date, most studies have used static pictures. Physical features such as luminance and spatial frequency can be easily extracted from any picture. Luminance is the light intensity of a source. In image treatment, the luminance corresponds to the grey-scale level of the colored image. This grey-scale level is obtaining for a RGB image by the relationship: luminance = 0.299 R + 0.587 G + 0.114 B. Spatial frequency is analogous of a temporal frequency in the spatial dimension. Temporal frequency is defined by the inverse of a period of time. Spatial frequency is the inverse of a distance. The unit of spatial frequency is in cycles per degree of visual angle. Figure 1 shows different spatial frequencies. The high spatial frequency exhibits rapid changes in the image, for example edges, etc. The low spatial frequency represents small changes in an image.

Figure 1 : Definition of spatial frequency
Left panel shows low spatial frequency. Right panel shows high spatial frequency
(Downloaded from www.Wikipedia,org**)**

The treatment of the visual system can be described along 3 complementary aspects of organization. The cellular aspect describes the early stages of visual processing. The regional specialization aspect describes the different visual areas and their functions. Finally, the dynamic and functional interaction between regions describes the propagation of information through two main (though non-exclusive) pathways: one for recognition and the other for localization

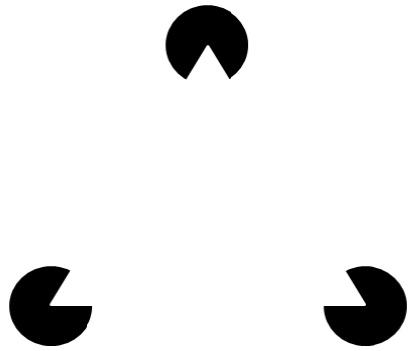

Figure 2: Kanizsa illusory contour.
Subjective borders are observed in the form of a triangle, such that there is a perceived brightness enhancement of the triangle shape.

1.1.1 Cellular aspect

The primary differentiation in the visual system comes from the distinction between two kinds of ganglion cells: parvocellular (P) and magnocellular (M) cells. These two kinds of cell types engender two distinct pathways that begin in the retina and project, via the lateral geniculate nucleus (LGN), to the primary visual cortex (striate cortex, V1).

Anatomically and functionally, parvocellular cells are smaller in size and have a smaller receptive field compared to magnocellular cells (Kaplan, 1991). A receptive field is the region of the visual space where an appropriate stimulus elicits action potentials. Parvocellular cells have a lower conduction velocity compared to the magnocellular cells (Kaplan, 1991). These physical characteristics have a direct implication on the treatment of visual stimuli. Indeed, their sensitivity to contrast is different. The magnocellular cells saturate at a low luminance contrast (~10 %), while parvocellular cells are sensitive at a higher luminance contrast >~8% (Kaplan, 1991). Similarly, parvocellular cells respond to chromatic (colors) contrast, while magnocellular cells do not (Kaplan, 1991). Parvocellular cells are sensitive to high spatial frequencies, whereas magnocellular cells are sensitive to low spatial frequencies. Magnocellular cells are sensitive to movement compared to parvocellular cells (Kaplan, 1991). Finally, magnocellular cells are activated vigorously by stimulus elements that are relatively large, whereas parvocellular cells are activated more strongly by stimulus elements that are relatively small (Jindra and Zemon, 1989; Dacey and Petersen, 1992).

On the one hand, the magnocellular system treats “low-resolution” visual information (i.e. low luminance contrast and achromatic) as well as moving images. It conducts these kinds of information rapidly to the visual cortex. This M pathway is involved in attention and processing of overall stimulus organization (Merigan and Maunsell, 1993; Steinman et al., 1997; Vidyasagar, 1999). On the other hand, the parvocellular system treats “high-resolution” visual information (i.e. high luminance contrast, chromatic) and static objects. It conducts these kinds of information slower to the visual cortex. This P pathway is involved in processing of fine-grained stimulus configurations and object identification (Merigan and Maunsell, 1993; Norman, 2002).

1.1.2 The Organization of Visual Regions

This section focuses on the different visual areas located within the occipital cortex. The visual cortex is composed of the primary visual cortex (called striate cortex or V1) and of the extra-striate visual regions including V2, V3, V4, and V5. The visual cortex can be subdivided in sub-areas, as Felleman and Van Essen (1991) proposed for the macaque monkey (Figure 3). In Figure 3 we may observe (at least) two different levels. The first level starts from the retina and projects to primary visual cortex and is composed of M and P pathways described in Section

1.1.1. The second level is cortico-cortical projections between areas. This level is more complex as there are many connections between areas, including multiple projections from one area to many others. Of note, in this figure no direction of the processing along this connection is specified because typically connections are bi-directional. Communication from low-level to high-level regions is called "bottom-up", and communication from high-level to low-level regions is called "top-down". These two types of communication will be important for the article in Section 6.3 where the debate of top-down vs. bottom-up processing of V1/V2 activation to illusory contours is treated. As V1/V2 are believed to be playing a critical role in illusory contour sensitivity, we will discuss them in more details. Recently another extra-striate visual area, the lateral occipital complex (LOC), is also believed to be playing a critical role in illusory contour and will also be described in more detail below.

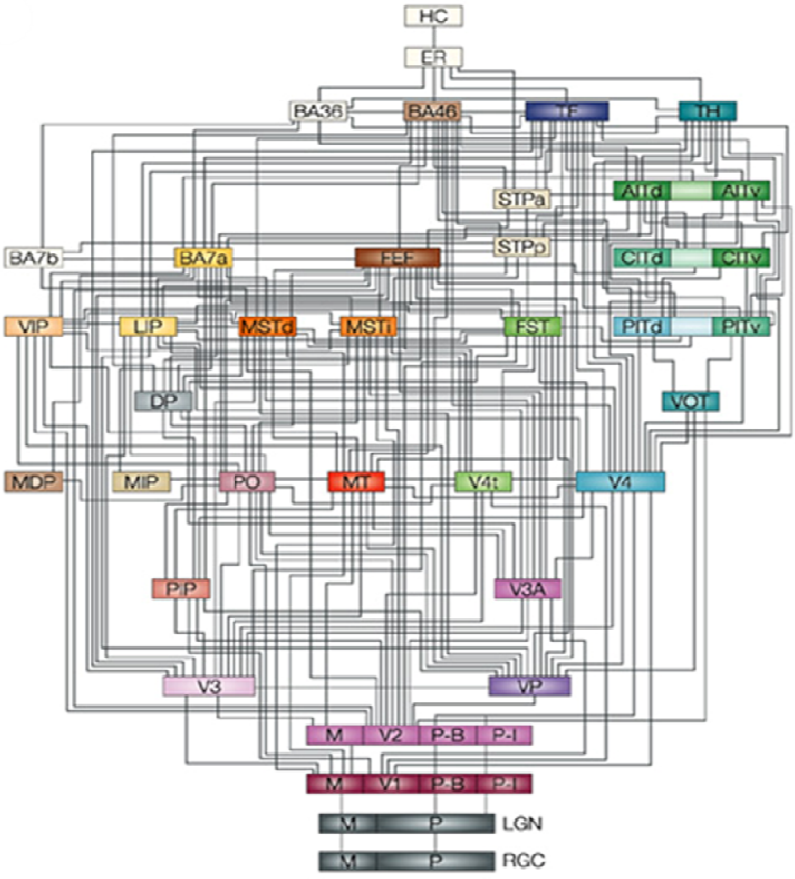

Figure 3 : Organization of the visual cortex in macaque,
32 visual areas could be shown (from **Felleman and Van Essen (1991)**

Primary visual cortex is located in the most posterior portion of the occipital lobe within the calcarine sulcus (Brodmann area 17). Visual area V2 is located around V1 in Brodmann areas 18

and 19, as can be seen in Figure 4. In terms of projections, V1 sends a large proportion of its connections to area V2 (Felleman and Van Essen (1991). Most of the V2 neurons have properties similar to the V1 neurons, although some V2 neurons are responding to more complex forms. These properties will be described below.

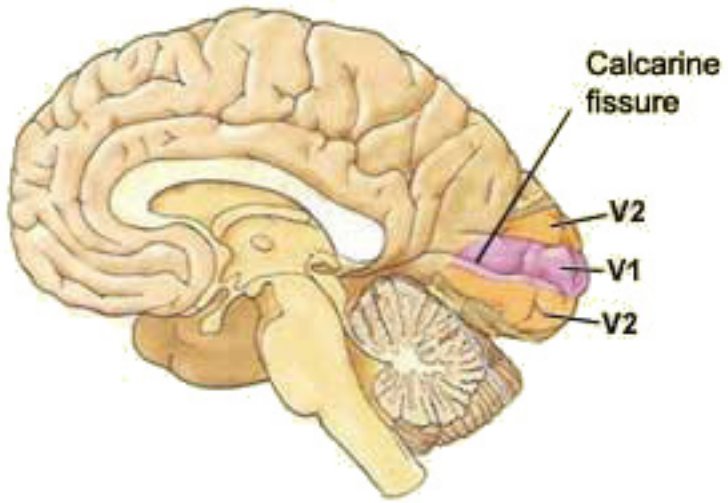

Figure 4 : Anatomical localization of V1 and V2
Midsagital view of the brain that highlights the anatomic localization of visual areas V1 and V2 (Downloaded from http://thebrain.mcgill.ca)

Functionally speaking, areas V1 and V2 are mainly involved in extracting low-level features and physical information from visual stimuli (in animals: (Hubel and Wiesel, 1977); and humans: Tootell et al., 1998; Romani et al., 2003). Hubel and Wiesel (1977) have shown early sensitivity to luminance, spatial frequency, and line orientation in areas V1 and V2. This bar orientation sensitivity was used in the article appearing in Section 6.3 to compare this well known activity in V1 and V2 to conditions involving illusory contours (ICs).

Areas V1 and V2 are organized retinotopically. Each point in visual space corresponds to one and only one sub-region within V1 and V2. Furthermore, two contiguous points in the visual space are represented contiguously in the cortex. The geometrical structure of an object is thus preserved in its cortical representation within V1 and V2. However the proportions of this projection are changed. Indeed, the central information of the visual field (i.e. the fovea) is disproportionately represented relative to the periphery. This is referred to as foveal magnification.

Another important visual area when considered the neural basis of illusory contour processing is the lateral occipital complex (LOC). This area is a high-level cortical area compared to V1 and

V2 described above. (Malach et al., 1995) described the responsiveness of this region and in particular how it responds more strongly to photographs of everyday objects compared to visual textures without shapes. This cortical area was located on the lateral bank of the fusifrom gyrus extending ventrally and dorsally. This result suggests that the LOC is involved in object recognition. Grill-Spector et al.(2001) review functions of the LOC with respect to object recognition. Importantly, the research they review shows that the LOC is sensitive to shapes in a cue-invariant and perspective-invariant manner, but is not sensitive to low-level features such as line orientation or contrast (or significantly less so; see e.g. Mendola et al. (1999) for a study of illusory contours). This information is relevant for article in Section 6.3 that shows the first illusory presence vs. absence differentiation in the LOC.

The major associative areas (V3, V4, and V5) have their own functional specificity. They are located peripherally to V1 and V2 as we can see in Figure 5. In terms of functionality, these areas are more specific. Indeed area V3 is associated with the treatment of dynamic shapes. Moreover, the V3 subdivision V3a is associated with the treatment of static shapes (Tootell et al., 1997). Area V4 is sensitive to colors and forms (Tootell and Hadjikhani, 2001; Tootell et al., 2004). Area V5 is associated with object movement (Tootell et al., 1995).

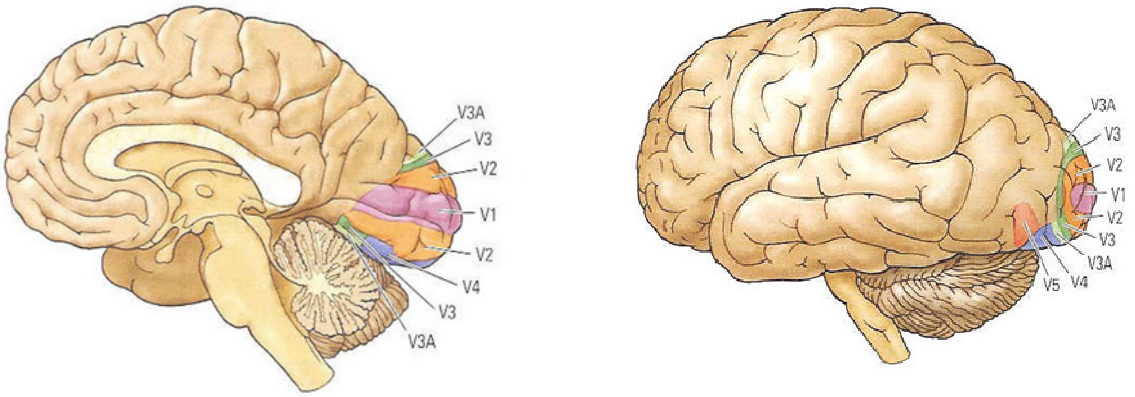

Figure 5 : Anatomical representation of visual areas V1 to V5
Midsagital view of the brain that highlights the anatomic localization of visual areas V1, V2, V3, V4, and V5 (Downloaded from http://thebrain.mcgill.ca)

1.1.3 Dynamic and functional interactions between visual regions

This section focuses on a more general treatment of visual information. Visual information is generally-speaking separated into two pathways. The first pathway, the ventral pathway, extends to the temporal lobe, and is involved in object recognition (therefore, this pathway is also called the "What" pathway). The second pathway, the dorsal pathway, projects to the parietal lobe, and appears to be essential for locating objects in space (therefore this pathways is

also called "Where" pathway). These two pathways are well described in animals and humans. These studies have stated that the flow of information is starting from V1 and V2 and is processed in parallel within the two pathways (Ungerleider and Mishkin, 1982). This parallel processing ability raised the important concept that recognition can be performed without spatial localization and vice versa. Studies on neurologic and neuropsychologic patients have shown there to be patients with normal spatial localization ability but impaired recognition (agnosia (Ungerleider and Mishkin, 1982)). The inverse situation was also reported (Ungerleider and Mishkin, 1982). It would be remiss to not mention the existence of the same functional sub-division into pathways for processing auditory and tactile information (De Santis et al., 2007)

Schroeder et al. (1998) showed there to be latency differences between the dorsal and ventral pathways (see also Schmolesky et al., 1998). They likewise showed that the first inputs into ventral stream regions exhibit a lateral or top-down profile rather than bottom-up profile. This would suggest that information treated along the dorsal pathway can influence the manner in which information is treated along the ventral pathway before that information activates these regions. Interactions between the pathways is also supported by Merigan and Maunsell (1993) who showed that while the dorsal visual pathway is more sensitive to magnocellular inputs and the ventral pathway is more sensitive to parvocellular inputs, this division is not exclusive. Rather, there is an intermixing of both magnocellular and parvocellular inputs within both dorsal and ventral pathways. These concepts impact the design and interpretation of the studies presented in Chapter 6.

1.2 Illusory contour processing

It is well established that our brain is able to reconstruct visual information without sensory input. This reconstruction is called completion or perceptual "filling-in". A simple definition could be: "the filling-in of information that is not directly given to the sensory input". In this frame the illusory contour (Figure 2) is one example of completion. In this example our brain is able to reconstruct the triangle that is absent. The triangle does not come from physical luminance differences. Indeed, the background inside and outside the triangle exhibit identical physical properties. This fact suggests that the perception of the triangle comes from the computations within the brain because it is not present at the retina.

The type of illusory contour used in the article described in section 1.1.1.a was Kanizsa-type and misaligned gratings for the article described in section 6.3.4.b. The misaligned gratings were used in the article presented in section 6.3 because they do not exhibit salient regions, whereas Kanizsa-type stimuli do. The salient region comes from computer vision and is defined as: "*a set*

of contiguous image pixels that likely correspond to a major surface in the scene" (Stanley and Rubin, 2003*).*

The following paragraph presents three different neurophysiological models for illusory contour sensitivity in the brain. Figure 6 shows a schematic representation of these models.

The first model states that illusory contour differentiation starts in V1/V2 and the other activities in parietal regions and LOC come from feed-forward modulation driven byV1/V2 activity. This model is supported by some microelectrode studies in macaque monkeys (e.g. von der Heydt and Peterhans, 1989; Peterhans and von der Heydt, 1989; Ramsden et al., 2001). Similarly, this model receives some support from hemodynamic imaging in humans ((e.g. Ffytche and Zeki, 1996).

The second model states that the illusory contour differentiation starts in LOC (lateral occipital complex). The activities in V1/V2 and other parietal regions are instead driven by feedback modulations from the LOC. This model is supported by some studies in humans, using misaligned gratings and Kanizsa stimuli with different physiological measurement (EEG, fMRI, MEG, TMS) (e.g Mendola et al., 1999; Pegna et al., 2002; Murray et al., 2002, 2004, 2006; Halgren et al., 2003; Brighina et al., 2003; Foxe et al., 2005). This model is also supported by animal studies using abutting line gratings stimuli (e.g Sáry et al., 2007, 2008).

The third model states that the LOC differentiates the salient region induced by the stimuli. The presence of the illusion should itself be differentiated first within V1/V2 in a manner under the control of feedback modulations from this LOC activity. This kind of hypothesis is supported by Stanley and Rubin (2003) and Yoshino et al.(2006) with fMRI and EEG data, respectively.

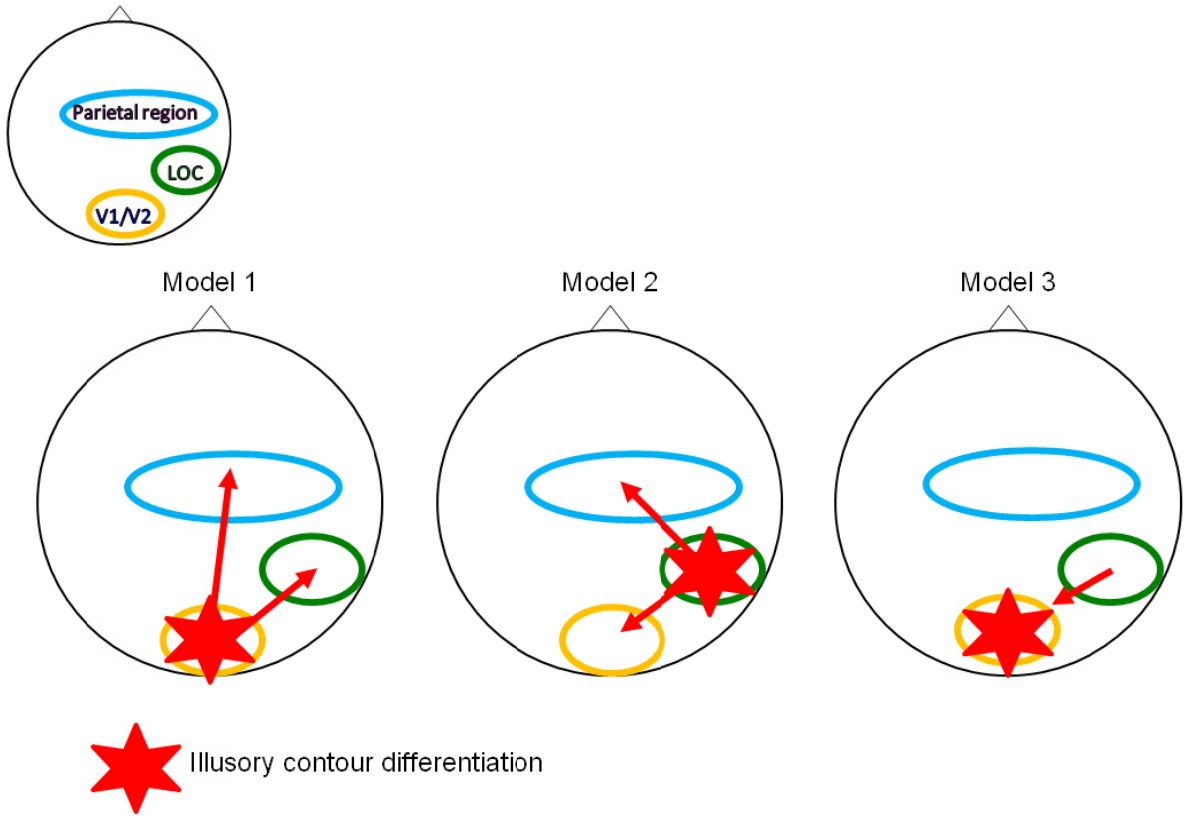

Figure 6 : Schematic of three competing models of illusory contour (IC) sensitivity
. For simplicity, only 3 brain regions are illustrated: lower-tier cortices (V1/V2), the lateral occipital cortex (LOC), and parietal cortex. Model 1 supports initial IC sensitivity within V1/V2 that is driven by feedforward inputs and/or local lateral interactions. Model 2 supports initial IC sensitivity within the LOC with later effects within V1/V2. Model 3 proposes that the LOC is sensitive to salient regions of the stimuli and not to the IC itself, though feedback from the LOC is required to effectuate IC sensitivity within V1/V2..

These models are discussed in the article in section 6.3.

1.3 Schizophrenia

1.3.1 Definition

The most-used standardized criteria for diagnosing schizophrenia come from the American Psychiatric Association's Diagnostic and Statistical Manual of Mental Disorders, version DSM-IV-TR.

According to this fourth edition three diagnostic criteria must be observed to establish a diagnosis of schizophrenia: (Spitzer et al., 1992)

" ***Characteristic symptoms:*** *if two or more of the following symptoms are observed during one-month (and less than one month if the patient is treated)*

- *Delusions*

- *Hallucinations*
- *Disorganized speech, which is a manifestation of formal thought disorder*
- *Grossly disorganized behavior (e.g. dressing inappropriately, crying frequently) or catatonic behavior*
- *Negative symptoms: blunted affect (lack or decline in emotional response), alogia (lack or decline in speech), or avolition (lack or decline in motivation)*

If the delusions are judged to be bizarre, or hallucinations consist of hearing one voice participating in a running commentary of the patient's actions, or of hearing two or more voices conversing with each other, only that symptom is required above.

Social/occupational dysfunction: *For a significant period of time since the onset of the disorders, one or more major domains, such as work, interpersonal relationships, or self-care, are markedly below the level of behaving before the disorders.*

Duration: *Continuous signs of the disorders persist for at least six months. This six-month period must include at least one month of symptoms (or less, if symptoms remitted with treatment).*"

Multiple forms of schizophrenia can be diagnosed, for example schizoaffective disorder.

1.3.2 Cognitive deficits (high-level)

This section is an overview of important findings on cognitive impairments in schizophrenic patients.

Selective attention is the ability to focus on target stimuli in the presence of distracters or competing stimuli (Sohlberg and Mateer, 2001), This ability is often impaired in schizophrenic patients (Egeland et al., 2003). Moreover, Liu et al. (2002) showed greater impairment in sustained attention in schizophrenia relative to other psychiatric diseases, like bipolar disorder or depression.

Another well-established deficit of schizophrenic patients is their poor memory skills. In fact, each stage of processing is impaired: encoding, storage and retrieval (Sohlberg and Mateer, 2001). The encoding deficit is linked to their visual search difficulties, as a result of their poor selective attention resources (Oltmanns et al., 1978; Hofer et al., 2003; Hartman et al., 2003). Working memory, which involves short term storage and manipulation of information, is considered among the most severe cognitive dysfunction of schizophrenic patients. It was first

described by (Baddeley, 1992). Coming to retrieval, (Kenny and Meltzer, 1991) have shown that people with schizophrenia have more problems with retrieval of episodic information than semantic information

Executive functions are also impaired. Based on the hierarchical system of cognition, this impairment can be seen as an integration of basic cognitive skills like attention to higher cognitive domains like executive functions (McGurk and Mueser, 2003).). Deficits in executive functions included lack of concept comprehension, absence of planning, abstract reasoning, and problem solving (Jaeger et al., 2003). For example, impairment in Schizophrenic patients has been found in early psychosis stage, such as poor sequence organization, lack of flexibility in responses, poor inhibition skills, absence of planning and strategy (Hutton et al., 1998; Mohamed et al., 1999).

1.3.3 Early visual deficits (Low-level)

Recently, the investigation in deficits related to schizophrenia has focused on early perceptual treatment. This section will focus its attention on the visual system investigated with EEG methods. For literature concerning other senses (e.g. audition), the reader may refer to Michie (2001) ; Turetsky et al. (2007) ; Näätänen and Kähkönen (2009) who describe patterns of deficits in generation of the mismatch negativity.

In the literature, the primary approach to investigating the visual system in schizophrenic patient is the steady-state VEPs (ssVEPs) (Spekreijse, 1966). Butler et al. (2005) using ssVEP showed a dysfunction of the magnocellular pathway in schizophrenia. This study used luminance contrast to bias responses to the magnocelluar or parvocelluar pathways. The authors founded only responses in the magnocellular condition. Additionally, the control group showed an incensement of the response to low luminance contrast stimuli (~1-10 %), which saturated once the luminance contrast was ~16-32 %. The parvocellular condition was obtained at a contrast level of 48%. At this contrast the magnocellular response were saturated. The patient group exhibited a much smaller gain and a much lower plateau for the magnocellular condition, but no difference was found in the parvocellular condition.

The second ssVEP experiment demonstrated a magnocellular impairment in schizophrenia. This was performed by Kim et al.(2005) using windmill-dartboard and partial-windmill stimuli. These kinds of stimuli were investigated across harmonic level responses. The first and the second harmonic levels (second harmonic is twice the first one) are the most important harmonics used in this study. The first harmonic was above the magnocellular-specific range (Zemon and Ratliff, 1982). This information showed that the first harmonic is more sensitive to the parvocellular pathway (Tootell et al., 1998). Additionally, the second harmonic is caused by

achromatic (McKeefry et al., 1996) and low spatial stimuli (Murray et al., 1983; Grose-Fifer et al., 1994). This result showed that the second harmonic is more sensitive to the magnocellular pathway. Kim et al.(2005) showed in schizophrenic patients compared to a control group a reduced amplitude and coherence of the second harmonic response for both stimuli presented above as well as normal first harmonic responses. This result supports a magnocellular pathway deficit in schizophrenia.

More recently, VEP studies also demonstrated early visual impairment in schizophrenia. These studies were analyzed in the time domain with more slowly presentation of the stimuli. They showed an impairment of the P1 component (Foxe et al., 2001, 2005; Doniger et al., 2002).

In conclusion ssVEP suggest an magnocellular pathway impairment and VEP studies added information on the early timing of this deficit

1.4 Methods

1.4.1 Electroencephalography

Electroencephalography (EEG) measures the electrical brain activity through electrodes placed at the scalp. EEG data are presented generally as traces across time. The electrical brain activity signal is due to the summation of synchronous post-synaptic potentials from neuronal ensembles. Because the electrical signals of the brain are relatively small, particularly those evoked by external stimuli, the recorded signal must be amplified, and approaches such as signal averaging are typically applied.

EEG is quantified at the scalp as a potential difference, which consequently required a reference location. The choice of the reference is critical, because changing the reference changes the waveforms, their local maxima and their amplitude. To better understand this critical notion, we can compare it to measurement of the altitude of a mountain (an analogy often used by Professor D. Lehmann). For example, the Jungfrau Mountain is 4158m high if referenced to sea-level, but is at 3786m if referenced to Lake Geneva. In practice, one of the electrodes is defined as reference for the recordings. The earth reference is not used for technical reasons (poor signal). There are a lot of different classical recording reference locations (noise, mastoids, vertex, etc.). Some systems also use “two” electrodes (Biosemi) as a loop to better simulate a zero potential. In the offline data treatment we generally use the average reference. The average reference is defined as the mean across electrodes (calculated against original reference (Desmedt et al., 1990; Pascual-Marqui and Lehmann, 1993; Michel et al., 2004) give general commentaries on the average reference. To be correctly computed the source estimation data

must be calculated against an average reference. This constraint derives from the source estimation hypotheses see Grave de Peralta Menendez et al. (2004) for more details.

1.4.2 EEG Analysis (ERP,Seg,IS)

This section focuses on high-density EEG. High-density EEG is used in research, compared to low-density recordings usually used clinics.

Stimulus-evoked brain activity is of relatively small amplitude in comparison to spontaneous EEG and sources of noise. Typically, signal averaging is performed to increase the visibility of stimulus-evoked activity by taking many epochs of EEG around a stimulus event. This procedure assumes that stimulus-related brain activity is time-locked and all other activity is distributed randomly (across trials) with respect to stimulus presentation.

Because the analyses presented in this thesis are based on data re-calculated against the average reference, it is critical to identify and remove (via interpolation) any "bad" channels (Perrin et al., 1987). Determination of "bad" channels can be based on poor electrode-skin contact, broken electrodes, etc. To complete the pre-processing steps, a grand mean (mean across subjects per condition) is computed and the single subject data are kept. Sometimes a baseline correction may be applied (though this also has a set of assumptions; see Lehman (1987)). At the end of the pre-processing of the data, we obtain one ERP per subject and per condition, as well as one grand mean per condition.

At this level, we can perform statistical analyses. They go in 3 directions: 1) strength of the field, using Global Field Power (GFP) as the dependent measure, 2) topographic analysis using scalp electrical maps as measure, and 3) source estimation using estimated activity in brain as the dependent measure. GFP and topographical analyses are orthogonal. This means that these two measures are independent. By contrast, source estimations are linked to either or both GFP and topographic results.

GFP was introduced by Lehmann and Skrandies (1980)) and corresponds to the standard deviation of all electrodes at a given instant in time (Equation 1) and expresses the average power of the signal across the electrode montage. The definition of GFP has several properties. It is expressed in μV, it is reference-free, and it is non-linear, (i.e. the mean of GFP is not equal to GFP of the mean).). Furthermore, GFP keeps temporal information, but loses the spatial distribution information across electrodes on the scalp. The GFP values are null or positive. A GFP value of zero involves that all electrodes express the same potential. Opposite high values express big differences, between positive and negative potential across scalp electrodes. In terms of analysis, we performed statistics (T-test, ANOVA) at each time-frame of this measure.

To account for temporal auto-correlation, only effects persisting for at least a certain time were considered reliable. This analysis gives only big temporal differences but is less to noisy.

$$GFP(t) = \sqrt{\frac{\sum_{i=1}^{n} \left(u_i(t) - \bar{u}(t)\right)^2}{n}}$$

n = Number of electordes

$u_i(t)$ = one electrodres

$\bar{u}(t)$ = average acrosse electrodes

Equation 1: Global Field Power

Topographic analysis is based on the distribution of the electric field across electrodes. This analysis is also reference-free. To better understand why the data are reference free, an analogy with cartography can be useful. On a topographical map, usually used for walking in the mountains, there are contours that indicate if it is steep or flat. These contours are totally independent of any references (sea-level vs. “Lac Leman”). For example the “Eiger” mountain is steep independently of whether we calculate the altitude from sea-level or “Lac Leman”. It is exactly the same way on EEG topography, which derives from pure spatial considerations. In terms of timing, there is also a consideration that is called microstate (Michel et al., 1999, 2004). This supports relative stability of maps across time. A map (or state) is stable for a certain period of time. This state will change to another that also will be stable in time, etc. The analysis of topography identifies these microstate properties using cluster analyses. This clustering reduces the data to a certain number of consecutive states represented by maps. Typical clustering analyses are K-means and hierarchical clustering (Murray et al., 2008a). The clustering being performed on the grand average, the output microstates are “artificial”. To solve this, a fitting procedure on individual subjects is performed, given the occurrence of each state, first onset, last onset or Global explain variance for each subject and condition. Finally, a statistical analysis of these measures is performed and gives the interpretable results. This fitting is based on the spatial correlation of the clustering output at the group-average level and the single-subject ERP.

The study of maps can also be performed time-frame by time frame using a metric named global dissimilarity (Lehmann and Skrandies, 1980), this analysis gives complementary information. They indicate at each time frame if the two different average maps across condition are significantly different.

In terms of interpretation, two different maps implicate different brain networks. But two different brain networks might express the same map. This property is critical, because it implies that only map differences inform us unequivocally about brain function. By contrast, similarity of maps does not provide us unambiguous information.

Source estimations refer to the mathematical reconstruction of brain activity producing the electric field at the scalp. In this thesis we used a distributed linear inverse solution (ELECTRA) applying the local autoregressive average (LAURA) regularization approach to address the non-uniqueness of the inverse problem (Grave de Peralta Menendez et al., 2001, 2004; Michel et al., 2004). The inverse solution algorithm is based on biophysical principles derived from the quasi-static Maxwell's equations; most notably the fact that independent of the conductor volume model used to describe the head, only irrotational and not solenoidal currents contribute to the EEG (Grave de Peralta Menendez et al., 2001, 2004). As part of the regularization strategy, homogenous regression coefficients in all directions and within the whole solution space are used. LAURA uses a realistic head model, and the solution space includes n nodes (we used classically 3005), selected from a 6 × 6 × 6 mm grid equally distributed within the gray matter of the Montreal Neurological Institute's average brain (courtesy of Grave de Peralta Menendez and Gonzalez Andino; http://www.electrical-neuroimaging.ch/). The head model and lead field matrix were generated with the Spherical Model with Anatomical Constraints (SMAC;Spinelli et al., 2000). As an output, LAURA provides current density measures; the scalar values of which were evaluated at each node. Prior basic and clinical research has documented and discussed in detail the spatial accuracy of this inverse solution (e.g. (Grave de Peralta Menendez et al., 2004; Michel et al., 2004; Gonzalez Andino, Michel, et al., 2005; Gonzalez Andino, Murray, et al., 2005; Martuzzi et al., 2009). This method may be used in two ways. First, we may use a period of interest corresponding to previous results generally obtained by the methods above. In this period of interest, data from each subject and condition are first averaged as a function of time to generate a single data point. Then an inverse solution is calculated for each of the nodes in the solution space. The second method is a time-frame by time-frame source estimation, which is calculated for each subject and condition. Each of these two methods has advantages. The first one is less sensitive to noise, but loses fine temporal information. The second is sensitive to noise, but keeps all the temporal information. Finally, statistical methods are applied to these data on each node for the first method and for each node and time-frame for the second method. To address the multiple testing problems, a spatial extent criterion for significant nodes is applied for both methods described above. Additionally, for the second way a consecutive significant timing criterion is also applied.

1.4.3 Visual components of the ERP

They are three major early visual components (C1, P1, N1) describing the ERP. This section presents these three components from their definition in terms of timing and topography to their presumed main brain sources. Additionally, a more detailed treatment of the P1 component will be provided here given its importance in the article in Chapter 6.

The C1 component was first described by (Jeffreys and Axford, 1972). It peaks typically from 50-90ms and its polarity and scalp distribution are related to the localization of the stimulus in space. For example, the C1 exhibits a negative polarity for a stimulus in the upper half of the visual field and exhibits a positive polarity for a stimulus in the lower half of the visual field. Its topographical scalp distribution exhibits positivity in the occipito-parietal electrodes contralateral to the stimulus presentation. The spatial dependency of the C1 component suggests a retinotopic dependence of this component (Jeffreys and Axford, 1972). In addition, Clark et al.(1995) and Di Russo et al.(2003) attribute the C1 component modulation to activity in primary visual cortex using source estimation method. More recently, Foxe et al. (2008) showed that the C1 component is related to the parvocellular pathway more than the magnocellular pathway.

The P1 component was attributed to (Spehlmann R, 1965). It is characterized by a positive peak around ~80-130ms. Its topographical scalp distribution is characterized by a maximum positivity over later occipital regions also described as posterior positivity. Studies of Simpson et al. (1995),Woldorff et al. (1997) and Murray et al.(2002) suggest that the P1 represents the activity of generators in both the dorsal and the ventral pathways. In terms of modulation, P1 amplitude is strongly dependent on attention (Mangun and Hillyard (1991).

The N1 component is define by a negative peak against a mastoid reference over ~150-200 ms. Its topographical distribution at the scalp is a posterior negativity. In terms of brain generators study of Allison et al. (1999) in intracranial grid-electrodes recording and studies of Bentin et al. (1999, Doniger et al. (2000, 2001) , Murray et al. (2002) on scalp distribution suggest that N1 is related to the ventral visual pathway.

1.4.4 Time frequency analysis

The classical frequency analysis uses a Fourier transformation. This kind of analysis transforms the time/amplitude signal into a frequency/amplitude (in). The Fourier transformation loses an important variable: The time. To preserve time and frequency, we decomposed the time/amplitude signal on small segments and performed a Fourier transform on each of the small element. This is called Short time-Fourier transformation. This method keeps both time and frequency, but lose time resolution or frequency resolution due to Heisenberg‘s uncertainty

principle. Many new approaches have tried to address this problem. In this manuscript we will focus on one of them: the Stockwell transformation (Stockwell et al., 1996). A summary of the Stockwell transform is: "*The S transform is a generalization of the Short-time Fourier transform, extending the Continuous wavelet transform and overcoming some of its disadvantages. For one, modulation sinusoids are fixed with respect to the time axis; this localizes the scalable Gaussian window dilations and translations in S transform. Moreover, the S transform does not have a cross-term problem and yields a better signal clarity than Gabor transform. However, the S transform has its own disadvantages: it requires higher complexity computation (because FFT can't be used), and the clarity is worse than Wigner distribution function and Cohen's class distribution function*". Technically the S transform gives us good time and frequency resolution at the EEG frequency of interest (0-100 Hz). This is not the only Time-frequency transformation; wavelets may also provide good results with EEG.

After this short presentation of the Time-frequency transformation, we will show different treatments and considerations for time-frequency analysis. First, time-frequency representations are reference-dependent. Results obtained in this manuscript were valid for only the chosen reference (arbitrarily the original reference will be used here). The S transform was performed on each single trial and then averaged. This averaging was done in four directions. First only the power (norm of the complex number) was extracted before the averaging. This analysis gives as we called induced power frequency (non-phase-locked to the stimulus). Second, the phase (angle of the complex number) was extracted before the averaging as we called induced phase. Third, complex numbers were averaged. This will give the evoked frequency. After this the power was calculated. Evoked frequencies are frequencies that are in phase across trails. This is exactly the same as performing the S transform on ERP. The fourth direction is the phase of the evoked responses.

Additionally to these four different approaches of the S transform (see above), we performed two different statistical models independent of the condition model. The first one uses electrodes as repetition, this increases power, but looses the spatial information. The second uses electrodes as factor. This keeps spatial information, with the interaction term between electrodes and condition factor, but is time-consuming and has less power.

To take into account if the multiple testing problems a binary morphology was applied following this procedure. The results of these statistical analyses were transformed into a binary image with 1 for significant points and 0 for non-significant. Then on these images a mathematical binary morphology (Serra, 1982) was applied.

The definition if binary mathematical morphology could be (Serra, 1982) :" An approach designed to fill the physical property of objects to their structure". To use this mathematical morphology a structuring element must be defined. This element is a shape (square, disk, or a cross) and contributes to the morphology. There are two types of morphology "erosion" and "dilatation" the others are combinations of theses basics. Practically the center of the shape is placed on a pixel. Depending on the type (erosion or dilatation) and the state of the neighbors (0 or 1) covered by the shape, the center pixel changes their state or not (1 to 0, 0 to 1, or no change). The next step is that the shape moves to the next pixel and the same procedure is applied. This technique cleans images by removing spot (erosion) and filling holes (dilatation). The quality of the clearing depends on the shape (form and size). The example in Figure 7 shows the difference before and after treatment. The grey pixels are the adding or excluding pixels

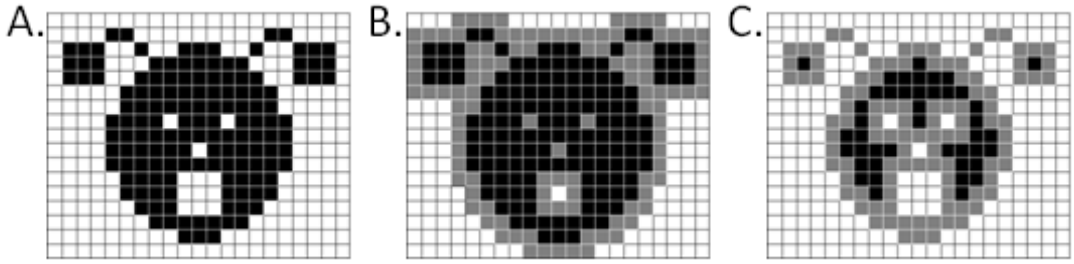

Figure 7: mathematical morphology erosion and dilatation:
Panel A shows original image. Panel B shows after dilatation with 3 X 3 square. C shows after erosion with 3 X 3 square. © www.wikipedia.org

In the statistical image case we used the mathematical morphology "opening". An "opening" is an "erosion" followed by a "dilatation. This Clear small element as we can see in Figure 8.The shape is a disk to take into account points at equal distances to the target pixels. The target pixel in the statistical image is in time/frequency domain.

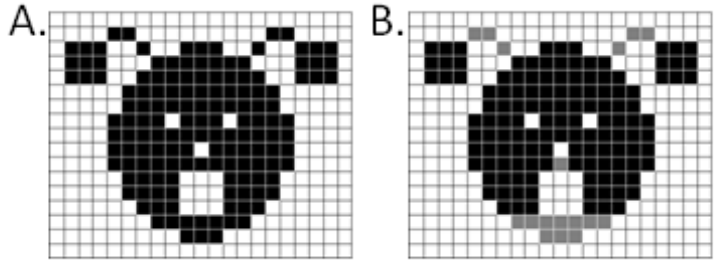

Figure 8 : Mathematical morphology, opening

Panel A shows original image. Panel B shows after opening with 3 X 3 square. © www.wikipedia.org

CHAPTER 2 RESULTS

2.1 Generating Controlled Image Sets in Cognitive Neuroscience Research

Jean-François Knebel, Ulrike Toepel, Julie Hudry,Johannes le Coutre, Micah M. Murray (2008)

Brain Topogr. 2008 Jun;20(4):284-9. Epub 2008 Mar 13.

Contribution: The candidate contributed decisively to the main idea of the method, development of the methods, data acquisition, and writing of the paper.

2.1.1 Abstract

The investigation of perceptual and cognitive functions with non-invasive brain imaging methods critically depends on the careful selection of stimuli for use in experiments. For example, it must be verified that any observed effects follow from the parameter of interest (e.g. semantic category) rather than other low-level physical features (e.g. luminance, or spectral properties). Otherwise, interpretation of results is confounded. Often, this issue is circumvented by including additional control conditions or tasks, both of which are flawed and also prolong experiments. Here, we present some new approaches for controlling classes of stimuli intended for use in cognitive neuroscience, however these methods can be readily extrapolated to other applications and stimulus modalities. Our approach is comprised of two levels. At a first level, individual stimuli are equalized in terms of their mean luminance. Each data point in the stimulus is adjusted to a standardized value based on a standard value across the stimulus battery. At a second level, two populations of stimuli are controlled in their spectral properties (i.e. spatial frequency) using a dissimilarity metric that equals the root mean square of the distance between two populations of objects as a function of spatial frequency along x- and y-dimensions of the image. Randomized permutations are used to obtain a minimal value between the populations. While another paper in this issue applies these methods in the case of acoustic stimuli (Aeschlimann *et al.*, this issue), we illustrate this approach here in detail for complex visual stimuli.

2.2 Impaired early visual response modulations to spatial information in chronic schizophrenia

Jean-François Knebel, Daniel C. Javitt, Micah M. Murray

Accepted for publication in Psychiatry Research: Neuroimaging

Contribution: The candidate contributed decisively to the, analyses and writing of the paper.

2.2.1 Abstract

Early visual processing stages have been demonstrated to be impaired in schizophrenia patients and their first-degree relatives. The amplitude and topography of the P1 component of the visual evoked potential (VEP) are both affected; the latter of which indicates alterations in active brain networks between populations. At least two issues remain unresolved. First, the specificity of this deficit (and suitability as an endophenotype) has yet to be established, with evidence for impaired P1 responses in other clinical populations. Second, it remains unknown whether schizophrenia patients exhibit intact functional modulation of the P1 VEP component; an aspect that may assist in distinguishing effects specific to schizophrenia. We applied electrical neuroimaging analyses to VEPs from chronic schizophrenia patients and healthy controls in response to variation in the parafoveal spatial extent of stimuli. Healthy controls demonstrated robust modulation of the VEP strength and topography as a function of the spatial extent of stimuli during the P1 component. By contrast, no such modulations were evident at early latencies in the responses from patients with schizophrenia. Source estimations localized these deficits to the left precuneus and medial inferior parietal cortex. These findings provide insights on potential underlying low-level impairments in schizophrenia.

2.3 Towards a resolution of conflicting models of illusory contour processing in humans

Jean-François Knebel, Micah M. Murray

Under review in Journal of neuroscience

Contribution: The candidate contributed decisively to the elaboration of the experimental design, data acquisition, analyses and writing of the paper.

2.3.1 Abstract

Despite numerous studies, the neurophysiologic mechanism mediating illusory contour (IC) sensitivity remains controversial. Three general models can be distinguished. One favors effects within lower-tier cortices, V1/V2, mediated by feed-forward inputs and/or long-range horizontal interactions. Another situates IC sensitivity within higher-tier cortices, principally lateral-occipital cortex (LOC), with feedback effects in V1/V2. Still others postulate that the LOC is sensitive to salient regions demarcated by the inducing stimuli, whereas effects within V1/V2 reflect specifically IC sensitivity. The present study resolved discordances between these models by using misaligned line gratings, oriented either horizontally or vertically, to induce ICs. These particular stimuli lack salient regions otherwise present in Kanizsa-type stimuli. Plus, varying line orientation one can assay early, low-level (V1/V2) modulations independently of IC presence. Using this 2x2 within subject design, we recorded 160-channel visual evoked potentials (VEPs) from 15 healthy humans and disambiguated the relative timing and localization of IC sensitivity with respect to that for grating orientation (as well as any interactions between these features). Millisecond-by-millisecond analyses of VEPs, response strength, as well as of distributed source estimations revealed a main effect of grating orientation beginning at 65ms post-stimulus onset within the calcarine sulcus (and elsewhere) that was followed by a main effect of IC presence beginning at 85ms post-stimulus onset within the LOC and extending dorsally into inferior parietal cortices. There was no evidence for differential processing of ICs as a function of the orientation of the grating. The collective results support models wherein IC sensitivity occurs first within the LOC.

2.4 Time-frequency

These results were based on data presented in the article in section 6.2. These results are exploratory and are not published yet. The statistical design is: one between subject factor called group (control vs. patient) and one within subject factor called eccentricity (wide vs. narrow).

This choice is based on previous results showed in article of section 6.2. The epoch properties are: a duration of one second (-300 ms to 700 ms) and frequency sampling of 500Hz. The Stockwell transformation with these values gives a time step of 2 ms and a frequency step of 1Hz, but the scale of the frequency is limited to 76Hz.

The two statistical methods presented in section 1.4.4 will be presented. This will be divided in 8 results figures; each panel will present data without and with mathematical morphology.

2.4.1 Electrode as repetition results

This section will present the results for the interaction group * eccentricity condition using electrodes as repetition. The statistical threshold was $p<0.05$. Additionally a mathematical morphology was applied to Figure 10, Figure 11, and Figure 12respectively with a 2, 4, and 6 radius disk. In Figure 9 no mathematical morphology was applied. Black color indicates significant differences and white color indicates no differences. A discussion of these results appears in Chapter 3. However, the reader should already note a difference between power (homogeneous) and phase (heterogeneous) information. Additionally, this difference shows the quality of the mathematical morphology methods to avoid false positive problems linked to statistical multiple testing. Finally, this section shows that electrodes as repetition is too conservative. Indeed, this analysis did not show differences observed with other EEG methods (GFP, Topography) see section 6.2 for details.

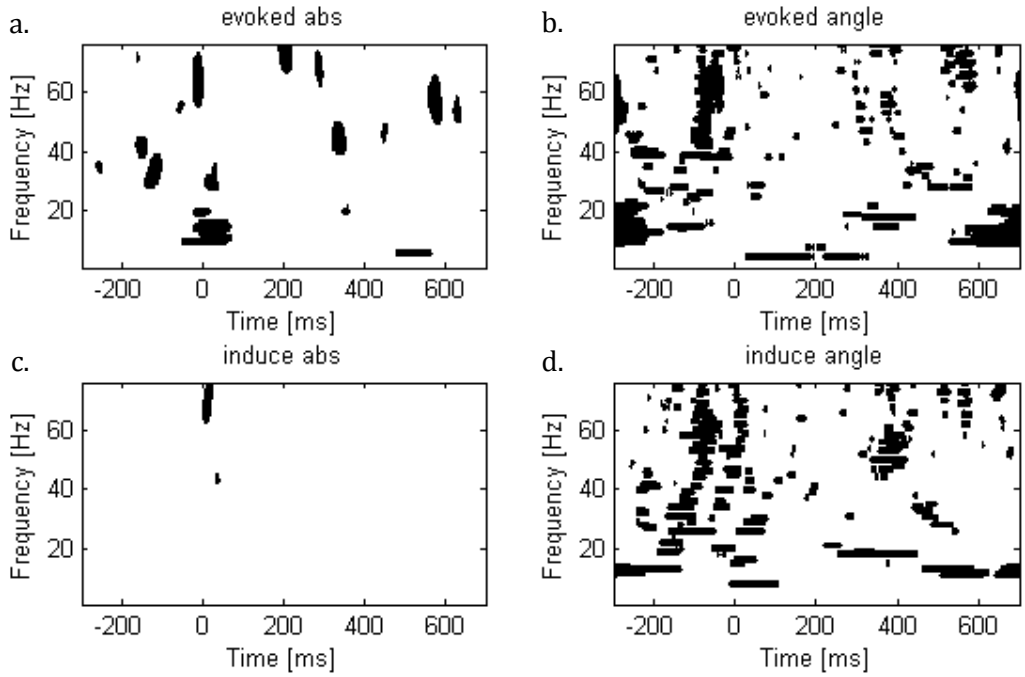

Figure 9 : Time-frequency Statistical map; Interaction group * eccentricity with electrodes as repetition and no mathematical morphology.

Panel a represents the power of evoked response; Panel b represents the phase of evoked response; Panel c represents the power of induced response; Panel d represents the phase of induced response

.

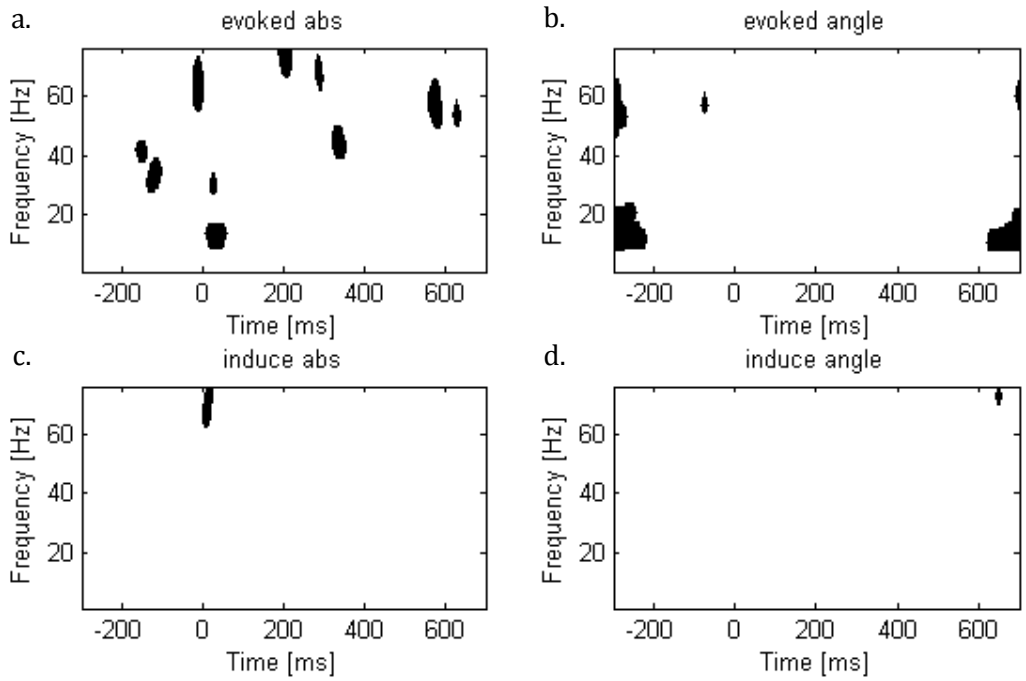

Figure 10 : Time-frequency Statistical map; Interaction group * eccentricity with electrodes as repetition using a 2 radius disk.

Panel a represents the power of evoked response; Panel b represents the phase of evoked response; Panel c represents the power of induced response; Panel d represents the phase of induced response.

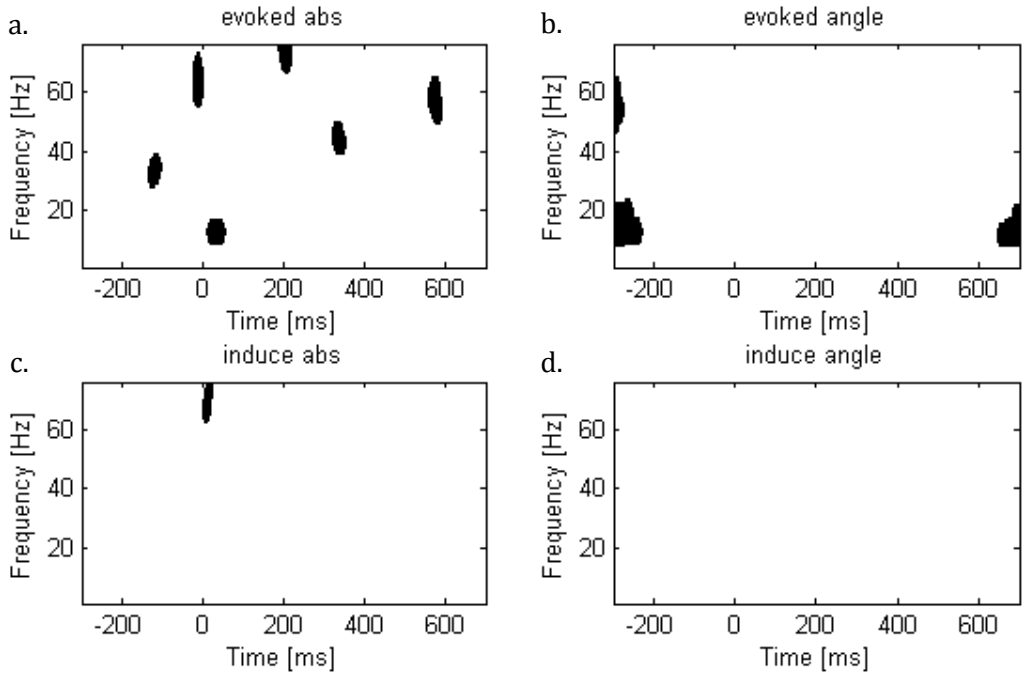

Figure 11 : Time-frequency Statistical map; Interaction group * eccentricity with electrodes as repetition using a 4 radius disk.

Panel a represents the power of evoked response; Panel b represents the phase of evoked response; Panel c represents the power of induced response; Panel d represents the phase of induced response**.**

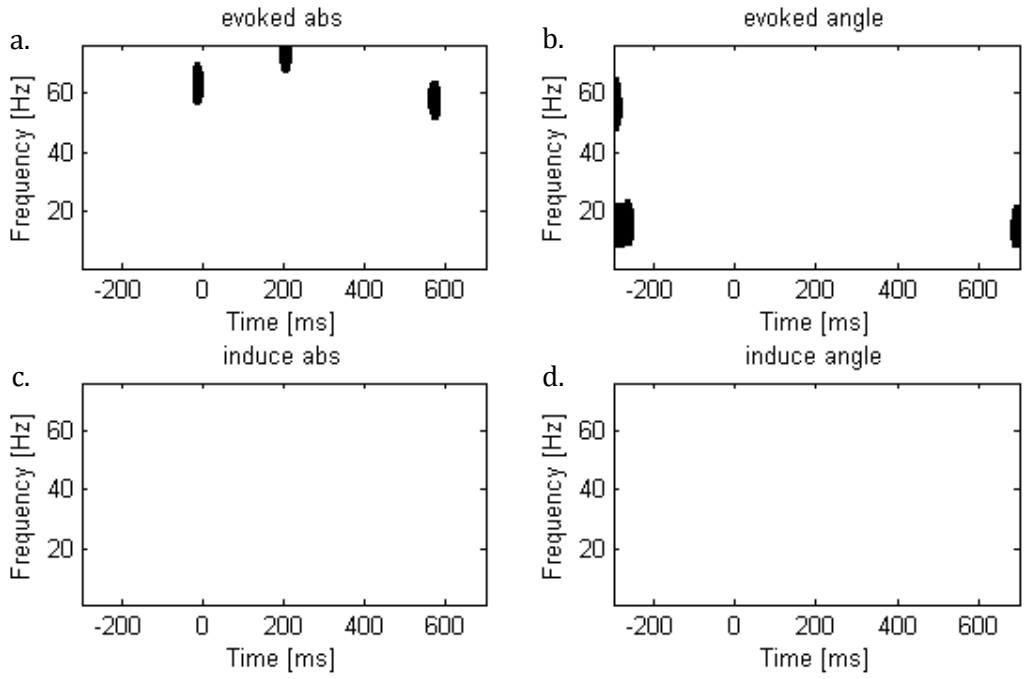

Figure 12 : Time-frequency Statistical map; Interaction group * eccentricity with electrodes as repetition using a 6 radius disk.
Panel a represents the power of evoked response; Panel b represents the phase of evoked response; Panel c represents the power of induced response; Panel d represents the phase of induced response.

2.4.2 Electrode as factor results

This section will present the results for the interaction electrodes * group * eccentricity condition. The statistical threshold was $p<0.05$. Additionally a mathematical morphology was applied to Figure 14, Figure 15, and Figure 16respectively with a 2, 4, and 6 radius disk. In Figure 13 no mathematical morphology was applied. Black color indicates significant differences and white color indicate no differences. A discussion of these results appears in Chapter 3. However, the reader should already note a difference between power (homogeneous) and phase (heterogeneous) information. Additionally, this difference shows the quality of the mathematical morphology methods to avoid false positive problems linked to statistical multiple testing. Finally, this section shows that electrodes as factor is less conservative compared to the previous section. Indeed, this analysis is congruent with other EEG methods (GFP, Topography) showed in section 6.2.

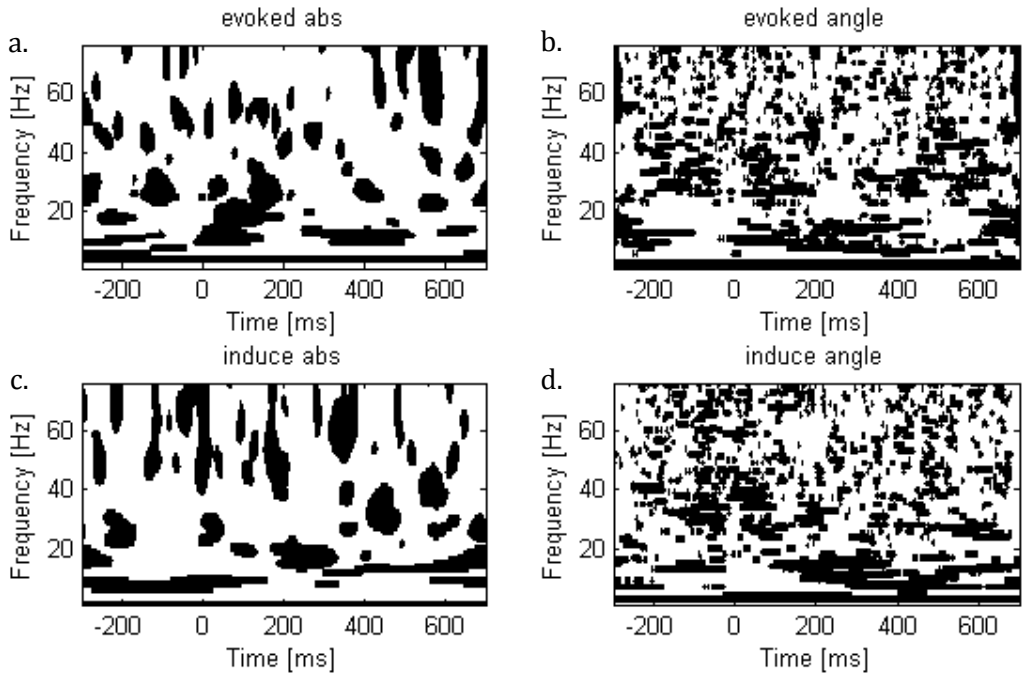

Figure 13 : Time-frequency Statistical map; Interaction electrodes * group * eccentricity and no mathematical morphology.
Panel a represents the power of evoked response; Panel b represents the phase of evoked response; Panel c represents the power of induced response; Panel d represents the phase of induced response.

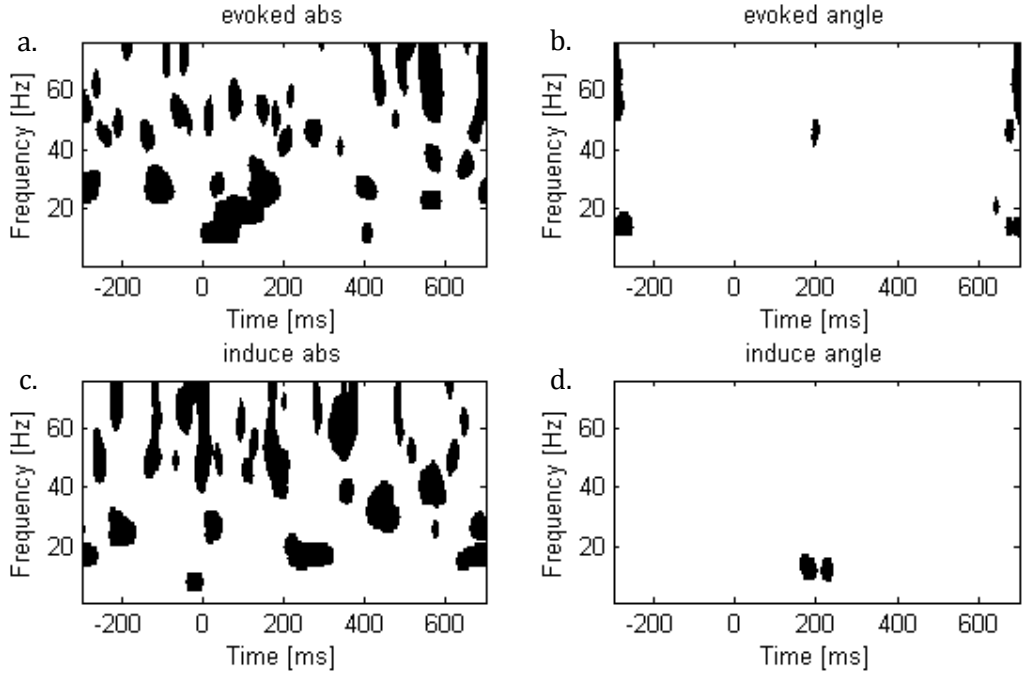

Figure 14 : Time-frequency Statistical map; Interaction electrodes * group * eccentricity using a 2 radius disk.
Panel a represents the power of evoked response; Panel b represents the phase of evoked response; Panel c represents the power of induced response; Panel d represents the phase of induced response.

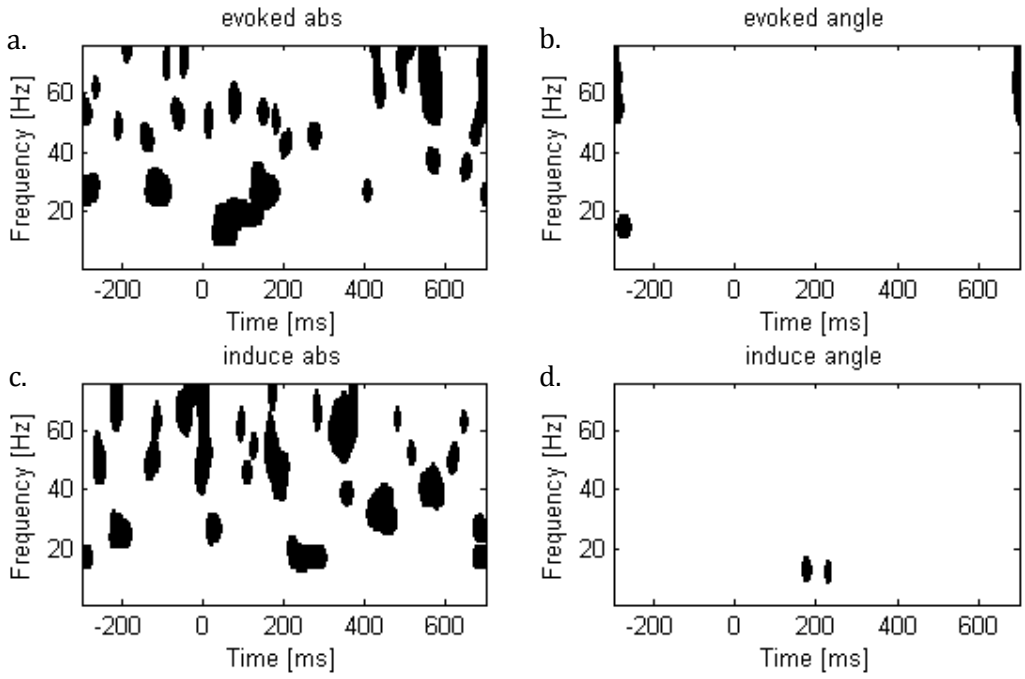

Figure 15 : Time-frequency Statistical map; Interaction electrodes * group * eccentricity using a 4 radius disk. Panel a represents the power of evoked response; Panel b represents the phase of evoked response; Panel c represents the power of induced response; Panel d represents the phase of induced response.

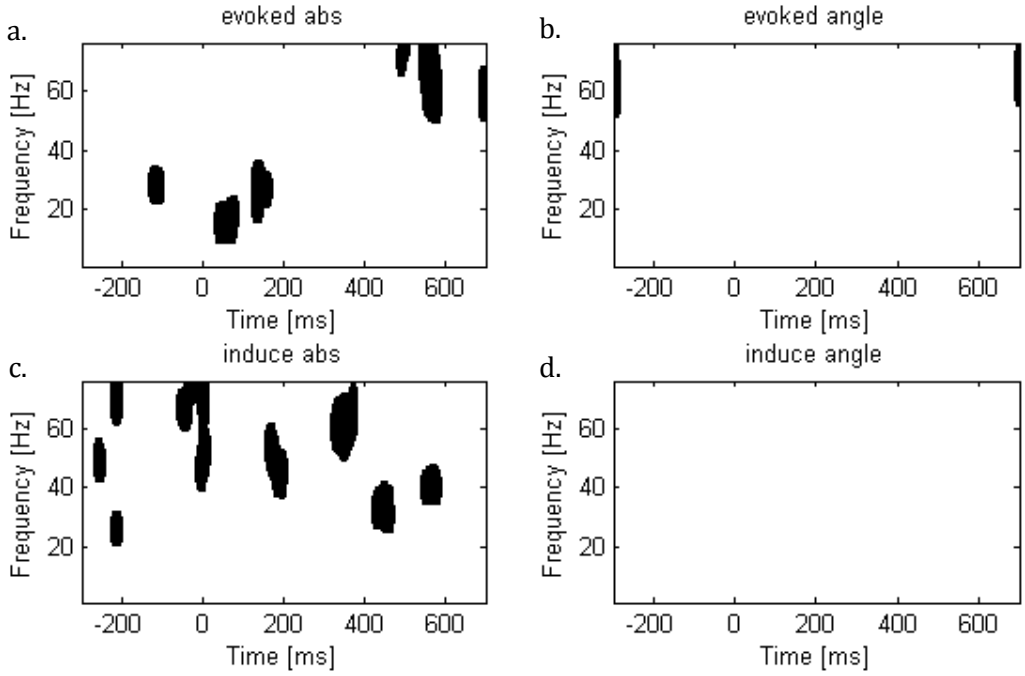

Figure 16 : Time-frequency Statistical map; Interaction electrodes * group * eccentricity using a 6 radius disk . Panel a represents the power of evoked response; Panel b represents the phase of evoked response; Panel c represents the power of induced response; Panel d represents the phase of induced response.

CHAPTER 3 DISCUSSION

The present findings in the articles in Chapter 6 and the method presented in section 1.4.4 will be discussed in this chapter. The first part presents a discussion on the time-frequency method and novelty for a reference-free statistical analysis. The second part presents a general discussion of the articles. The three scientific articles treat different topics as presented in the Introduction. The first article focused on methods for stimulus control (Section 6.1 : Generating Controlled Image Sets in Cognitive Neuroscience Research). The second article characterized visual dysfunction in schizophrenia (Section 6.2 : Impaired early visual response modulations to spatial information in chronic schizophrenia). The third article focused on mechanisms of illusory contour sensitivity in healthy control subjects (Section 6.3 : Towards a resolution of conflicting models of illusory contour processing in humans). The discussion will be divided between the stimulus treatment article (6.1) and the neurophysiologic articles (6.2; 6.3).

3.1 Time-frequency

This section is divided into two subsections. The first subsection will be a general comment on the results obtained in Section 2.4. This discussion will focus on the methods used. This will be specifically on the dataset information (evoked vs. induced frequencies), frequency information (absolute value vs. angle or phase), the statistical approach (electrodes as factor or repetition), and mathematical morphology correction. The second subsection will be on future developments in time-frequency analysis methods. This section will present a method to address the reference-dependence of typical such analyses. No subsection about the interpretation in terms of neurophysiologic aspects will be presented here. This choice based on my point of view, and I think that the only interpretation of such data should be descriptive (at present). In addition, the results in section 2.4 are reference-dependent. This limitation alone curtails the correct interpretation of the underlying neurophysiological process. This kind of method needs further investigation and should be presented in addition to the “classical” ones (ERP, GFP, Topography, etc.).

3.1.1 Methods

It is important to remember that the reference used was the average reference, which is an arbitrary choice. This section is built from general to specific comments on dataset information (evoked vs. induced frequencies), frequency information (absolute value vs. angle or phase), statistical approach (electrodes as factor or repetition), and mathematical morphology correction. The first remark concerns the figures in Section 2.4. These figures showed statistical

differences before stimulus onset. This difference could be a problem and may be removed by applying a baseline correction in the time-frequency space for each frequency. This correction followed the same idea applied to the time-amplitude space across electrodes.

The second remark concerns panel b and d of Figure 9 and Figure 13. These figures showed heterogeneity of the significant points in the phase/angle space. This heterogeneity means that no pattern could be distinguishable. This heterogeneity suggests that the phase information is not relevant for a neurophysiologic interpretation. The heterogeneity may come from the property of the electrical wave itself. Indeed, from the Maxwell equation the phase of an electrodynamics wave might be flip to 180° in the border between two media (Kind of refraction). This change is driven by the magnetic permeability (called ?r) of each medium. This flip presence cannot be predictable because it is dependent of the different media of each subject. This last consideration explains the heterogeneity across subject

In contrast, the absolute value (abs) or power is homogeneous. Figures without mathematical morphology (Figure 9(a, c)), Figure 13 (a, c)) suggest blobs of significant points. This reflects a strong correlation across frequency and time. In addition, the Maxwell equations stipulate that the oscillation of the electric and magnetic field of an electrodynamics wave is not modified by successive media. Only the wave length of propagation is altered.

The quality of the mathematical morphology methods applied for multiple statistical tests is showed by comparing the figures without (Figure 9 and Figure 13) and with (Figure 10 to Figure 12 and Figure 14 to Figure 16) corrections. A good method for the statistical multiple testing problems should remove the heterogeneity in one hand and should keep the original pattern in the other hand. In this sense the data in section 2.4 present two types of data. Some data (panel a.c) are homogeneous data (we can identify some pattern). The other (panel b,d) are heterogeneous (we cannot identify pattern). The treatment for panel b and d remove the heterogeneity. Note that a small criterion is enough (a disk with a radius of two that takes into account only the two neighbors in each direction). This methods applied in panels a and c showed conservation of big regions and removed small regions of significant points. This observation suggests that mathematical morphology keep the original important pattern. Another interesting pattern is shown on Figure 13 where we show a thin frequency band of significant points of all the time (bottom of each panel).The mathematical morphology removes this pattern because it is too thin in terms of frequency. These examples show the quality of this mathematical morphology criterion that it takes into account time and frequency simultaneously. This kind of criteria might also be applied in the source estimation across time, where the timing criterion is applied before the spatial criterion.

The different datasets (evoked and induced frequencies) exhibited in all statistical designs showed different patterns. This information suggests that these two datasets are informative for physiological interpretation. A careful study should be on both evoked and induced information.

In the following paragraphs deferent statistical approaches will be discussed. The statistical design with electrodes as repetition seems to be too restrictive. Indeed, a statistical difference on few electrodes may be suppressed by the rest of the electrodes that are not significant. This statistical design suggests that all electrodes recorded the same experiment. This kind of hypothesis appears too strong in this case (63 electrodes). This could be enough for a few electrodes. The advantage of this method was to increase the statistical power and reduce the sensitivity to noise.

By contrast, the other statistical approach with a statistical design with electrodes as factor seems to be more adaptive to these data. Indeed, in Figure 16 panel a, the power evoked response showed a statistical difference at the P1 latency. This statistical difference is compatible in latency to results in section 6.2 on the GFP, topographical and source estimation analyses for the same interaction effect term. Additionally, the evoked time-frequency response is the Stockwell transformation of the visual evoked potential. It is not surprising to find this difference and this could prove the quality of this approach. To validate definitively this approach it will be interesting to vary the reference electrode and to observe the dependency of this statistical difference across these different references.

The statistical approach presented above informs us about the importance of the topographical distribution of the time-frequency measure. Indeed, the approach using electrodes as factor maintains this information and is safer than the other.

3.1.2 Future Directions

This section presents a proposition for a statistical approach that is reference-free. For the moment this statistical test only compares 2 conditions, such as a t-test, but it takes into account the scalp distribution of the electrodes. Koenig and Pascual-Marqui (2009) showed that the relative distances in the complex plane of the electrodes are reference-free. In this figure Koenig and Pascual-Marqui (2009) also show that the reference is at the zero of the axes. This property means that two different conditions could be represented in the same space if and only of these two conditions are measured against the same reference. For example, we could choose a reference defined by the average across conditions, subjects and electrodes. This consideration is very important.

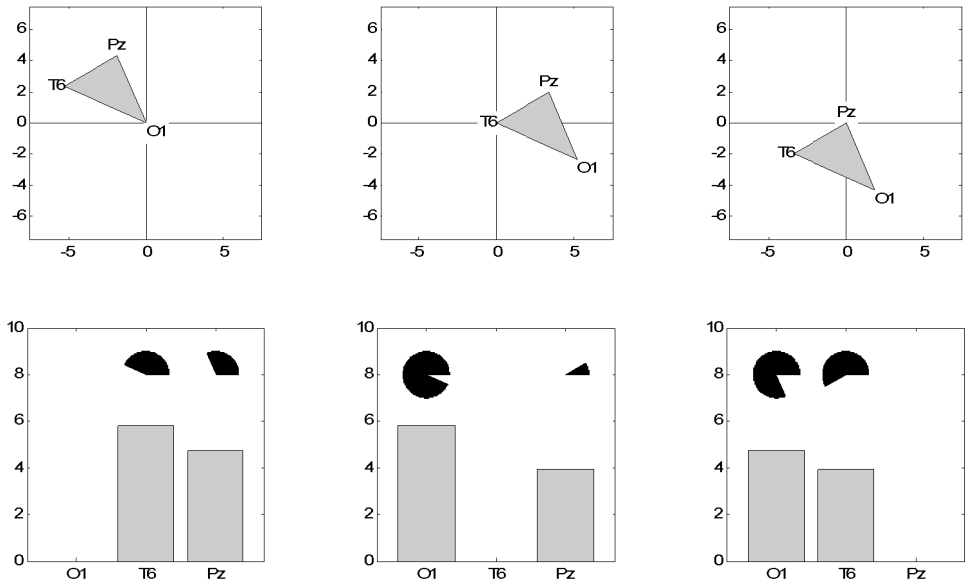

Figure 17 : Distance differences independent of the reference in complex space
Image from **Koenig and Pascual-Marqui (2009)** showed the invariance of references change of relative distance in the complex plan (panel a). Panel b showed the dependency of reference of phase and power information

.

Similar to time-amplitude topography analysis, a mathematical metric could be used to measure the distance between conditions. In the time-amplitude space this metric is called global dissimilarity (Lehmann and Skrandies, 1980). This global dissimilarity at a given point in time measures the mathematical distance between two maps. To compute the statistical information the dissimilarity metric between two average conditions were compared to the distribution of dissimilarities obtained on average condition created by permutation of subject condition (see Murray et al., 2008 for more details).

These two considerations lead me to create a metric such as dissimilarity for time-frequency information. Indeed, as in the dissimilarity methods for EEG potentials, we might calculate for each time and frequency a distance between two condition maps. This will be reference-free if the metric is calculated in the complex plane. The best-known metric in a two dimensional plan is the Euclidean distance (Euclide (323-285 B.C.), translated by Bernard Vitrac 1990). The metric could be the sum of the Euclidian distances across electrodes (Equation 3) .This metric could be named global Euclidean. To perform statistical analysis, a similar kind of permutation used for global dissimilarity (TANOVA) might be used on the global Euclidean distance.

$$\sum_{i=1}^{n}\sqrt{\left(r_{i,1}-r_{i,2}\right)^2+\left(c_{i,1}-c_{i,2}\right)^2}$$

$r_{i,1}$ = real part for electrodes i for condtion 1

$r_{i,2}$ = real part for electrodes i for condtion 2

$c_{i,1}$ = complex part for electrodes i for condtion 1

$c_{i,2}$ = complex part for electrodes i for condtion 2

n= number of elecrtordes

Equation 2: Definition of the global Euclidean metric

As the previous section demonstrates, the evoked and the induced information are important. The evoked complex plane is easily obtained by transforming ERP's with a time-frequency transformation. For the induced activity, it is a little bit more complex. To obtain the induced complex plane, we suggest performing power and phase of each epoch separately and to perform an average afterwards. This is the classical way to obtain an induced phase and power frequency information. At this step we can easily reconstruct the real and the complex part with this phase and power information. Equation 3 shows this kind of transformation.

$$a=\sqrt{\frac{r^2}{1+\left(\tan(\alpha)\right)^2}}$$

$$b=\sqrt{r^2-a^2}$$

$$\alpha\in[-\pi;\pi]$$

$$r\geq 0$$

where a = real part ; b= complex part
r = length (power) α=phase

if $\alpha<-\frac{\pi}{2}\Rightarrow a=-a$ and $b=-b$

else $-\frac{\pi}{2}<\alpha<0\Rightarrow b=-b$

else $\alpha>\frac{\pi}{2}\Rightarrow a=-a$

Equation 3: Transformation from polar complex number to real / complex representation.

Another method will be to compute the source estimation, after dealing with the time-frequency methods. This method is not currently practical because of the time of calculation.

Finally, other methods using time-frequency exist. One interesting method is the frequency tracking (Van Zaen et al., 2010). This method tracks a frequency and describes its temporal evolution, using and adaptive filter.

3.1.3 Methodological study

This article generated signal processing methods for controlling low-level visual features (luminance and spatial frequencies) of stimuli. The luminance treatment method appeared to be safe, because it changes the stimuli. That is, the new stimuli created are similar in luminance. The only limitation of this method is the saturation that may impact stimulus identification. This saturation is equivalent to an over-exposed photograph.

The second method focuses on controlling spatial frequency and identifies subsets of stimuli from among a larger initial set. The basic idea is to find two subsets of stimuli where the averages of the spatial frequencies are relatively close. This problem may lead to two subsets that exhibit an absolute grand distance together. To illustrate this, we took a set of 10 objects with arbitrary values from 1 to 10 (called group 1) and another set of 10 objects with arbitrary value from 90 to 100 (called group 2). The subsets are composed of three elements per group (3 in group 1 and 3 in group 2). The metric or distance is the difference between the averages of each subset group. With this configuration, the smallest distance is obtained with subset of value 8,9,10 (mean = 9) in group 1 and 90, 91, 92 (mean = 91) in group 2. The “absolute” distance between these subsets is big (91-9 = 82). This illustrates the limitation of this method given only the relative distance between two groups of stimuli. This method gives good results if sets of object are heterogeneous.

Figure 18, adapted from Toepel et al. (2009), used stimulus images treated in the article in section 6.1. Electrophysiological responses suggest sufficient treatment (luminance and spatial frequencies) to exclude low-level stimulus features as an explanation for the results from this experiment. As showed in section 1.1.2 low-level feature is differentiated in the primary visual cortex. In addition the section 1.4.3 showed in electrophysiology that the primary visual cortex is involved in the generation of the C1 component (Clark et al., 1995; Di Russo et al., 2003).The latency of the C1 component is around ~50-90 ms at occipital electrodes. As demonstrated in Figure 18, there were no differences at any level (waveform, GFP, topography) around the C1 latency. The C1 component may be useful for defining a period of interest where visual differences might be due to the activity of the primary visual cortex. The earliest differences appeared around ~160ms. Additionally, in Toepel et al. (2009) source estimations did not appear in the primary visual cortex. All of these considerations suggest enough similarity between the two sets of images in terms of low-level physical features.

This is not surprising because food pictures are heterogeneous in spatial frequencies. Additionally, it would be interesting to test with fMRI the difference in activity in V1 to these two subsets. This kind of experiment may promote further advances to the image treatment method developed here.

From a computational point of view, the algorithm may be improved by evolutionary algorithms. This kind of algorithm is inspired by natural evolution and expresses a better convergence to the optimal result. For example, a genetic algorithm will improve the time of calculation and converge to the optimal solution compared to a random algorithm.

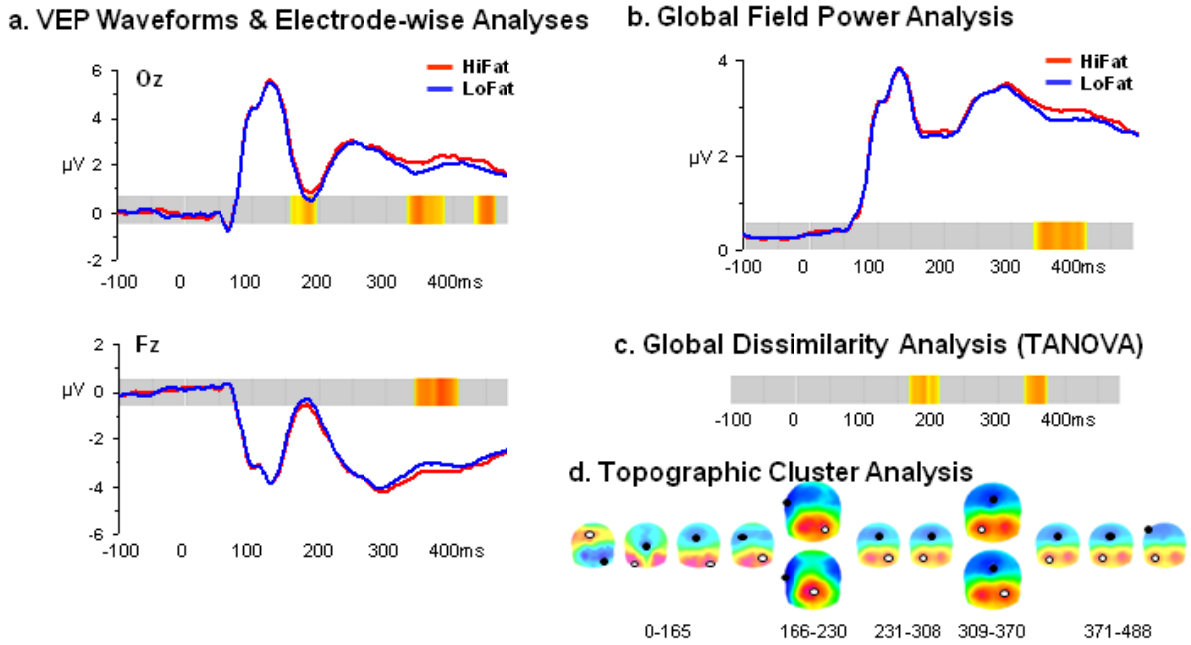

Figure 18: electrophysiological result Adapted from (Toepel et al., 2009b)
All panel does not show differences at C1 latency (~50 to 90ms)

3.2 Neurophysiologic studies

The neurophysiologic articles (6.2; 6.3) presented in this manuscript focused on early stages of visual processing. One compared control subjects to schizophrenic patients (6.2); the other is based only on healthy subjects (6.3). This difference leads us to treat this section in two ways. First, the conclusion of each article will be presented. Second, several ideas will be presented (coming from the articles) to more precisely investigate early visual processing.

3.2.1 Summary of general conclusions

The article presented in section 6.2 confirmed a dorsal stream deficit in schizophrenia using Kanizsa stimuli (Figure 2 and Figure 23). This deficit was exhibited by a functional impairment of the P1 component as a function of stimulus eccentricity and independent of the presence of illusory contours (in VEP waveforms, GFP waveforms, VEP topography, and source estimations). Variation in the stimulus eccentricity was performed with the localization of the inducers ("pacmen").

By contrast, there was no evidence for impaired processing of illusory contours, suggestive of intact ventral stream processes. As Foxe et al.(2005) demonstrated schizophrenic patients performed the illusory detection task like controls. Additionally in the same study, the N1 component that modulated according to illusory contour presence versus absence is preserved and is localized to regions of the lateral occipital complex (LOC).

The article presented in section 6.3 addressed the debate concerning the mechanism of illusory processing in the healthy brain. This article suggests that the illusory contour sensitivity previously observed in areas V1 and V2 in the macaque monkey is a top-down modulation from a high-level cortex (LOC). Indeed, we located the first VEP differentiation to the illusory contour presence vs. absence in the LOC (Figure 32) and a later in V1/V2 (Figure 33). This was also showed at waveform (Figure 30) and GFP (Figure 31) levels by comparison between timings of orientation and illusory presence vs. absence conditions differentiation. To obtain this result and to overcome salient regions present in the often-used Kanizsa stimuli, misaligned grating stimuli were used. Two properties of these grating stimuli were compared: their orientation (which involves early visual areas) and the presence or absence of an illusory contour.

3.2.2 General comments and Future Directions

The section will present comments suggested by the articles in section 6.2 and 6.3. This will be done in multiple subsections describing future directions or comment topics that may refer to one or both articles. The discussion of the articles themselves are presented in Sections 6.2.5, and 6.3.6

3.2.2.a Relation between illusory shapes and their eccentricity within the visual field

In both articles the illusory contours were composed of different geometrical shapes (squares, circles and diamonds). In the article about schizophrenia (6.2) the different shapes generated variation in the eccentricity of the inducers across the visual field (square vs. circle). Additionally, in the gratings article (6.3) the different shapes (diamond vs. circle) did not exhibit differences in terms of electrophysiological measures.

The absence of differences between shapes in the gratings article (6.3) suggests that differences observed in the schizophrenia article (6.2) were likely due to eccentricity and not due to the shape itself. Additionally, Murray et al.(2002) included more variation in the shapes and number of inducers used. They showed systematic differences between five different Kanizsa shapes as well as their control orientations (triangle, square, circle, star, and pentagon; cf. Table 1 in Murray et al. ,2002) as a function of inducer eccentricity and not as a function of other low-level features (e.g. number of inducers, support ratio, induced surface area, etc.).

There was no evidence that different shapes were treated differently in schizophrenic patients.

3.2.2.b Misaligned grating stimuli used for eccentricity condition

The article in section 6.2 did not exhibit an interaction between the illusion presence or absence condition and the eccentricity condition. The investigation of an interaction between illusion detection condition and eccentricity condition could highlight functional interactions between ventral and dorsal visual processing pathways. Another problem with the stimuli used in section 6.2 is different image size between stimuli. Indeed, the stimuli image size of Kanizsa type is defined by their inducers. The inducers exhibited the border of the image. This image size difference could be explaining the eccentricity differences.

To investigate more carefully this interaction, misaligned gratings could be used. With this kind of stimulus, the image size is equal for all stimuli and only the eccentricity shape (within image stimuli) may vary. Additionally, with these stimuli any variation in eccentricity is obtained only when the gratings are misaligned and therefore induce an illusory contour. This property could be used for investigating interactions between ventral and dorsal pathways. Finally, the physical information outside the illusory shape (grating bars go from one side to the other side of the screen) could be used for investigating the relationship between spatial detractors and the processing of illusory contours specifically.

An experiment with illusory misaligned gratings using different eccentricity generates some hypotheses in healthy control subjects.

In terms of interaction between ventral and dorsal pathways, the first hypothesis states that the eccentricity condition differences are exhibited at the P1 latency. This would predominantly involve the dorsal visual pathway such as was the case with the Kanizsa illusion types. This hypothesis suggests sensitivity to eccentricity prior to the detection of the illusory contour. Indeed, the illusory contour sensitivity peaks during the N1 component. This suggests a treatment of illusory presence in the dorsal pathways or an interaction between dorsal and ventral pathways. The second difference between these kinds of stimuli is the physical distracter

present in misaligned gratings. This first hypothesis above states that a physical distracter does not perturb early visual differentiation. This would likely involve an earlier treatment to extract only the relevant information.

The second hypothesis states that the differentiation of the eccentricity condition comes after the N1 component (i.e. the index of illusory contour sensitivity). This hypothesis states that the detection of the illusory is necessary for perceiving differences in stimulus eccentricity. This hypothesis suggests a later eccentricity differentiation. This consideration would show a role of the ventral visual pathway in eccentricity differentiation. This would in turn involve an interaction between ventral and dorsal pathways.

3.2.2.c Local spatial frequency in misaligned gratings

In the article 6.3 illusory stimuli were obtained by a misalignment of the gratings lines. This misalignment creates a local change in spatial frequency. In other term, this is the phase shift of the misaligned gratings lines. In this article this local spatial frequency was twice the spatial frequency of the grating itself (phase shift of π). This was performed by a misalignment of half of the distance between two lines (horizontal or vertical). Indeed, the gratings could be misaligned in a way to create different local spatial frequency. For example, one third (phase shift of $2/3\ \pi$) or two third (phase shift of $4/3\ \pi$) of the distance between two lines could be used.

The dependency of the local change of spatial frequency in the illusion perception could be interesting. Indeed, they could suggest an automatic process by comparing the behavioral and electrophysiological threshold to detection of illusion.

The psychophysical threshold could be used as condition for the electrophysiological studies. Indeed, it would be interesting to test the local spatial frequency around the behavioral threshold in EEG. This kind of experiment suggests two different hypotheses for the EEG response.

The first hypothesis states that conditions above and below behavioral threshold do not exhibit early visual differences. This suggests that the differentiation between presence and absence of the illusion is proceeding in high level treatment, opposite to low level treatment. This kind of result adding with results in article section 6.3 and other studies (e.g. Murray et al., 2002) suggest different areas in brain involved in illusion detection. These different areas would be depending on the difficulty to extract the illusory contour. Previous study from Murray et al. (2006) using “fat” and “thin” Kanizsa type did not show difference between correct and incorrect detection in ICs and NCs conditions. This study suggests that completion is independent of the accuracy of the subjects.

The second hypothesis state that conditions above and below behavioral threshold exhibits early visual differences. This suggests that the detection of illusion is an automatic process but the capacity to extract this information is not automatic. Additionally it will be interesting to compare conditions below behavioral threshold to non-illusion conditions. Using the condition below behavioral threshold as non illusory condition will permit to construct a design similar to the one in section 6.2 with an eccentricity condition in illusory and an eccentricity condition in non illusory stimuli. This kind of stimuli could be used for non illusory condition in Section 3.2.2.b.

3.2.2.d Task relative to eccentricity compare to illusory presence

In the article on schizophrenia (6.2), the task was performed in the presence or absence of illusion. This task was not related to the eccentricity condition where patients exhibit deficits. Additionally no differences were found at the behavioral level as shown in section 6.2.4.a . This is not surprising, because the illusion presence condition was preserved (see Foxe et al., 2005). It would be interesting to test a task related to the detection of eccentricity. This kind of question could inform about the relation between task attention and early visual deficit in schizophrenia. This could be performed on two illusory and non illusory square shapes at different eccentricity levels. This could be also performed on non-illusory shape or shape, but the task dependency on the illusory detection would be lost. The task will be to detect wide or narrow condition independently of the presence or absence of the illusion. This will involve a presentation of both squares before the experiment to define to the subject the wide and the narrow condition.

Behavioral and physiological responses using EEG in this task might help to better understand the early visual deficit in schizophrenia.

The first hypothesis states that a P1 deficit will be shown. This would suggest that there is no relationship between attention and early visual deficit in schizophrenia. This deficit will be exhibited independently of the task, and thus will not be related to attention. However deficit in P1 added to normal behavior suggests that illusory detection processing is involved in spatial task attention. This could highlight interaction between spatial attention and detection of illusion.

The second hypothesis states that no deficit in P1 will be found. This would suggest a relation between early visual deficit and attention. However a behavioral deficit added to the P1 deficit would suggest importance of P1 to perform this kind of task. No behavioral deficit added to the P1 deficit would suggest a later treatment of eccentricity for schizophrenic patients. The later treatment hypothesis was shown in section 6.2 where eccentricity differences after P1 were preserved in the schizophrenic patient group. In addition to the second hypothesis it would be

interesting to show the N1 component. The N1 component as Foxe et al. (2005) showed is preserved. The eccentricity task may provide two different N1 process. The first process, the N1 is preserved. This would be performed within and without specific attention. The second process would be an impairment of the N1 component. This suggests in addition with consideration above that there is a relationship between attention and dorsal and ventral pathways. They also suggest that attention play a critical role in early preservation in schizophrenic patients. This kind of information would involve studies on early visual deficit should be passive to avoid the attention.

3.2.2.e Sensitivity deficit or global deficit in schizophrenia dorsal pathway

The Article on schizophrenic patients (6.2) showed impairment in the eccentricity condition for two different conditions (wide vs. narrow). This suggested a deficit in the dorsal visual pathway. This kind of experiment did not explain if the deficit in the dorsal visual pathway is a sensitivity deficit or a global deficit.

To address this issue it would be interesting to test schizophrenic patients with linear increment of eccentricity stimuli. This kind of experiment will not use ICs stimuli, NCs stimuli is enough. This will be performed only in central visual field to avoid well know differences between central and peripheral vision. Results of an experiment with these stimuli in schizophrenic patients might show two different results.

The first result could show no differences across all eccentricity levels at P1 latency compared to control subjects which exhibit differences at a certain eccentricity level. This would suggest a general impairment of the schizophrenic patients in dorsal visual pathway

The second result could show differences between at least two eccentricities at P1 latency. This would suggest a partial deficit in the dorsal visual pathway. This impairment may be due to the sensitivity deficit in the dorsal visual pathway.

The information would be important to a better understanding of this early deficit. A sensitivity deficit is very different to a global deficit. A sensitivity deficit may suggest that patient could perform P1 modulation as control for example with medication. Contrariwise a global deficit is deeper and it might not be treated. In another way, a sensitivity deficit might reflect a functional deficit opposite to an anatomical deficit that might reflect a global deficit. Finally a study from van der Stelt et al. (2004) did not report P1 deficit. This finding would suggest a sensitivity deficit.

3.2.2.f Stimuli bias to parvocellular/magnocellular pathway neurophysiology implication

The article on the P1 deficit in schizophrenia (6.2) demonstrated a deficit in the visual dorsal pathway. Additionally, previous studies (Butler and Javitt, 2005) generalized this impairment to a magnocellular pathway deficit. It would be interesting to investigate this impairment further, to understand more precisely where the deficit starts. More precisely, it would be interesting to investigate if this deficit appears in magnocellular/parvocellular pathways or dorsal/ventral pathways.

To further investigate this processing, stimulus biased to the parvocellular or magnocellular pathway would be a good way. A stimulus bias toward the parvocellular pathway could be a colored stimulus. For example, we could use Kanizsa stimuli presented in the schizophrenia article with colored inducers and a colored background. Additional control of the stimuli must be performed in order to create the colored inducer and the colored background with iso-luminance. Iso-lumiance means that both colors (inducer and background) exhibit the same gray scale level. This ensures that inducer and background cannot be differentiated by their contrast but only by their color information. A stimulus bias towards the magnocellular pathway could be a low contrast stimulus in the gray scale level. As in paragraph above, Kanizsa type stimuli could be used.

These stimuli would show the role of parvocellular and magnocellular pathway in the visual dorsal and ventral pathway. To address this we could replicate the experiment of the article in section 6.2 with the stimuli described above. An experiment using colored stimuli will involve the parvocellular pathway, as explained in the section 1.1.1. Additionally the colored Kanizsa of section 6.2 would activate the dorsal pathway in the eccentricity condition and the ventral pathway in the illusion condition. Differentiation of eccentricity or illusion would exhibit a relation of the parvocellular pathway to visual dorsal/ventral pathways. Opposite, Kanizsa stimuli with low contrast (which activate the magnocellular pathway) would exhibit a relation between the Magnocellular pathway and the visual dorsal/ventral pathways.

Many neurophysiological hypotheses are related to these stimuli .The next paragraph will be divided into two parts. First the hypothesis will be related in healthy control group. Second, this hypothesis will be related to schizophrenic patients group

There are three different hypotheses for the healthy controls group. The first hypothesis states that the eccentricity condition shows differences for both stimuli presented above (similar to the article in section 6.2). This would mean independency of the dorsal pathway to the parvocellular

and magnocellular pathways. The second hypothesis state that the eccentricity condition shows differences for one of the two stimuli above and no eccentricity condition difference for the other. This would mean a dorsal visual pathway dependency for one of the parvocellular or magnocellular pathways depending on the stimulus what will not exhibit the difference. The Third hypothesis states that the will be no eccentricity condition differences. This would mean a dependency of the dorsal visual pathway to parvocellular and magnocellular pathways. These considerations can be extrapolated in the illusion presence condition and the ventral visual pathway.

In this paragraph the three healthy controls hypotheses will be related to schizophrenic patients. This relation between patients and controls should go in two directions. The first direction is that patients could exhibit the same differences like controls for the hypotheses above. This could reveal that there is no impairment. The second direction is that patients do not exhibit differences where controls exhibit them. This will reveal impairment. The second direction will be the most probable direction. The next paragraphs will discuss the implication of these two types of stimuli above (colored and low--contrasted) for schizophrenic patients and healthy controls.

This paragraph will list all the different possibilities of colored stimuli for the eccentricity condition. The choice of the eccentricity condition is guided by previous results (see article in section 6.2). There are three different hypotheses between controls and schizophrenic patients. The first hypothesis states that controls and schizophrenic patients will exhibit no differences in the eccentricity condition. This could suggest that the parvocellular pathway alone is not sufficient to exhibit dorsal visual pathway differences to eccentricity. This suggests no interaction between parvocellular pathway and dorsal visual pathway. The second hypothesis states that controls and patients will differentiate similarly the eccentricity condition. This could mean that the parvocellular pathway is sufficient to exhibit dorsal visual difference for the eccentricity condition. This suggests interaction between parvocellular pathway and dorsal visual pathway. Additionally, this hypothesis could demonstrate a magnocellular pathway deficit and a preserved parvocellular pathway in schizophrenic patients. Indeed, schizophrenic patients exhibit normal response (i.e. same differences for patients than controls) without magnocellular activity. This would reflect a dominance of magnocellular pathway to the dorsal visual pathway. Indeed, article in section 6.2 showed a deficit with stimuli without parvocellular or magnocellular bias. The third hypothesis states that controls will exhibit differences, while patient will not. This could suggest that the parvocellular pathway is sufficient to exhibit dorsal visual pathway differences in control. Additionally, this third hypothesis suggests an impairment in dorsal visual pathway without magnocellular pathway activity. This impairment could be in

the dorsal visual pathway or an interaction deficit between parvocellular pathway and dorsal visual pathway. By analogy, the same kind of hypothesis may be applied to the colored stimuli in the presence/absence illusion condition.

The hypotheses showed in previous paragraphs for the eccentricity condition and the illusion condition should be combined in order to obtain better understanding interaction between the parvocellular pathway and dorsal/ventral pathway and early visual deficits in the schizophrenic patients.

This paragraph will list all the different possibilities for low-contrast stimuli for the eccentricity condition. Similar to the paragraph above, three different hypotheses will be put forth. The first hypothesis states that controls and schizophrenic patients exhibit no differences. This could mean that magnocellular pathway alone is not sufficient to exhibit dorsal visual pathway differences to eccentricity. This suggests an interaction between parvocellular pathway and dorsal visual pathway. The second hypothesis states that controls and patients will differentiate similarly the eccentricity condition. This could suggest that the magnocellular pathway is sufficient to exhibit dorsal visual differences in the eccentricity condition. Additionally, this hypothesis would demonstrate no deficit in the magnocellular pathway (i.e. no deficit between retina and primary visual cortex) because patients exhibit normal response (i.e. same differences for patients than controls) within stimuli bias to magnocellular pathway. This possible absence of deficit for schizophrenic patients in the magnocellular pathway added with the article in section 6.2 would suggest that the P1 deficit is related to the parvocellular pathway interaction to the dorsal pathway or appear in the dorsal visual pathway itself. The third hypothesis states that controls will exhibit differences, while patient will not. This could mean that the magnocellular pathway is sufficient to exhibit dorsal visual pathway differences for controls. Additionally, this third hypothesis suggests an impairment in the magnocellular pathway and perhaps no impairment in the dorsal visual pathway. By analogy the same kind of hypothesis may be applied to the low-contrast stimuli in the presence/absence of illusion condition. The hypothesis for eccentricity condition and illusion condition should by combine to obtain better understanding of the interaction of the magnocellular pathway to the dorsal/ventral pathways and the early visual deficit in the schizophrenic patients.

Finally a combination of these two experiments, will investigate: the link between parvocellular/magnocellular pathways and Dorsal/Ventral visual pathways, the interaction between parvocellular pathway and magnocellular pathway. Additionally, this could clarify the early visual deficit in schizophrenia. Indeed, these kinds of studies might highlight to which

pathway(s) is impaired and especially if the P1 deficit is due to the dorsal pathway alone, the magnocellular pathway alone or both.

3.2.2.g Relation of P1 deficit and high level

It would be interesting to find a relation between the P1 deficit and the cognitive deficit (e.g. working memory, attention, etc.). To address this problematic, we could use other physiological methods; Trans Magnetic Stimulation (TMS) would be relevant. Indeed, single pulses or repetitive pulses might be applied on the dorsal pathway, in addition a complex cognitive task such as working memory task, selective attention task, etc could be tested. For example, the TMS single pulse would be applied at different timing to the dorsal pathway during a cognitive task. The dependency of the task performance (reaction time, accuracy, etc) to the timing of the TMS pulse should be measured. This dependency would exhibit the relation between dorsal pathway and cognitive task by given the timing of the dependency. In term of schizophrenia this kind of experiment could link early visual deficit to cognitive deficit depending of the timing of TMS of the dependency. The choice of single pulses or repetitive pluses will be defined by the complexity of the cognitive task and some technical procedures.

CHAPTER 4 **CONCLUSION**

A major issue in research on schizophrenia will be to define a biomarker. A biomarker is an objective measure to evaluate a pathological process. This will be helpful for diagnosis and early detection of schizophrenia. In the one hand, as we showed in section 1.3.1, the diagnosis is only based on observation and subjective perception of the clinician. In this context a biomarker could help to diagnosis by given a objective measure to diagnosis. In the other hand, schizophrenia as well as all diseases an early detection provides a better chance for helping the patients. In this case the biomarker because it is objective could be a signal to detect the disorder.

Addressing this early perceptual deficit could be a good biomarker. Indeed, early processes are automatic due to the timing of this effect. This automatism is the major point, because it is uncontrollable and more stable across subjects.

In this field early visual deficits may play a critical role. Indeed, the P1 deficit would be a schizophrenia biomarker. A recent study from Yeap et al. (2006) demonstrated a reduction of the P1 between clinically unaffected first-degree relatives of patients with schizophrenia patients with schizophrenia and controls. This confirmed the efficacy of using the P1 as an endophenotype.

To go further, the experiments described above could give additional details on P1 deficit in schizophrenic patients. For example section 3.2.2.f could show interaction between the magnocellular/parvocellular pathway and the dorsal/ventral pathway or precise the early visual deficit in schizophrenic patients. These details adding to investigation in different schizophrenic patient groups and control groups may be conducted to a robust biomarker. These groups should be first episodic patients, chronic patients, first relatives of schizophrenia patients, and non-psychiatric controls. In addition to these groups, subgroups based on specific schizophrenia disorder (e.g. schizoaffective) could be interesting. The most interesting population will be homozygote twins where one exhibits schizophrenia disorder and the other does not. This kind of population is very difficult to find, but it may provide very interesting information.

Finally as Yeap et al. (2009) suggested it would also be interesting to investigate other psychiatric diseases like bipolar disorder. This study opens the question of the classification of psychiatric disorders. A large longitudinal study including different psychiatric disorders, risk population of teenagers (genetic, suspicion of disorder), new pharmacological treatment using

P1 as a biomarker could establish the real effect of the P1 as biomarker. Seen as this kind of study is very long, it is important to be sure that the P1 is really a good biomarker.

CHAPTER 5 REFERENCES

Allison, T., Puce, A., Spencer, D.D., McCarthy, G., 1999. Electrophysiological studies of human face perception. I: Potentials generated in occipitotemporal cortex by face and non-face stimuli. Cereb. Cortex 9, 415-430.

Baddeley, A., 1992. Working memory. Science 255, 556-559.

Bentin, S., Mouchetant-Rostaing, Y., Giard, M.H., Echallier, J.F., Pernier, J., 1999. ERP manifestations of processing printed words at different psycholinguistic levels: time course and scalp distribution. J Cogn Neurosci 11, 235-260.

Brighina, F., Ricci, R., Piazza, A., Scalia, S., Giglia, G., Fierro, B., 2003. Illusory contours and specific regions of human extrastriate cortex: evidence from rTMS. Eur. J. Neurosci 17, 2469-2474.

Butler, P.D., Javitt, D.C., 2005. Early-stage visual processing deficits in schizophrenia. Curr Opin Psychiatry 18, 151-157.

Clark, V., Fan, S., Hillyard, S., 1995. Identification of early visual evoked potential generators by retinotopic and topographic analyses. Human Brain Mapping 2, 170-187.

Dacey, D.M., Petersen, M.R., 1992. Dendritic field size and morphology of midget and parasol ganglion cells of the human retina. Proc. Natl. Acad. Sci. U.S.A 89, 9666-9670.

De Santis, L., Clarke, S., Murray, M.M., 2007. Automatic and intrinsic auditory "what" and "where" processing in humans revealed by electrical neuroimaging. Cereb. Cortex 17, 9-17.

Desmedt, J.E., Tomberg, C., Noël, P., Ozaki, I., 1990. Beware of the average reference in brain mapping. Electroencephalogr Clin Neurophysiol Suppl 41, 22-27.

Di Russo, F., Martínez, A., Hillyard, S.A., 2003. Source analysis of event-related cortical activity during visuo-spatial attention. Cereb. Cortex 13, 486-499.

Doniger, G.M., Foxe, J.J., Murray, M.M., Higgins, B.A., Snodgrass, J.G., Schroeder, C.E., Javitt, D.C., 2000. Activation timecourse of ventral visual stream object-recognition areas: high density electrical mapping of perceptual closure processes. J Cogn Neurosci 12, 615-621.

Doniger, G.M., Foxe, J.J., Schroeder, C.E., Murray, M.M., Higgins, B.A., Javitt, D.C., 2001. Visual perceptual learning in human object recognition areas: a repetition priming study using high-density electrical mapping. Neuroimage 13, 305-313.

Doniger, G.M., Foxe, J.J., Murray, M.M., Higgins, B.A., Javitt, D.C., 2002. Impaired Visual Object Recognition and Dorsal/Ventral Stream Interaction in Schizophrenia. Arch Gen Psychiatry 59, 1011-1020.

Egeland, J., Rund, B.R., Sundet, K., Landrø, N.I., Asbjørnsen, A., Lund, A., Roness, A., Stordal, K.I., Hugdahl, K., 2003. Attention profile in schizophrenia compared with

depression: differential effects of processing speed, selective attention and vigilance. Acta Psychiatr Scand 108, 276-284.

Euclide (0323-0285 av. J. -C.), 1990. Les éléments. 1, Livres I-IV / Euclide d'Alexandrietrad. du texte de Heiberg : géométrie plane / trad. et commentaires par Bernard Vitrac ; introd. générale par Maurice Caveing

Felleman, D.J., Van Essen, D.C., 1991. Distributed hierarchical processing in the primate cerebral cortex. Cereb. Cortex 1, 1-47.

Ffytche, D.H., Zeki, S., 1996. Brain activity related to the perception of illusory contours. Neuroimage 3, 104-108.

Foxe, J.J., Doniger, G.M., Javitt, D.C., 2001. Early visual processing deficits in schizophrenia: impaired P1 generation revealed by high-density electrical mapping. Neuroreport 12, 3815-3820.

Foxe, J.J., Strugstad, E.C., Sehatpour, P., Molholm, S., Pasieka, W., Schroeder, C.E., McCourt, M.E., 2008. Parvocellular and magnocellular contributions to the initial generators of the visual evoked potential: high-density electrical mapping of the "C1" component. Brain Topogr 21, 11-21.

Foxe, J.J., Murray, M.M., Javitt, D.C., 2005. Filling-in in Schizophrenia: a High-density Electrical Mapping and Source-analysis Investigation of Illusory Contour Processing. Cereb. Cortex 15, 1914-1927.

Gonzalez Andino, S.L., Michel, C.M., Thut, G., Landis, T., Grave de Peralta, R., 2005. Prediction of response speed by anticipatory high-frequency (gamma band) oscillations in the human brain. Hum Brain Mapp 24, 50-58.

Gonzalez Andino, S.L., Murray, M.M., Foxe, J.J., de Peralta Menendez, R.G., 2005. How single-trial electrical neuroimaging contributes to multisensory research. Exp Brain Res 166, 298-304.

Grave de Peralta Menendez, R., Gonzalez Andino, S., Lantz, G., Michel, C.M., Landis, T., 2001. Noninvasive localization of electromagnetic epileptic activity. I. Method descriptions and simulations. Brain Topogr 14, 131-137.

Grave de Peralta Menendez, R., Murray, M.M., Michel, C.M., Martuzzi, R., Gonzalez Andino, S.L., 2004. Electrical neuroimaging based on biophysical constraints. Neuroimage 21, 527-539.

Grill-Spector, K., Kourtzi, Z., Kanwisher, N., 2001. The lateral occipital complex and its role in object recognition. Vision Res 41, 1409-1422.

Grose-Fifer, J., Zemon, V., Gordon, J., 1994. Temporal tuning and the development of lateral interactions in the human visual system. Invest. Ophthalmol. Vis. Sci 35, 2999-3010.

Halgren, E., Mendola, J., Chong, C.D.R., Dale, A.M., 2003. Cortical activation to illusory shapes as measured with magnetoencephalography. Neuroimage 18, 1001-1009.

Hartman, M., Steketee, M.C., Silva, S., Lanning, K., Andersson, C., 2003. Wisconsin Card

Sorting Test performance in schizophrenia: the role of working memory. Schizophr. Res 63, 201-217.

von der Heydt, R., Peterhans, E., 1989. Mechanisms of contour perception in monkey visual cortex. I. Lines of pattern discontinuity. J. Neurosci 9, 1731-1748.

Hofer, A., Weiss, E.M., Golaszewski, S.M., Siedentopf, C.M., Brinkhoff, C., Kremser, C., Felber, S., Fleischhacker, W.W., 2003. An FMRI study of episodic encoding and recognition of words in patients with schizophrenia in remission. Am J Psychiatry 160, 911-918.

Hubel, D.H., Wiesel, T.N., 1977. Ferrier lecture. Functional architecture of macaque monkey visual cortex. Proc. R. Soc. Lond., B, Biol. Sci 198, 1-59.

Hutton, S.B., Puri, B.K., Duncan, L.J., Robbins, T.W., Barnes, T.R., Joyce, E.M., 1998. Executive function in first-episode schizophrenia. Psychol Med 28, 463-473.

Jaeger, J., Czobor, P., Berns, S.M., 2003. Basic neuropsychological dimensions in schizophrenia. Schizophr. Res 65, 105-116.

Jeffreys, D.A., Axford, J.G., 1972. Source locations of pattern-specific components of human visual evoked potentials. II. Component of extrastriate cortical origin. Exp Brain Res 16, 22-40.

Jindra, L.F., Zemon, V., 1989. Contrast sensitivity testing: a more complete assessment of vision. J Cataract Refract Surg 15, 141-148.

Kanizsa, G., 1976. Subjective contours. Sci. Am 234, 48-52.

Kaplan, E., 1991. The receptive field structure of retinal ganglion celles in cat and monkey, in: Vision and visual dysfunction. leventhal AG, pp. 10-40.

Kenny, J.T., Meltzer, H.Y., 1991. Attention and higher cortical functions in schizophrenia. J Neuropsychiatry Clin Neurosci 3, 269-275.

Kim, D., Zemon, V., Saperstein, A., Butler, P.D., Javitt, D.C., 2005. Dysfunction of early-stage visual processing in schizophrenia: harmonic analysis. Schizophr. Res 76, 55-65.

Koenig, T., Pascual-Marqui, R.D., 2009. Multichannel frequency and time-frequency analysis, in: Electrical Neuroimaging. Cambridge University press, pp. 145-168

Lehman, D., 1987. Principles of spatial analysis, in: Methods of analysis of brain electrical and magnetic signals, Handbook of electroencephalography and clinical neurophysiology. Gevins AS, Remond A, pp. 309-354.

Lehmann, D., Skrandies, W., 1980. Reference-free identification of components of checkerboard-evoked multichannel potential fields. Electroencephalogr Clin Neurophysiol 48, 609-621.

Liu, S.K., Chiu, C., Chang, C., Hwang, T., Hwu, H., Chen, W.J., 2002. Deficits in sustained attention in schizophrenia and affective disorders: stable versus state-dependent markers. Am J Psychiatry 159, 975-982.

Malach, R., Reppas, J.B., Benson, R.R., Kwong, K.K., Jiang, H., Kennedy, W.A., Ledden, P.J., Brady, T.J., Rosen, B.R., Tootell, R.B., 1995. Object-related activity revealed by functional magnetic resonance imaging in human occipital cortex. Proc. Natl. Acad. Sci. U.S.A 92, 8135-8139.

Mangun, G.R., Hillyard, S.A., 1991. Modulations of sensory-evoked brain potentials indicate changes in perceptual processing during visual-spatial priming. J Exp Psychol Hum Percept Perform 17, 1057-1074.

Martuzzi, R., Murray, M.M., Meuli, R.A., Thiran, J., Maeder, P.P., Michel, C.M., Grave de Peralta Menendez, R., Gonzalez Andino, S.L., 2009. Methods for determining frequency- and region-dependent relationships between estimated LFPs and BOLD responses in humans. J. Neurophysiol 101, 491-502.

McGurk, S.R., Mueser, K.T., 2003. Cognitive functioning and employment in severe mental illness. J. Nerv. Ment. Dis 191, 789-798.

McKeefry, D.J., Russell, M.H., Murray, I.J., Kulikowski, J.J., 1996. Amplitude and phase variations of harmonic components in human achromatic and chromatic visual evoked potentials. Vis. Neurosci 13, 639-653.

Mendola, J.D., Dale, A.M., Fischl, B., Liu, A.K., Tootell, R.B., 1999. The representation of illusory and real contours in human cortical visual areas revealed by functional magnetic resonance imaging. J. Neurosci 19, 8560-8572.

Merigan, W.H., Maunsell, J.H., 1993. How parallel are the primate visual pathways? Annu. Rev. Neurosci 16, 369-402.

Michel, C.M., Murray, M.M., Lantz, G., Gonzalez, S., Spinelli, L., Grave de Peralta, R., 2004. EEG source imaging. Clin Neurophysiol 115, 2195-2222.

Michel, C.M., Seeck, M., Landis, T., 1999. Spatiotemporal Dynamics of Human Cognition. News Physiol. Sci 14, 206-214.

Michie, P.T., 2001. What has MMN revealed about the auditory system in schizophrenia? Int J Psychophysiol 42, 177-194.

Mohamed, S., Paulsen, J.S., O'Leary, D., Arndt, S., Andreasen, N., 1999. Generalized cognitive deficits in schizophrenia: a study of first-episode patients. Arch. Gen. Psychiatry 56, 749-754.

Murray, I., MacCana, F., Kulikowski, J.J., 1983. Contribution of two movement detecting mechanisms to central and peripheral vision. Vision Res 23, 151-159.

Murray, M.M., Brunet, D., Michel, C.M., 2008a. Topographic ERP analyses: a step-by-step tutorial review. Brain Topogr 20, 249-264.

Murray, M.M., Brunet, D., Michel, C.M., 2008b. Topographic ERP analyses: a step-by-step tutorial review. Brain Topogr 20, 249-264.

Murray, M.M., Foxe, D.M., Javitt, D.C., Foxe, J.J., 2004. Setting boundaries: brain dynamics of modal and amodal illusory shape completion in humans. J. Neurosci 24, 6898-6903.

Murray, M.M., Imber, M.L., Javitt, D.C., Foxe, J.J., 2006a. Boundary completion is automatic and dissociable from shape discrimination. J. Neurosci 26, 12043-12054.

Murray, M.M., Imber, M.L., Javitt, D.C., Foxe, J.J., 2006b. Boundary completion is automatic and dissociable from shape discrimination. J. Neurosci 26, 12043-12054.

Murray, M.M., Wylie, G.R., Higgins, B.A., Javitt, D.C., Schroeder, C.E., Foxe, J.J., 2002. The spatiotemporal dynamics of illusory contour processing: combined high-density electrical mapping, source analysis, and functional magnetic resonance imaging. J. Neurosci 22, 5055-5073.

Näätänen, R., Kähkönen, S., 2009. Central auditory dysfunction in schizophrenia as revealed by the mismatch negativity (MMN) and its magnetic equivalent MMNm: a review. Int. J. Neuropsychopharmacol 12, 125-135.

Norman, J., 2002. Two visual systems and two theories of perception: An attempt to reconcile the constructivist and ecological approaches. Behav Brain Sci 25, 73-96; discussion 96-144.

Oltmanns, T.F., Ohayon, J., Neale, J.M., 1978. The effect of anti-psychotic medication and diagnostic criteria on distractibility in schizophrenia. J Psychiatr Res 14, 81-91.

Pascual-Marqui, R.D., Lehmann, D., 1993. Comparison of topographic maps and the reference electrode: comments on two papers by Desmedt and collaborators. Electroencephalogr Clin Neurophysiol 88, 530-531, 534-536.

Pegna, A.J., Khateb, A., Murray, M.M., Landis, T., Michel, C.M., 2002. Neural processing of illusory and real contours revealed by high-density ERP mapping. Neuroreport 13, 965-968.

Perrin, F., Bertrand, O., Pernier, J., 1987. Scalp current density mapping: value and estimation from potential data. IEEE Trans Biomed Eng 34, 283-288.

Peterhans, E., von der Heydt, R., 1989. Mechanisms of contour perception in monkey visual cortex. II. Contours bridging gaps. J. Neurosci 9, 1749-1763.

Ramsden, B.M., Hung, C.P., Roe, A.W., 2001. Real and illusory contour processing in area V1 of the primate: a cortical balancing act. Cereb. Cortex 11, 648-665.

Romani, A., Callieco, R., Tavazzi, E., Cosi, V., 2003. The effects of collinearity and orientation on texture visual evoked potentials. Clin Neurophysiol 114, 1021-1026.

Sáry, G., Chadaide, Z., Tompa, T., Köteles, K., Kovács, G., Benedek, G., 2007. Illusory shape representation in the monkey inferior temporal cortex. Eur. J. Neurosci 25, 2558-2564.

Sáry, G., Köteles, K., Kaposvári, P., Lenti, L., Csifcsák, G., Frankó, E., Benedek, G., Tompa, T., 2008. The representation of Kanizsa illusory contours in the monkey inferior temporal cortex. Eur. J. Neurosci 28, 2137-2146.

Schroeder, C.E., Mehta, A.D., Givre, S.J., 1998. A spatiotemporal profile of visual system

activation revealed by current source density analysis in the awake macaque. Cereb. Cortex 8, 575-592.

Serra, J.P., 1982. Image analysis and mathematical morphology. Academic Press.

Simpson, G.V., Foxe, J.J., Vaughan, H.G., Mehta, A.D., Schroeder, C.E., 1995. Integration of electrophysiological source analyses, MRI and animal models in the study of visual processing and attention. Electroencephalogr Clin Neurophysiol Suppl 44, 76-92.

Sohlberg, M.M., Mateer, C.A., 2001. Cognitive rehabilitation: an integrative neuropsychological approach. Guilford Press.

Spehlmann R, 1965. The averaged electrical responses to diffuse and to patterned light in the human. Electroencephalography Clinical Neurophysiology 19, 560-569.

Spekreijse, H., 1966. Analysis of EEG responses in man, Thesis, University of Amsterdam. ed.

Spinelli, L., Andino, S.G., Lantz, G., Seeck, M., Michel, C.M., 2000. Electromagnetic inverse solutions in anatomically constrained spherical head models. Brain Topogr 13, 115-125.

Spitzer, R.L., Williams, J.B., Gibbon, M., First, M.B., 1992. The Structured Clinical Interview for DSM-III-R (SCID). I: History, rationale, and description. Arch. Gen. Psychiatry 49, 624-629.

Stanley, D.A., Rubin, N., 2003. fMRI activation in response to illusory contours and salient regions in the human lateral occipital complex. Neuron 37, 323-331.

Steinman, B.A., Steinman, S.B., Lehmkuhle, S., 1997. Transient visual attention is dominated by the magnocellular stream. Vision Res 37, 17-23.

van der Stelt, O., Frye, J., Lieberman, J.A., Belger, A., 2004. Impaired P3 generation reflects high-level and progressive neurocognitive dysfunction in schizophrenia. Arch. Gen. Psychiatry 61, 237-248.

Stockwell, R., Mansinha, L., Lowe, R., 1996. Localization of the Complex Spectrum: The S Transform. IEEE TRANSACTIONS ON SIGNAL PROCESSING, 998-1001.

Toepel, U., Knebel, J., Hudry, J., le Coutre, J., Murray, M.M., 2009a. The brain tracks the energetic value in food images. Neuroimage 44, 967-974.

Toepel, U., Knebel, J., Hudry, J., le Coutre, J., Murray, M.M., 2009b. The brain tracks the energetic value in food images. Neuroimage 44, 967-974.

Tootell, R.B., Hadjikhani, N., 2001. Where is 'dorsal V4' in human visual cortex? Retinotopic, topographic and functional evidence. Cereb. Cortex 11, 298-311.

Tootell, R.B., Hadjikhani, N.K., Vanduffel, W., Liu, A.K., Mendola, J.D., Sereno, M.I., Dale, A.M., 1998. Functional analysis of primary visual cortex (V1) in humans. Proc. Natl. Acad. Sci. U.S.A 95, 811-817.

Tootell, R.B., Mendola, J.D., Hadjikhani, N.K., Ledden, P.J., Liu, A.K., Reppas, J.B., Sereno,

M.I., Dale, A.M., 1997. Functional analysis of V3A and related areas in human visual cortex. J. Neurosci 17, 7060-7078.

Tootell, R.B., Reppas, J.B., Dale, A.M., Look, R.B., Sereno, M.I., Malach, R., Brady, T.J., Rosen, B.R., 1995. Visual motion aftereffect in human cortical area MT revealed by functional magnetic resonance imaging. Nature 375, 139-141.

Tootell, R.B.H., Nelissen, K., Vanduffel, W., Orban, G.A., 2004. Search for color 'center(s)' in macaque visual cortex. Cereb. Cortex 14, 353-363.

Turetsky, B.I., Calkins, M.E., Light, G.A., Olincy, A., Radant, A.D., Swerdlow, N.R., 2007. Neurophysiological endophenotypes of schizophrenia: the viability of selected candidate measures. Schizophr Bull 33, 69-94.

Ungerleider, L., Mishkin, M., 1982. Two cortical visual systems, in: Visual Behavior. D.J. Ingle, M.A. Goodale & R.J.W. Mansfield, pp. 549–586.

Van Zaen, J., Uldry, L., Duchêne, C., Prudat, Y., Meuli, R.A., Murray, M.M., Vesin, J., 2010. Adaptive tracking of EEG oscillations. J. Neurosci. Methods 186, 97-106.

Vidyasagar, T.R., 1999. A neuronal model of attentional spotlight: parietal guiding the temporal. Brain Res. Brain Res. Rev 30, 66-76.

Woldorff, M.G., Fox, P.T., Matzke, M., Lancaster, J.L., Veeraswamy, S., Zamarripa, F., Seabolt, M., Glass, T., Gao, J.H., Martin, C.C., Jerabek, P., 1997. Retinotopic organization of early visual spatial attention effects as revealed by PET and ERPs. Hum Brain Mapp 5, 280-286.

Yeap, S., Kelly, S.P., Reilly, R.B., Thakore, J.H., Foxe, J.J., 2009. Visual sensory processing deficits in patients with bipolar disorder revealed through high-density electrical mapping. J Psychiatry Neurosci 34, 459-464.

Yeap, S., Kelly, S.P., Sehatpour, P., Magno, E., Javitt, D.C., Garavan, H., Thakore, J.H., Foxe, J.J., 2006. Early visual sensory deficits as endophenotypes for schizophrenia: high-density electrical mapping in clinically unaffected first-degree relatives. Arch. Gen. Psychiatry 63, 1180-1188.

Yoshino, A., Kawamoto, M., Yoshida, T., Kobayashi, N., Shigemura, J., Takahashi, Y., Nomura, S., 2006. Activation time course of responses to illusory contours and salient region: a high-density electrical mapping comparison. Brain Res 1071, 137-144.

Zemon, V., Ratliff, F., 1982. Visual evoked potentials: evidence for lateral interactions. Proc. Natl. Acad. Sci. U.S.A 79, 5723-5726.

CHAPTER 6 ARTICLES

6.1 Generating Controlled Image Sets in Cognitive Neuroscience Research

Jean-François Knebel[1,*], Ulrike Toepel[1,2,*], Julie Hudry[3], Johannes le Coutre[3], Micah M. Murray[1,2,4]

The Functional Electrical Neuroimaging Laboratory,

[1]Neuropsychology and Neurorehabilitation Service and [2]Radiology Service,

Centre Hospitalier Universitaire Vaudois and University of Lausanne, Switzerland

[3]Nestlé Research Center, Vers-chez-les-Blanc, Lausanne, Switzerland

[4]EEG Brain Mapping Core, Center for Biomedical Imaging, Lausanne and Geneva, Switzerland

*These authors contributed equally to this report.

Address correspondence to either:

Jean-François Knebel

Neuropsychology and Neurorehabilitation Service

Centre Hospitalier Universitaire Vaudois (CHUV)

Hôpital Nestlé, 5, Rue Pierre Decker

CH-1011 Lausanne, Switzerland

jean-francois.knebel@chuv.ch

or

Micah M. Murray

EEG Brain Mapping Core, Centre for Biomedical Imaging

Centre Hospitalier Universitaire Vaudois

Radiology Service, BH08.078

Bugnon 46

CH-1011 Lausanne, Switzerland

Micah.murray@chuv.ch

6.1.1 Abstract

The investigation of perceptual and cognitive functions with non-invasive brain imaging methods critically depends on the careful selection of stimuli for use in experiments. For example, it must be verified that any observed effects follow from the parameter of interest (e.g. semantic category) rather than other low-level physical features (e.g. luminance, or spectral properties). Otherwise, interpretation of results is confounded. Often, researchers circumvent this issue by including additional control conditions or tasks, both of which are flawed and also prolong experiments. Here, we present some new approaches for controlling classes of stimuli intended for use in cognitive neuroscience, however these methods can be readily extrapolated to other applications and stimulus modalities. Our approach is comprised of two levels. The first level aims at equalizing individual stimuli in terms of their mean luminance. Each data point in the stimulus is adjusted to a standardized value based on a standard value across the stimulus battery. The second level analyzes two populations of stimuli along their spectral properties (i.e. spatial frequency) using a dissimilarity metric that equals the root mean square of the distance between two populations of objects as a function of spatial frequency along x- and y- dimensions of the image. Randomized permutations are used to obtain a minimal value between the populations to minimize, in a completely data-driven manner, the spectral differences between image sets. While another paper in this issue applies these methods in the case of acoustic stimuli (Aeschlimann et al. ,2088), we illustrate this approach here in detail for complex visual stimuli.

Key words: visual perception, images, luminance adaptation, spectral frequency

6.1.2 Introduction

Investigating visual and auditory perception in humans by utilizing non-invasive brain imaging methods such as electroencephalography (EEG), magnetoencephalography (MEG), functional magnetic resonance imaging (fMRI), and near-infrared spectroscopy (NIRS) is a rapidly growing field within neuroscience. Many studies have been specifically concerned with categorical processing of object stimuli (e.g. Thorpe et al. 1996; Mouchtang-Rostaing *et al.* 2000; VanRullen and Thorpe 2001; Carmel and Bentin 2002; Goffaux et al. 2003; Delorme et al., 2004; Michel et al. 2004; Lewis et al. 2005; Murray et al. 2006; Harel et al., 2007). Because real-world objects are often quite difficult and infeasible to present within laboratory settings (i.e. due to their size, availability, and/or the associated difficulty in controlling their presentation), research on visual and auditory perception most often deals with replicas, including photographs and drawings, of real-world objects. Naturally, these objects and their photographed counterparts do not solely differ in their categorical attributes (e.g. cars vs. animals vs. houses, etc.). Low-level visual features also vary substantially between objects. For example, Delplanque and colleagues (2007) recently examined the International Affective Picture System (IAPS; Lang et al. 2005) and found that differences in affective ratings can co-occur with differences in the images' spectral power. In light of these considerations neuroscientific studies of discrimination and categorization certainly need to assure that observed effects are indeed due to the category specificity of an object and not to low-level perceptual features (e.g. photograph angle, luminance, spectral properties). Otherwise, data interpretation will likely be confounded.

Brain imaging methods, in particular those with a high temporal resolution like EEG and MEG, are prone to data misinterpretation caused by low-level visual attributes. For example, the temporal dynamics of emotional influences on face processing can vary, in part, due to the level of control of low-level visual attributes (see Murray et al. 2008 for discussion of some impacts of ERP data analysis methods). While categorization effects within ~80ms after stimulus onset have been reported (Pizzagalli et al. 1999), similar effects are only observed at ~130ms when stimuli are highly controlled for in their physical features (Pourtois et al. 2005). Moreover, some studies have challenged the specificity of a face-selective EEG component, the N170, by relating it to variance in the pixel arrangements between images conveying facial stimuli as opposed to other objects (Itier and Taylor 2004; Thierry et al. 2007; though see Bentin et al. 2007). Although both these and other studies have reported faces vs. objects ERP differences in the P100 component (i.e. substantially earlier than the N170), such effects could be driven by inter-category luminance differences and/or spectral variation (e.g. Johannes et al. 1995; McCourt and Foxe 2004; Butler et al. 2007 for effects of luminance and spatial frequency on ERPs).

In order to circumvent problems of low-level physical differences between stimulus conditions, researchers might choose to introduce additional control conditions or tasks in their experimental designs, both of which are imperfect and also prolong experiments (e.g. Doniger et al. 2000; VanRullen and Thorpe 2001; Murray et al. 2006; Rossion and Jacques 2007 for some examples). In this technical report, we present some new approaches for controlling classes of visual stimuli intended for use in cognitive neuroscience. These methods can also be readily extrapolated to auditory stimuli and other applications (see Aeschlimann et al., this issue).

Our approach is comprised of two levels. A first level serves to equate individual stimuli in terms of their mean intensity (i.e. the luminosity of images), while also addressing potential confounds of image saturation. Many neuroscientific studies on visual processing indeed equalize image luminosity, yet details on the utilized procedures are seldom given. Thus, one objective of the present technical report was to provide newcomers with the necessary tools and mathematical formulae. The second level of our approach aims at controlling two sets of stimuli with respect to their spectral properties (i.e. spatial power spectra; see also Delplanque et al. 2007), without requiring a priori filtering of the stimuli. The two levels should be applied consecutively since the luminosity treatment can have some influences on the spatial frequency properties of an image. As will be made clear below, because the luminance treatment adjusts all images to one standard value, this value will indeed stay stable even after the definition of image subsets obtained from the second level of our approach. We present analyses based on a photographic image database we developed to investigate the time course of food categorization.

6.1.3 Materials and Methods

The images for the analyses were obtained in the following way. Top-view photographs of food items were taken in front of equal backgrounds from identical angles. The photographs were subdivided into high- vs. low-fat food classes by means of official nutritional databases. All images were sized to 300x300 pixels. Yet, non-squared images can be utilized as well when equal in the number of pixels between images.

6.1.4 Intensity treatment

The intensity treatment serves to control adaptively the luminosity of images which can be mathematically defined as luminance or grayscale value, respectively. In the case of sounds, volume would be the analogue measure. In a first step, all images are defined in color space in terms of the YUV color model (e.g. Wyszecki and Stiles 1982), which is that used for the PAL British standard format. In this model, the Y component represents the luminance of an image. The U and V components, on the other hand, represent the chrominance of an image.

The luminance (= grayscale value) of a pixel is influenced by the color levels red (R), green (G) and blue (B) in varying proportions, such that Y= 0.299 x R + 0.587 x G + 0.114 x B. In this way, the Y component represents a particular image in its original dimensions as a matrix of its luminance values. In order to compare the luminance properties between images, we calculated one numerical value per image. The value $\overline{Y}$ expresses the weighted luminance of an image (see Figure 19a). In order to obtain the value $\overline{Y}$, we applied an equation that serves to calculate the mathematical expectation of a normalized histogram (Pascal and Huygens, 1657).

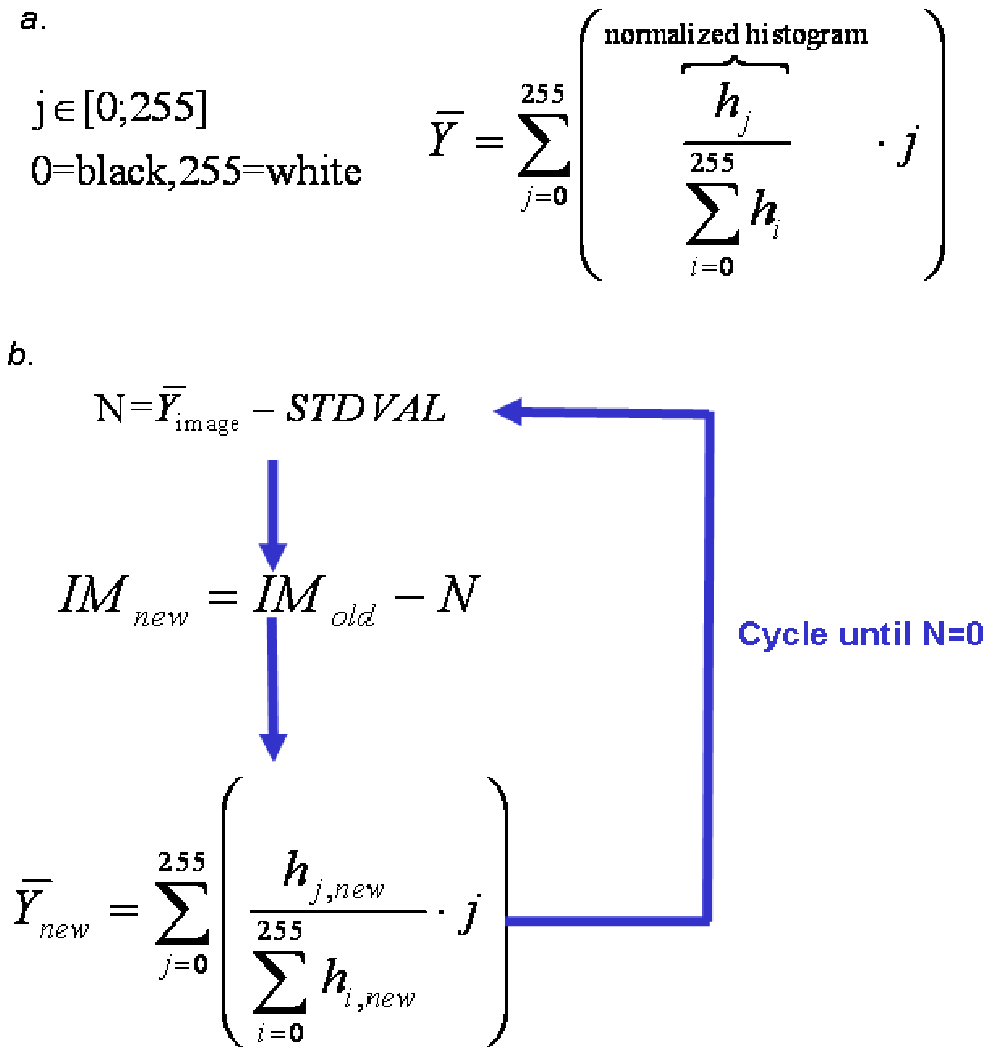

Figure 19 : Schema of the Algorithm for luminance control
a. This equation shows how one numerical value per image is obtained that represents its luminance. b. Illustration of the iterative cycle applied to adapt the luminance across images. (See text for details about the equations.)

In this equation, the factor j conveys the specific grayscale value which can range from 0 (=black) to 255 (=white). The factor h_j describes how often this particular grayscale value j is

present in the luminance matrix *Y* of one image. The value h_j is normalized by dividing it by the absolute sum of pixels h_i per image. In order to account for the arbitrary amount of pixels along the black-white dimension (0-255) the result of the normalization is multiplied with the factor *j*. Intrinsically, this weighting by multiplication with the factor j assumes that the luminance increases between black and white in a linear way. The value $\overline{Y}$ is calculated as the sum of all weighted values per image, resulting in one representative numerical value $\overline{Y}$ per image.

Figure 19b illustrates the procedure for a set of images. First, the $\overline{Y}$ value for each image is computed. In succession, one standard value has to be defined based on the obtained $\overline{Y}$ values across a set of images. In general, the particular standard value used can be defined by the experimenter (for example, it may be the mean or median $\overline{Y}$ value across all images). Second, this standard value (*STDVAL*) is subtracted from the $\overline{Y}$ value of each original image ($\overline{Y}_{\text{image}}$) resulting in a negative or positive value *N*. If the value *N* for an image is positive, the particular image conveys a higher luminance (i.e. is brighter) than the standard value. By contrast, obtaining a negative value *N* would indicate that an image is lower in luminance than the defined standard. In succession, a new image (IM_{new}) is created by subtracting the *N* value from the original image (IM_{old}). Consecutively, the mathematical expectation of a normalized histogram (see Figure 19) is recalculated to obtain the new $\overline{Y}$ value of each image. This new $\overline{Y}$ value is again submitted to the computation of the *N* value. The cycle is repeated until the value of *N* equaled 0 for all images that were submitted to the algorithm.

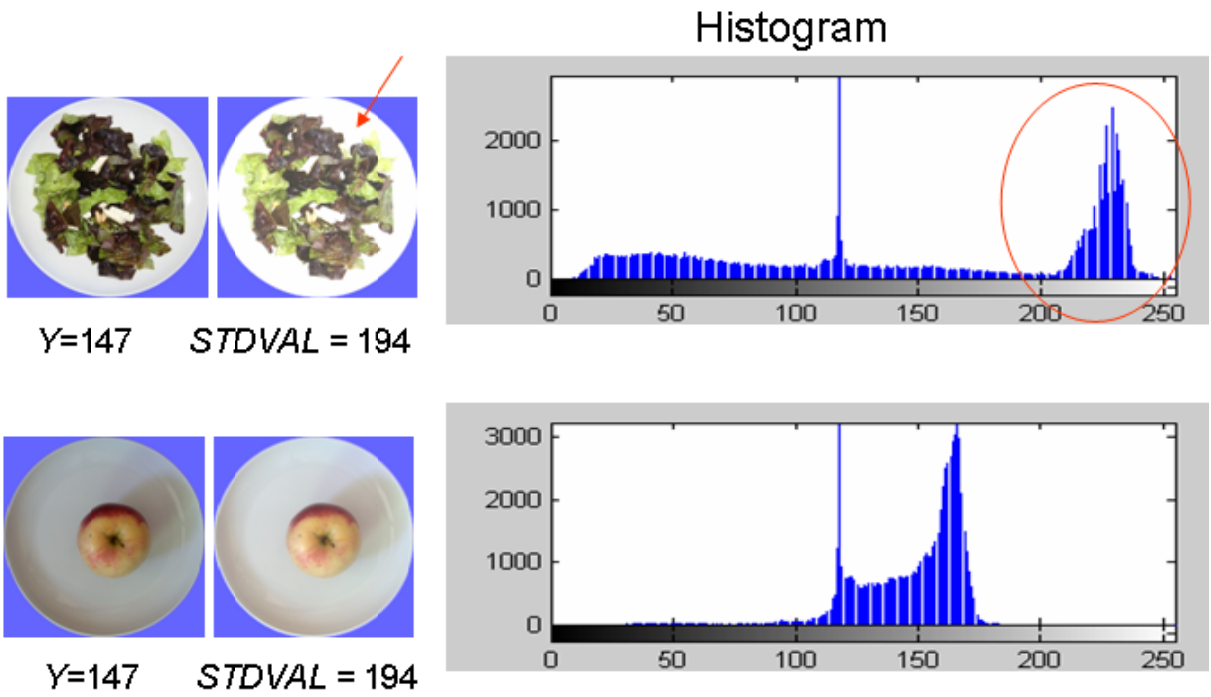

Figure 20 : Results and limitation of the luminance control
The left panel displays sample images before and after intensity treatment. The right panel displays the histograms of these images (the x-axis represents the intensity value of a given pixel and the y-axis the number of pixels) and how the images can become faded out when distributions are wide while also containing a concentration near extreme values of Y. (See text for details on how this issue can be addressed.)

Figure 20 illustrates the outcome of the luminance adaptation for two images from our database. Both images are adapted to a standard value of 194. The outcome for the two images also illustrates a limitation to the algorithm. When the histogram of an image, i.e. the distribution of pixels, is rather widely dispersed across the range of values 0-255 with a concentration of pixels close to the 255 value (i.e. white), the rendering of this image to the standard value can result in a further pixel concentration towards the 255 value. Thus, a saturation effect for the image can occur, which leads to a bright appearance of the image. The histogram of the pixel values within the example image in the upper panel of Figure 20 exhibits a widely distributed pixel range, but a high concentration of pixels between the values 220 and 250. Luminance adaptation for the images according to the previously calculated mean standard value substantially fades out the image. The problem can be overcome by lowering the standard value for all images to be rendered or by using the median. Therefore, using the mean $\overline{Y}$ value as a standard value might not always be satisfactory. Alternatively, images with high pixel concentrations towards the 255 value could be excluded. Note that the latter option would forcibly reduce the number of images available for the experiment.

6.1.5 Spectral distance optimization

The spectral analysis ensures equal arrangement of spectral properties within the visual objects themselves. In contrast to intensity properties, the spectral properties of an object cannot be readily altered without potentially impacting the recognizability, as this would change the overall arrangement of pixels within an image and the resultant appearance. The same constraint also applies to the spectral phase within an image as it plays a predominant role in image appearance (Oppenheimer and Lim 1981).

In some studies the spatial features are, however, specifically modified to examine the functional role of high vs. low spatial frequencies, e.g. for the processing of the emotional valence of facial expressions (Vuilleumier et al. 2003; Pourtois et al. 2005;). Here, we chose to closely match (sub)groups of images (i.e. images from experimental condition A with the images from condition B) in terms of their spatial frequencies to gain maximal physical approximation or minimal dissimilarity, respectively. Such notwithstanding, approaches that filter the spectral properties of images (Nasanen et al. 1999; Dakin et al. 2002) can gain even better or perfect approximations of similarity between image groups. However, these approaches alter the overall appearance of images by eliminating certain frequency bands, which our approach seeks to avoid. Thus, while the images here have not been filtered before applying the spectral distance optimization to ensure the quasi-natural appearance of objects in an image, the experimenter interested in the functional role of selective spatial frequencies could precede the analysis with the application of a filter.

A mathematically simple way to achieve maximal “alikeness” for subgroups of images is the Dissimilarity equation, which we have modified from the one often used in the analysis of EEG and MEG datasets to identify whether the topographies of responses differ (c.f. Lehmann and Skrandies 1980; Skrandies 1993; Murray et al , this issue). Dissimilarity as such bears no physical significance; rather, it is a singular measure of the difference along a given dimension (e.g. topography of an ERP or spatial frequency in the case of images) without any quantification of the variance in this difference. For this reason, Dissimilarity is interpretable when a distribution of values is generated based on permutations of a dataset (here, images whereas topographic maps in the case of EEG/ERP).

Inputs for the Dissimilarity equation are the mean spectra of two subgroups of images (i.e. two experimental conditions) selected from among a larger population of images. The equation compares the mean values between conditions using the root mean square of the difference between the spectra obtained for each subgroup. The values u and v represent the mean spatial

power spectra for two groups of images at a given location within the image space. This calculation yields a matrix that is then summed for all points (or coordinates) of the matrix. Finally, the result is normalized by dividing it by the factor, *k*, which represents the size of the image.

The subgroups yielding the lowest Dissimilarity value from a range based on all other possible subgroups of images can then be identified. The range of Dissimilarity values is based on numerous trial iterations. That is, different mean spectra are obtained by iteratively (re)selecting new subgroups of images from each original group and calculating their dissimilarity values. The subgroups yielding the lowest Dissimilarity value is selected to form the materials for the experiment, as these constitute the sets of images that are the spectrally most similar. This procedure is schematized in Figure 21.

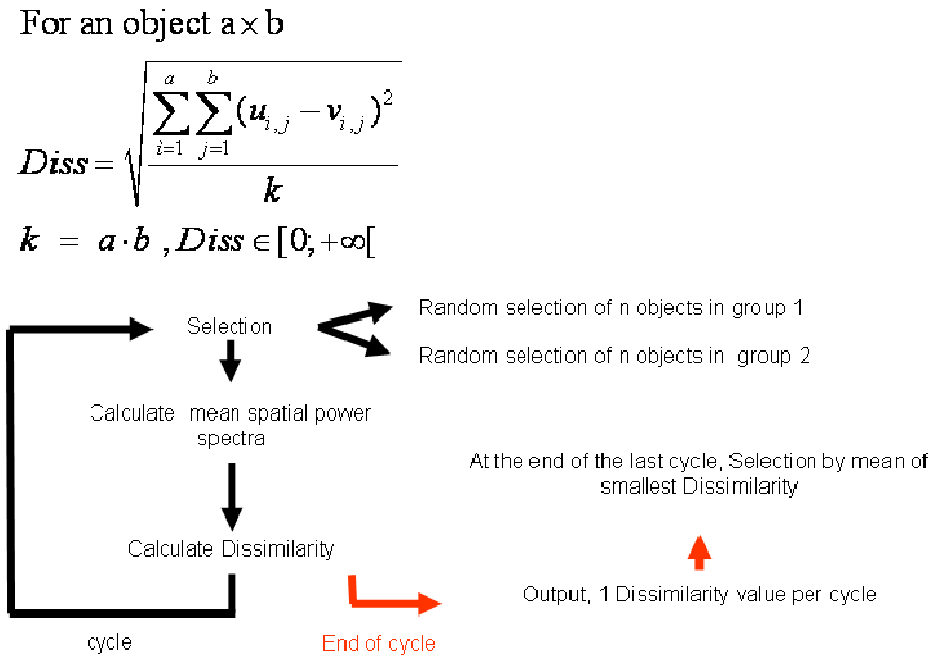

Figure 21 : Schema of the Algorithm for spatial frequency control
Dissimilarity equation (upper panel) and illustration of the computation cycle that enables the comparison of Dissimilarity values between the different choices of images for each stimulus condition (lower panel).

First, *n* images from the total population available for either condition are randomly selected. The mean spatial power spectrum for each of these subgroups of images is then calculated separately. Next, the Dissimilarity is calculated. The input (= image name) and output (= Dissimilarity) value of the equation are stored. Consecutively, the procedure undergoes a random number of cycles each of which is based on new selections of *n* images per group, saving

input and output properties as above. It is important to note that this procedure cannot be run on *all* of the original images, because the obtained Dissimilarity values would always be unchanged and no meaningful assertions could be made. After a sufficient number of iterations (e.g. 1000) the experimenter can identify the groups of images for use in the experiment whose comparison yielded the lowest dissimilarity value.

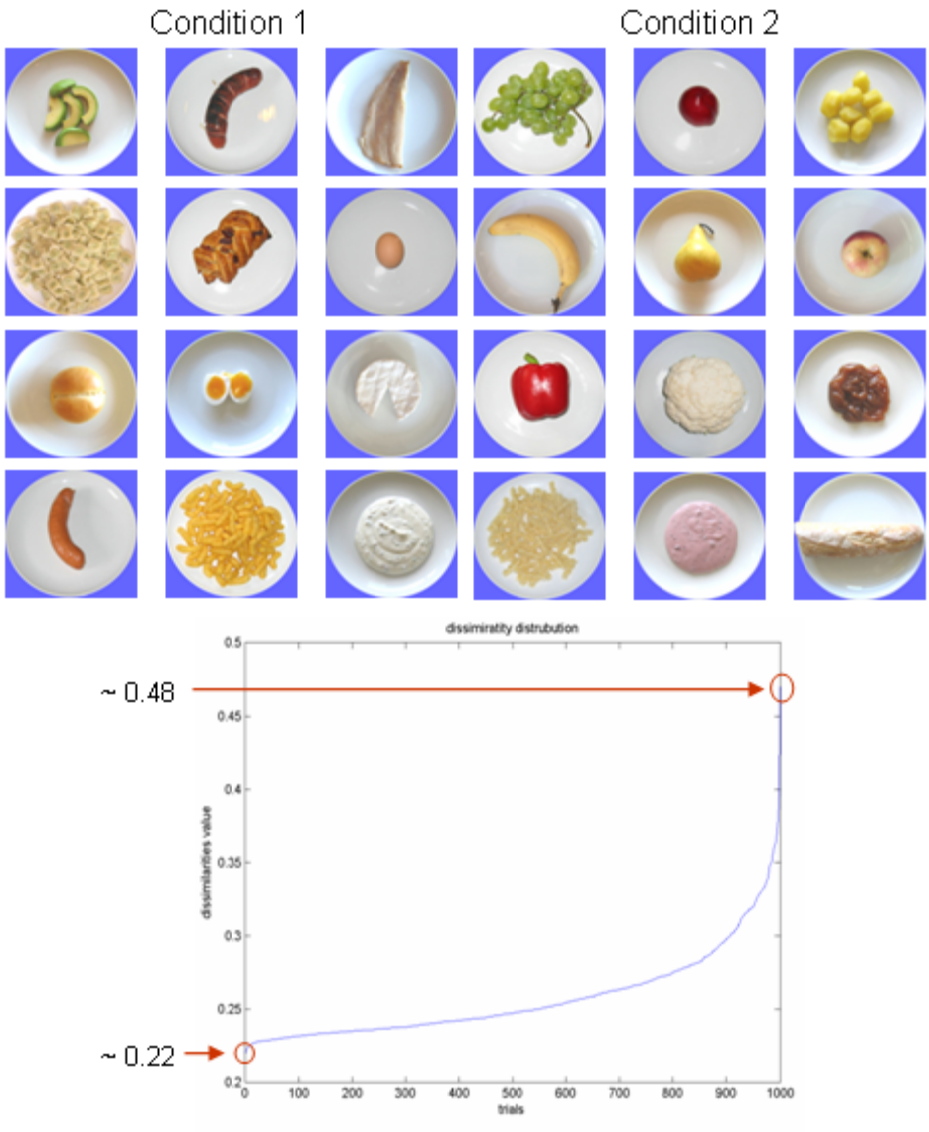

Figure 22 : Results of spatial frequency control
Output of the computation cycle depicted in Figure 3, which shows the distribution of Dissimilarity values across trial cycles, and the corresponding image set that yielded the lowest Dissimilarity value.

Figure 22 illustrates an example of the output of the algorithm. In this example, each of the original 2 groups of images comprised 50 different photographs. For each cycle where Dissimilarity is calculated a subgroup of 12 of these 50 images is selected. The upper graph

displays the Dissimilarity values on the y-axis, and the number of computed cycles on the x-axis. It becomes evident that one particular choice of photographs per group yields the lowest dissimilarity (~0.22), whereas another choice results in a Dissimilarity value twice as high (~0.48). The lower panel of Figure 22 shows the groups of images from each condition that yielded the lowest Dissimilarity value and therefore match most closely in terms of spatial frequencies.

Importantly, in contrast to the intensity treatment, the spectral distance optimization does not alter the physical properties of the images. Rather, it identifies the subgroup of images that are the closest spectrally from among the possible options (the bounds of which are defined by the available stimulus set). Consequently, the outcome of the spectral distance optimization is only true in a specific space (i.e. the specific content of groups of objects). Consequently, this method cannot reveal that the objects between groups are physically identical, but rather only that these groups of images are the least different.

6.1.6 Conclusion

Low-level differences in visual features often constitute a major caveat in the interpretation of neuroscientific studies of object processing. Here we present some intuitive and mathematically straightforward methods for controlling luminance and spectral properties within and between stimulus conditions. These methods are not solely applicable to visual feature control but can also be extrapolated to acoustic properties.

6.1.7 Acknowledgments

Financial support has been provided by the Leenaards Foundation (2005 Prize for the Promotion of Scientific Research to MMM). Researchers interested in obtaining the MatLab code for the procedures should either contact Jean-François Knebel (jean-francois.knebel@chuv.ch) or Micah Murray (micah.murray@chuv.ch).

6.1.8 References

Aeschlimann M, Knebel J-F, Murray MM, Clarke S (2008) Emotional pre-eminence of human vocalizations. Brain Topogr

Bentin S, Taylor MJ, Rousselet GA, Itier RJ, Caldara R, Schyns PG, Jacques C, Rossion B (2007) Controlling interstimulus perceptual variance does not abolish N170 face sensitivity. Nat Neurosci.10:801-802.

Butler PD Martinez A, Foxe JJ, Kim D, Zemon V, Silipo G, Mahoney J, Shpaner M, Jalbrzikowski M, Javitt DC (2007) Subcortical visual dysfunction in schizophrenia drives secondary cortical impairments. Brain. 130:417-30.

Carmel D, Bentin S (2002) Domain specificity versus expertise: factors influencing distinct processing of faces. Cognition 83:1-29.

Dakin SC, Hess RF, Ledgeway T, Achtman RL (2002) What causes non-monotonic tuning of fMRI response to noisy images? Curr Biol. 12:R476-477.

Delorme A, Rousselet GA, Mace MJ, Fabre-Thorpe M (2004) Interaction of top-down and bottom-up processing in the fast visual analysis of natural scenes. Brain Res Cogn Brain Res. 19: 103-113.

Delplanque S, N'diaye K, Scherer K, Grandjean D (2007) Spatial frequencies or emotional effects? A systematic measure of spatial frequencies for IAPS pictures by a discrete wavelet analysis. J Neurosci Methods 165:144-150.

Doniger GM, Foxe JJ, Murray MM, Higgins BA, Snodgrass JG, Schroeder CE, Javitt DC (2000) Activation timecourse of ventral visual stream object-recognition areas: high density electrical mapping of perceptual closure processes. J Cogn Neurosci. 12:615-621.

Goffaux V, Gauthier I, Rossion B (2003) Spatial scale contribution to early visual differences between face and object processing. Brain Res Cogn Brain Res. 16: 416-424.

Harel A, Ullman S, Epshtein B, Bentin S (2007) Mutual information of image fragments predicts categorization in humans: electrophysiological and behavioral evidence. Vision Res. 47:2010-2020.

Itier RJ, Taylor MJ (2004) N170 or N1? Spatiotemporal differences between object and face processing using ERPs. Cereb. Cortex 14: 132-142.

Johannes S, Münte TF, Heinze HJ, Mangun GR (1995) Luminance and spatial attention effects on early visual processing. Brain Res Cogn Brain Res. 2:189-205.

Lehmann D, Skrandies W (1980) Reference-free identification of components of checkerboard-evoked multichannel potential fields. Electroencephalogr Clin Neurophysiol. 48: 609-621.

Lewis JW, Brefczynski JA, Phinney RE, Janik JJ, DeYoe EA (2005) Distinct cortical pathways for processing tool versus animal sounds. J. Neurosci. 25: 5148-5158.

McCourt ME, Foxe JJ (2004) Brightening prospects for early cortical coding of perceived luminance: a high-density electrical mapping study. Neuroreport. 15:49-56.

Michel CM, Seeck M, Murray MM (2004) The speed of visual cognition. Suppl Clin Neurophysiol. 57: 617-627.

Mouchetant-Rostaing Y, Giard MH, Bentin S, Aguera PE, Pernier J (2000) Neurophysiological correlates of face gender processing in humans. E. J. Neurosci. 12: 303-310.

Murray MM, Brunet D, Michel CM (2008) Topographic ERP analyses: A step-by-step tutorial review. Brain Topogr

Murray MM, Camen C, Gonzalez Andino SL, Bovet P, Clarke S (2006) Rapid brain discrimination of sounds of objects. J. Neurosci. 26:1293-1302.

Nasanen R (1999) Spatial frequency bandwidth used in the recognition of facial images. Vis Res. 39:3824-3833.

Oppenheim AV, Lim JS (1981) The importance of phase in signals. Proc IEEE. 69:529-541.

Pascal B, Huygens C (1657) Treaty of mathematics “De rationiciis in ludo aleae”.

Pizzagalli D, Regard M, Lehmann D (1999) Rapid emotional face processing in the human right and left brain hemispheres: an ERP study. Neuroreport. 10: 2691-2688.

Pourtois G, Dan ES, Grandjean D, Sander D, Vuilleumier P (2005) Enhanced extrastriate visual response to bandpass spatial frequency filtered fearful faces: time course and topographic evoked-potentials mapping. Hum Brain Mapp. 26: 65-79.

Rossion B, Jacques C (2007) Does physical interstimulus variance account for early electrophysiological face sensitive responses in the human brain? Ten lessons on the N170. Neuroimage. doi:10.1016/j.neuroimage.2007.10.011.

Skrandies W (1993) EEG/EP: new techniques. Brain Topogr. 5: 347-350.

Thierry G, Martin CD, Downing P, Pegna AJ (2007) Controlling for interstimulus perceptual variance abolishes N170 face selectivity. Nat. Neurosci. 10: 505-511.

Thorpe SJ, Fize D, Marlot C (1996) Speed of processing in the human visual system. Nature. 381: 520-522.

VanRullen R, Thorpe SJ (2001) The time course of visual processing: from early perception to decision-making. J Cogn Neurosci. 13: 454-461.

Vuilleumier P, Armony JL, Driver J, Dolan RJ (2003) Distinct spatial frequency sensitivities for processing faces and emotional expressions. Nat Neurosci. 6:624-631.

Wyszecki G, Stiles WS (1982) Color Science: Concepts and Methods, Quantitative Data and Formulae. John Wiley & Sons, New York.

6.2 Impaired early visual response modulations to spatial information in chronic schizophrenia

Jean-François Knebel[a,b], Daniel C. Javitt[c], Micah M. Murray[a,b,c,*]

[a]Neuropsychology and Neurorehabilitation Service, Department of Clinical Neuroscience, Centre Hospitalier Universitaire Vaudois and University of Lausanne, Switzerland

[b]Radiology Department, Centre Hospitalier Universitaire Vaudois and University of Lausanne, Switzerland

[c]Program in Cognitive Neuroscience and Schizophrenia, The Nathan S. Kline Institute for Psychiatric Research, Orangeburg, NY, USA

[d]The Electroencephalography Brain Mapping Core, Center for Biomedial Imaging, Lausanne, Switzerland

Corresponding author:

Micah Murray

Department of Clinical Neurosciences,

CHUV

BH08.078

Rue du Bugnon 46

1011 Lausanne, Switzerland

Tel : +41 21 3141321; Fax : +41 21 3141319

Email : micah.murray@chuv.ch

6.2.1 Abstract

Early visual processing stages have been demonstrated to be impaired in schizophrenia patients and their first-degree relatives. The amplitude and topography of the P1 component of the visual evoked potential (VEP) are both affected; the latter of which indicates alterations in active brain networks between populations. At least two issues remain unresolved. First, the specificity of this deficit (and suitability as an endophenotype) has yet to be established, with evidence for impaired P1 responses in other clinical populations. Second, it remains unknown whether schizophrenia patients exhibit intact functional modulation of the P1 VEP component; an aspect that may assist in distinguishing effects specific to schizophrenia. We applied electrical neuroimaging analyses to VEPs from chronic schizophrenia patients and healthy controls in response to variation in the parafoveal spatial extent of stimuli. Healthy controls demonstrated robust modulation of the VEP strength and topography as a function of the spatial extent of stimuli during the P1 component. By contrast, no such modulations were evident at early latencies in the responses from patients with schizophrenia. Source estimations localized these deficits to the left precuneus and medial inferior parietal cortex. These findings provide insights on potential underlying low-level impairments in schizophrenia.

Keywords:

Electroencephalography (EEG), electrical neuroimaging, event-related potential (ERP); visual evoked potential (VEP)

6.2.2 Introduction

Historically schizophrenia has been considered as primarily a disturbance in higher-order functions (Goldman-Rakic 1994; Goldberg TE & Gold JM 1995; Weinberger & Gallhofer 1997; Green 1998). More recently, there has been increasing interest in the contributions of early and low-level processing impairments. This has been most notable in the case of auditory processing where impairments in sensory gating and in mismatch negativity generation are well-documented (Umbricht et al. 2000; Umbricht et al. 2006; Lavoie et al. 2008). With regard to visual dysfunctions, a number of studies support there being deficits that more strongly impact functions associated with the magnocellular than parvocellular pathway (e.g Martínez et al., 2008; Coleman et al., 2009; Kiss et al., 2010). In particular, such deficits have been interpreted as indicative of disturbed spatial processing that in turn may lead to and/or appear conjointly with higher-level deficits (Butler & Javitt, 2005; Javitt, 2009)

Studies that have focused on the time course of these low-level visual processing impairments have found that visual evoked potentials (VEPs) over the initial 100ms (i.e. the P1 component) are impaired in patients with schizophrenia. A P1 deficit has not only been identified in chronic patients (Foxe et al. 2001; Doniger et al. 2002; Foxe et al. 2005), but also in first-degree relatives (Yeap et al. 2006). In particular, Foxe et al. 2005 demonstrated that this P1 deficit is not simply a shift in the amplitude of an otherwise intact process, but instead follows from a change in the configuration of the underlying brain network as revealed by topographic modulations in the VEP.

At present, however, it remains unknown whether this perturbed network is capable of exhibiting intact functional modulations in response to parametric variations in stimulus features. For example, Foxe et al. 2001 examined P1 amplitude in healthy controls and chronic patients with schizophrenia as a function of the number of pixels present in the visual display. While healthy controls exhibited an incremental modulation with increased numbers of pixels (and by extension stimulus energy), such was not observed in patients. Based on its topographic distribution (Foxe et al. 2001), estimated sources (Foxe et al. 2005), and relative sensitivity to luminance contrast (Butler et al. 2001) the P1 deficit in schizophrenic patients has been generally ascribed to impairments within dorsal visual stream structures. This proposition is in solid agreement with additional research demonstrating impairments in visuo-spatial functions in such patients (Cadenhead et al. 1998; Schwartz et al. 1999; Brenner et al. 2002; Butler et al. 2003). However, at present it remains unknown whether the P1 deficit obtained in VEP studies reflects impaired spatial processing per se or instead a more general diminution in visual processing/sensitivity.

The present study focused on early visual processing in chronic schizophrenia patients with the objective of determining whether impaired responses reflect impaired sensitivity to spatial features. Prior work from our group has shown that in healthy controls the P1 is sensitive to small (<1°) variations in the spatial eccentricity of parafoveally presented stimuli (Murray et al., 2002). Here, we compared VEPs from patients in response to such variations in the spatial eccentricity of stimuli that were oriented to form an illusory contour shape or not. Given that patients have been shown to exhibit intact sensitivity to illusory contour forms (Foxe et al. 2005), we could thus dissociate spatial from form-related processes.

6.2.3 Materials and Methods

6.2.3.a Participants

A total of 16 individuals participated in this study. There were 8 chronic and medicated patients (all males; 2 left-handed), aged 36-47 years (mean±SD = 42±4 years) at the time of EEG recording and meeting DSM-IV criteria for schizophrenia. The control cohort included 8 individuals (all males; 1 left-handed), aged 25-53 years (mean±SD = 39±11 years) and with no history of or current neurological or psychiatric illness. There was no reliable difference in the ages of the patient and control populations ($t(14)=0.725$; $p=0.481$). All participants had normal or corrected-to-normal vision. These participants are a subset of those from our prior work (Foxe et al. 2005), which included 16 patients with schizophrenia and 17 healthy controls. Exclusion of data from 8 of the original 16 patients was due to poor signal quality in the VEPs when averaged according to the subset of stimuli described below. Data from control subjects were excluded to generate a cohort matched in size, age, and sex. Positive and Negative Symptoms Scale (PANSS) ratings were performed by a single rater, with factors defined according to White et al. (1997). At the time of testing, all patients were receiving antipsychotic medication. There was no evidence, however, for correlations between antipsychotic dose and any of the dependent measures evaluated in this study. Details regarding clinical evaluation and medication are provided in Table 1. Controls were free of psychiatric illness or symptoms by self-report using criteria from the SCID-NP (see Spitzer et al. 1992S), and all reported no history of alcohol or substance abuse.

Diagnosis: Schizophrenia/Schizoaffective Disorder	8/0
Neuroleptics: Atypical/Typical/Both	8/0/0
Chloropromazine (CPZ)-equivalent±SD, daily	1056.13±378.70
Clinical Global Impressions (CGI)±SD	4.25±0.46
Education±SD, y	11.14±3.34
Illness Duration±SD, y	17.88±6.27
Intelligence Quotient (IQ)±SD	96.0±9.32
Laterality Quotient±SD	0.62±0.70
PANSS: Positive Symptoms±SD	12.13±5.14
Negative Symptoms±SD	21.13±5.89
Autistic Preoccupation±SD	13.25±3.28
Activation±SD	6.88±2.03
Dysphoria±SD	11.38±2.26

Table 1. Demographic and Clinical Characteristics of Schizophrenia Patient Group (*N*=8)

6.2.3.b Stimuli and Task

Participants were instructed to centrally fixate an array of Kanizsa-type (Kanizsa 1976) 'pacmen' inducers that were oriented in one of two manners to either form or not form an illusory shape ('IC' and 'NC' conditions, respectively). The timing of the stimuli and response window is detailed below. The inducers were circular (subtending 3° of visual angle in diameter) and appeared black on a gray background. Stimuli were presented on a CRT computer monitor (Iiyama Vision Master Pro 502, model no. A102GT) located 114cm away from the participant. Their task was to indicate whether they perceived a gray shape on top of the pacmen.

Five shapes were induced in the original study of Foxe et al. 2005 from which the present data come: square, circle, triangle, pentagon and star. In order to produce illusory shapes of the same maximal width and height (6° in either plane), the eccentricity of inducers varied slightly across shapes (cf. Table 1 in Murray et al. 2002). The analyses in the present study focused on VEPs to the square and circle as well as their corresponding configurations that were oriented so as to not induce the perception of an illusory shape. That is, both IC and NC configurations were

analyzed. In the case of the square, the four inducers were centered at 4.25° eccentricity along 45° radii from central fixation. For the circle, the four inducers were located at 3° eccentricity along the horizontal and vertical meridians. The support ratio (i.e. the percentage of the perimeter of the illusory shape revealed by the inducers; Ringach & Shapley 1996) was 50% for the square and 64% for the circle. The surface area of the induced IC shapes was 36°2 in the case of the square and 28.3°2 in the case of the circle (Figure 23). Throughout this study, we refer to the IC and NC configurations of the square as "wide" and those of the circle as "narrow" (Figure 23). The reason for this choice is that studies in healthy controls have shown that early VEP responses to the square and circle (as well as their NC counterparts) differ due to the eccentricity of the inducers (Murray et al., 2002).

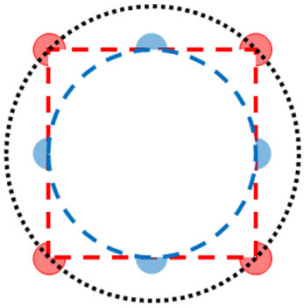

Figure 23 : Schematic of the relative eccentricity of the stimuli.
For simplicity, only the stimulus orientations forming an illusory contour shape are shown. The wide eccentricity is shown in red. The narrow eccentricity is shown in blue.

The timing of stimulus presentations during the course of a trial was such that each array of inducers appeared for 500ms, followed by a blank gray screen for 1000ms. Then a 'Y/N' response prompt appeared and remained on the screen until a response was made, allowing participants to fully control stimulus delivery. Another blank screen of 1000ms duration followed participants' responses. Subjects were instructed to press one button for a 'No' response, indicating that they did not perceive a gray shape 'pop-out' from the background, or a second button for a 'Yes' response, indicating that they perceived a gray shape on top of the inducers. IC and NC inducer configurations were randomly presented and were equally probable. Stimulus presentation and response collection were controlled using Neuroscan's STIM software and hardware. Subjects were encouraged to take breaks between blocks to maintain high concentration and prevent fatigue. Use of the response prompt was to displace in time the motor responses with respect to the sensory VEP. Consequently, however, reaction time data were not analyzed.

6.2.3.c EEG acquisition and pre-processing

Continuous EEG was acquired through Neuroscan Synamps (Neurosoft Inc. Sterling VA) from 64 Ag/AgCl electrodes (impedances <5kΩ, nose reference, 0.05 – 100Hz band pass filter, 500Hz sampling rate). For VEP calculation EEG epochs were time-locked to the presentation of inducer arrays and covered 100ms pre-stimulus and 500ms post-stimulus. Epochs with amplitude deviations in excess of ±80μV at any channel, with the exception of those labeled as 'bad' due to poor electrode-skin contact or damage, were considered artifacts and were excluded. Likewise, trials with blinks or other transients were excluded off-line based on vertical and horizontal electrooculograms. Data from 'bad' channels were interpolated using 3D splines (Perrin et al. 1987), and data were down-sampled to a 61-channel scalp montage used for source estimations. Prior to group-averaging VEPs, data were band-pass filtered (0.1-60Hz), re-calculated to an average reference, and baseline corrected using the pre-stimulus interval. For each participant, 4 VEPs were calculated, following the 2 condition (IC, NC) x 2 eccentricity (wide, narrow) within subject design. The number of accepted sweeps per condition was ~110 for controls ($\in$ [54,197]) and ~ 70 for patients ($\in$ [30,124]).

6.2.3.d EEG analyses

The analyses were performed using the Cartool software by Denis Brunet (http://brainmapping.unige.ch/Cartool.htm). This study followed a 2x2x2 mixed model design, using the within subjects factors of stimulus eccentricity (wide vs. narrow) and stimulus condition (IC vs. NC) and the between subjects factor of clinical status (patients vs. controls). Given the cohort size for each group, non-parametric statistics were used throughout. The repeated measures non-parametric F-test is a bootstrapping of the subjects on the one hand (taking with replacement the subject label) and permutation of the within subjects factors on the other. On each cycle we calculate for each randomization an F-value. Repeating this for 1000 cycles generates an empirical distribution of F-values from which a corresponding p-value can be obtained. This method has the advantage of keeping the intra-variance of the subjects and the only hypothesis is that our data represent the space that we would like to test. Unfortunately, this type of analysis does not readily allow for the calculation of effect size. Nor does the F-value itself (alongside its degrees of freedom) provide a direct indication of the statistically reliability of an effect/interaction, as one must instead consider it against the empirical distribution.

Effects were identified with a multi-step analysis procedure, which we refer to as electrical neuroimaging, examining reference-independent global measures of the electric field at the scalp (Michel et al. 2004; Murray et al. 2008). Briefly, electrical neuroimaging entails analyses of response strength and response topography to differentiate effects due to modulation in the

strength of responses of statistically indistinguishable brain generators from alterations in the configuration of these generators (viz. the topography of the electric field at the scalp). Electrical neuroimaging analyses, being reference-independent, have several advantages over canonical waveform analyses. The statistical outcome with voltage waveform analyses will change with the choice of the reference electrode (Murray et al. 2008). Our conclusions are based solely on reference-independent global measures of the electric field at the scalp. In addition, we utilized the local auto-regressive average distributed linear inverse solution (LAURA; Grave de Peralta Menendez et al. 2001) to visualize and statistically contrast the likely underlying sources of effects identified in the VEPs.

Changes in the strength of the electric field at the scalp were assessed using global field power (GFP) from each participant and experimental condition (Lehmann and Skrandies, 1980; Koenig and Melie-Garcia, 2010). Values at each time point were compared with a repeated measures non parametric F-test, as above. To account for temporal auto-correlation, only effects persisting for at least 10ms were considered reliable (see Guthrie and Buchwald, 1991).

A K-means clustering analysis of the VEP topography at the scalp identified time periods of stable topography independent of VEP strength (data are normalized), which is a data-driven measure (Murray et al. 2008; Murray et al. 2009). The optimal number of topographies or 'template maps' that accounted for the group-averaged data set (i.e. the post-stimulus periods of all conditions from both patients and controls, collectively) was determined by a modified cross-validation criterion (Murray et al. 2008; Murray et al. 2009). The pattern of template maps identified in the group-averaged data across patients and controls was then statistically tested in the data of each individual participant, using spatial correlation to label each data point as better matching one or another template map. The output is a measure of relative map presence for each participant that is in turn submitted to a repeated measures non parametric F-test with the within subject factors of condition, eccentricity, and map as well as the between subjects factor of clinical status. This procedure reveals whether and when VEPs are more often described by one map versus another, and therefore whether different intracranial generator configurations are engaged.

We estimated the sources in the brain underlying the VEPs using a distributed linear inverse solution (ELECTRA) applying the local autoregressive average (LAURA) regularization approach to address the non-uniqueness of the inverse problem (Grave de Peralta Menendez et al. 2001; Grave de Peralta Menendez et al. 2004; Michel et al. 2004). The inverse solution algorithm is based on biophysical principles derived from the quasi-static Maxwell's equations; most notably the fact that independent of the volume conductor model used to describe the head, only

irrotational and not solenoidal currents contribute to the EEG (Grave de Peralta Menendez et al. 2001; Grave de Peralta Menendez et al. 2004). As part of the regularization strategy, homogenous regression coefficients in all directions and within the whole solution space were used. LAURA uses a realistic head model, and the solution space included 3005 nodes, selected from a 6 × 6 × 6 mm grid equally distributed within the gray matter of the Montreal Neurological Institute's average brain (courtesy of Grave de Peralta Menendez and Gonzalez Andino; http://www.electrical-neuroimaging.ch/). The head model and lead field matrix were generated with the Spherical Model with Anatomical Constraints (SMAC; Spinelli et al. 2000). As an output, LAURA provides current density measures; the scalar values of which were evaluated at each node. Prior basic and clinical research has documented and discussed in detail the spatial accuracy of this inverse solution (e.g. Grave de Peralta Menendez et al. 2004; Michel et al. 2004; Gonzalez Andino et al. 2005; Gonzalez Andino et al. 2005; Martuzzi et al. 2009). The time periods used for source estimations were determined from the above VEP analyses. Data from each subject and condition were first averaged as a function of time to generate a single data point. The inverse solution was then calculated for each of the nodes in the solution space. These data matrices were then submitted to repeated measures non-parametric F-test as above. The results of the source estimations were rendered on the MNI brain with the Talairach & Tournoux (1988) coordinates of the largest statistical differences indicated.

6.2.4 Results

6.2.4.a Behavioral results

All participants readily performed the IC/NC discrimination task. Mean (s.d. indicated) accuracy for control subjects was 93±11.3%, 96±5.6%, 97±8.5%, and 98±5.6% for the IC_wide, IC_narrow, NC_wide, and NC_narrow conditions, respectively. These values for patients were 97±5.6%, 92±6%, 97±5.17.0%, and 90±11.3%. Values from individual participants were statistically analyzed with a 2x2x2 repeated measures non-parametric F-test using the within subjects factors of stimulus eccentricity (wide vs. narrow) and stimulus condition (IC vs. NC) and the between subjects factor of clinical status (patients vs. controls). There were no main effects or interactions (all $p>0.18$). Thus, VEP effects are not readily explained by performance differences. These performance results also provide one level of evidence that all participants were able to allocate their attention to the stimuli.

6.2.4.b Electrophysiological results

A first level of analysis of the VEP was performed using individual voltage waveforms, though we would remind the reader that our conclusions were based on reference-independent global

measures detailed below. Responses from a parietal midline electrode (Pz) are shown in Figure 24 for controls and patients as a function of stimulus condition and stimulus eccentricity. Visual inspection of these waveforms suggests several effects. First, there appears to be a main effect of group, such that patients would appear to have a generally smaller P1 than controls (see also Foxe et al., 2005). Second, healthy controls appear to exhibit modulation over P1 VEP latencies as a function of stimulus eccentricity, whereas patients with schizophrenia do not. Third and by contrast, responses from both populations appear to modulate over N1 VEP latencies as a function of stimulus condition (i.e. as a function of illusory contour presence). These observations were statistically evaluated via a time-point by time-point 2x2x2 mixed model repeated measures non parametric F-test. There was a main effect of eccentricity over the 56-104ms and 124-150ms post-stimulus intervals. Responses were generally larger for the 'wide' than 'narrow' inducer arrays. There was also a main effect of stimulus condition over the 116-184ms, 352-446ms and 460-500ms post-stimulus intervals. Responses were generally larger to IC than NC stimuli. There was a main effect of group over the 58-100ms post stimulus interval, with generally stronger responses for controls than patients. Additionally, there was a significant group x stimulus eccentricity interaction over the 66-108ms post-stimulus interval and a group x stimulus condition interaction over the 256-274ms post-stimulus interval.

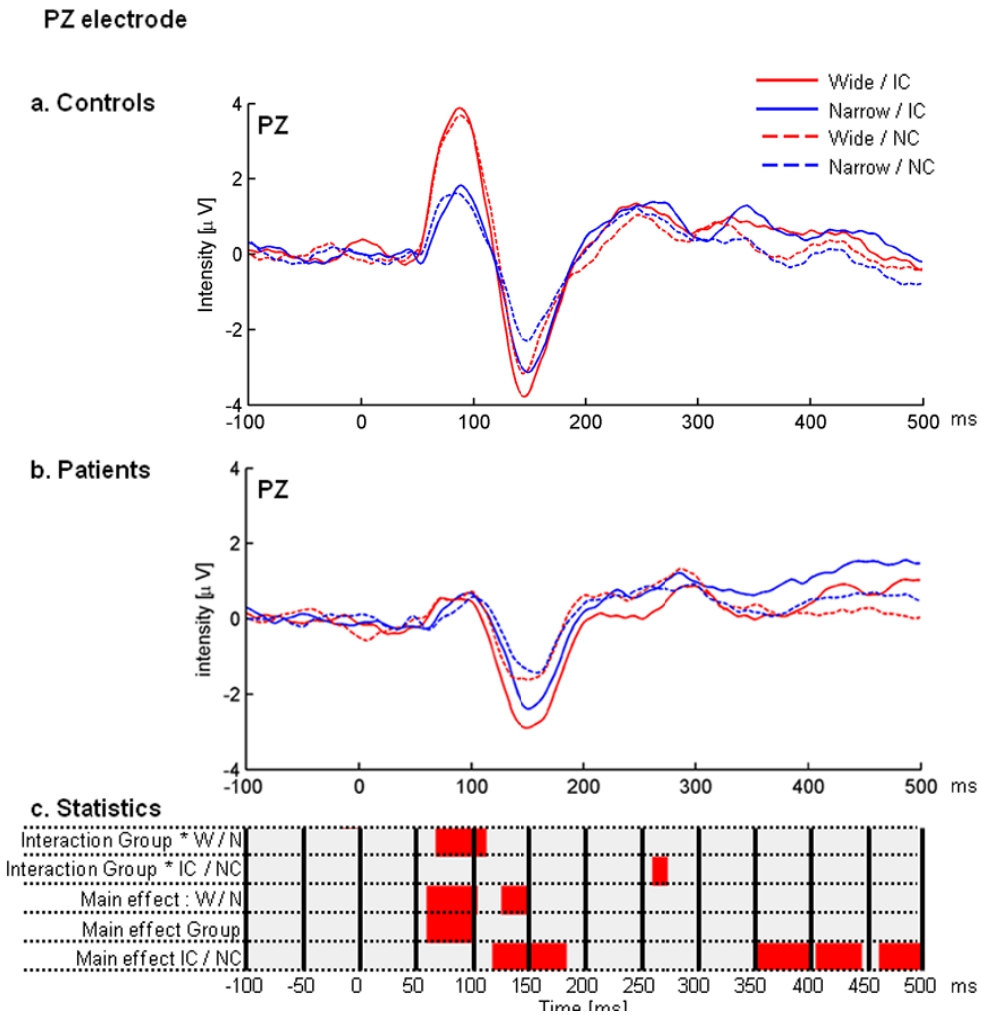

Figure 24 : Schizophrenia article ; Waveform results
Exemplar group-average VEPs from healthy controls (panel a) and chronic patients with schizophrenia (panel b) at a parietal midline scalp site (Pz). In these plots the solid lines represent the illusory contour (IC) stimulus condition and the dotted lines the non-illusory contour (NC) stimulus condition. Red lines refer to the wide stimulus eccentricity and blue to the narrow stimulus eccentricity. Panel c displays the results of a time-point by time-point non-parametric F-test on the VEP at electrode Pz (alpha ≤0.05; temporal criterion of at least 6 contiguous time-points).

As described in the Materials and Methods, the VEP data were analyzed using electrical neuroimaging methods to independently identify modulations in response strength and response topography. Mean GFP waveforms are displayed in Figure 25 in response to each condition for each population separately. As above, visual inspection of these waveforms suggests that healthy controls exhibit modulation over P1 VEP latencies as a function of stimulus eccentricity, whereas patients with schizophrenia do not. By contrast, responses from both populations appear to modulate over N1 VEP latencies as a function of stimulus condition (i.e. as a function of illusory contour presence). These observations were statistically evaluated via a time-point by time-point 2x2x2 mixed model repeated measures non parametric F-test. There was a main effect of eccentricity over the 74-96ms and 108-138ms post-stimulus intervals, with generally stronger responses to 'wide' than 'narrow' inducer arrays. There was also a main effect

of stimulus condition over the 126-170ms post-stimulus interval, with generally stronger responses to IC than NC stimuli. There was no evidence for a main effect of group at any latency, suggesting that clinical status did not lead to a general change in VEP strength. This also provides an argument against explanations in terms of attention differences or the fact that patients were medicated.

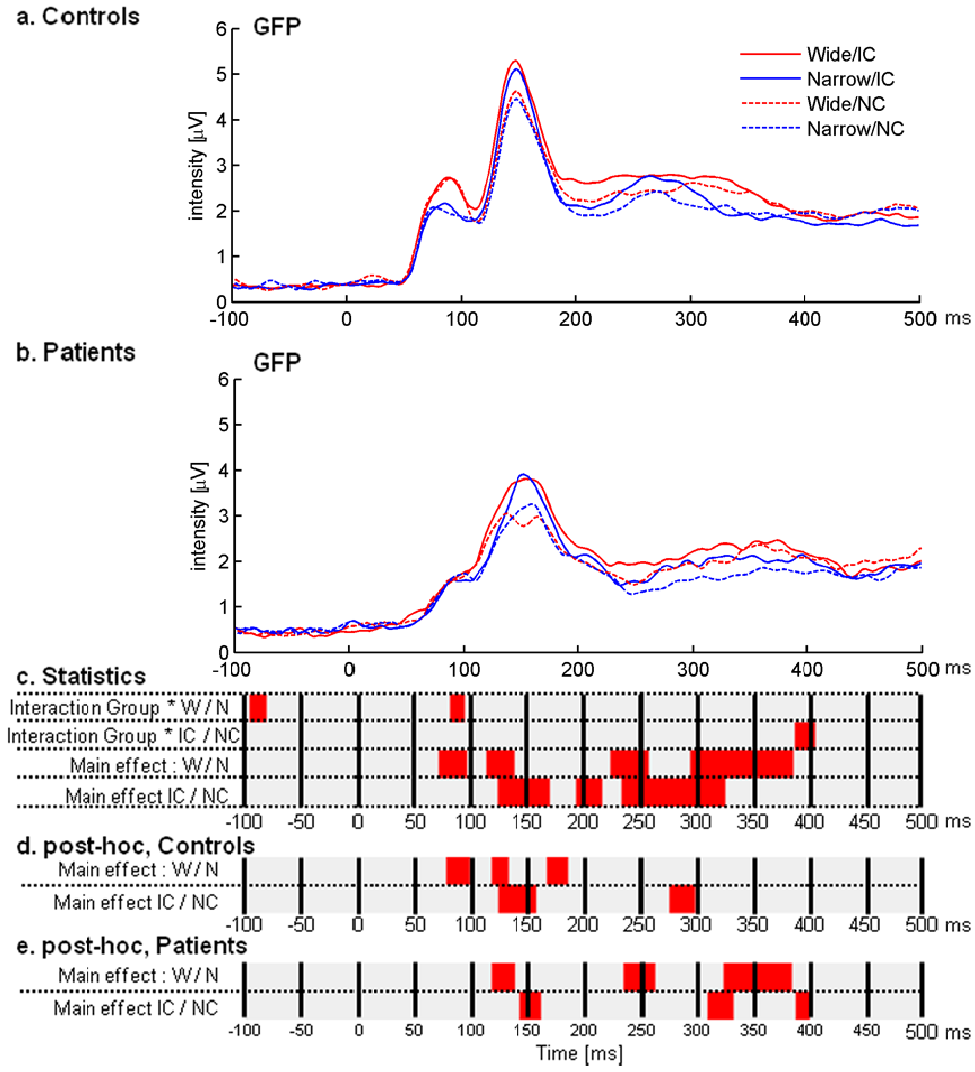

Figure 25 : Schizophrenia article ; GFP results
Group-average global field power (GFP) waveforms from healthy controls (panel a) and chronic patients with schizophrenia (panel b). Conventions for the plots are identical to those in Figure 2. Panel c displays the results of a time-point by time-point non-parametric F-test on the GFP (alpha ≤0.05; temporal criterion of at least 6 contiguous time-points). Panels d and e display the post-hoc analyses on each group using the same criteria as in panel c.

Of principal interest to the aims of the present study, there was a significant group x stimulus eccentricity interaction over the 84-94ms post-stimulus interval. In order to better identify the basis of this interaction, additional 2x2 within subject repeated measures non parametric F-tests

were performed as a function of time. In the case of healthy controls, there was a main effect of stimulus eccentricity over the 78-96ms, 118-130ms, and 168-184ms post-stimulus intervals. There was also a main effect of stimulus condition over the 124-156ms post-stimulus interval. In the case of patients with schizophrenia, there was a main effect of stimulus eccentricity over the 114-136ms interval. There was also a main effect of stimulus condition over the 144-160ms post-stimulus interval. Thus, controls but not patients exhibited robust modulation with stimulus eccentricity during the P1 period. We would add that there was also a significant interaction between group and stimulus condition over the 388-404ms post-stimulus interval. However, we do not discuss this effect in detail here for two main reasons. First, this effect is considerably subsequent to effects and interactions involving stimulus eccentricity. Second, this effect echoes that which we have previously reported in our original study (Foxe et al., 2005).

Modulations in response topography within and between groups were investigated using a cluster analysis. Across the concatenated dataset (i.e. the grand-average VEPs for the full 2x2x2 design), 13 template maps were identified that explained 96.06 % of the variance. Indistinguishable topographies were observed across groups, stimulus conditions, and stimulus eccentricities at all latencies, with the exception of the 54-108ms post-stimulus period (i.e. the P1 component). Over this time period, two maps were observed in the responses from healthy controls that differed between 'wide' and 'narrow' eccentricities irrespective of IC vs. NC stimulus condition. By contrast, all responses from patients with schizophrenia were described by a single map. These observations at the grand-average level were statistically examined at the single-subject level using a 2x2x2x2 repeated measures non-parametric F-test on the output of the fitting procedure described in Materials and Methods; the additional factor being map. This analysis revealed significant interactions between eccentricity and map ($p=0.001$) as well as between group, eccentricity, and map ($p=0.01$) see Figure 26. Because topographic differences forcibly follow from differences in the configuration of the underlying sources (Lehmann, 1987), this pattern of results demonstrates that patients and controls differ in the brain networks recruited to differentiate between wide and narrow stimulus eccentricities over the 54-108ms period.

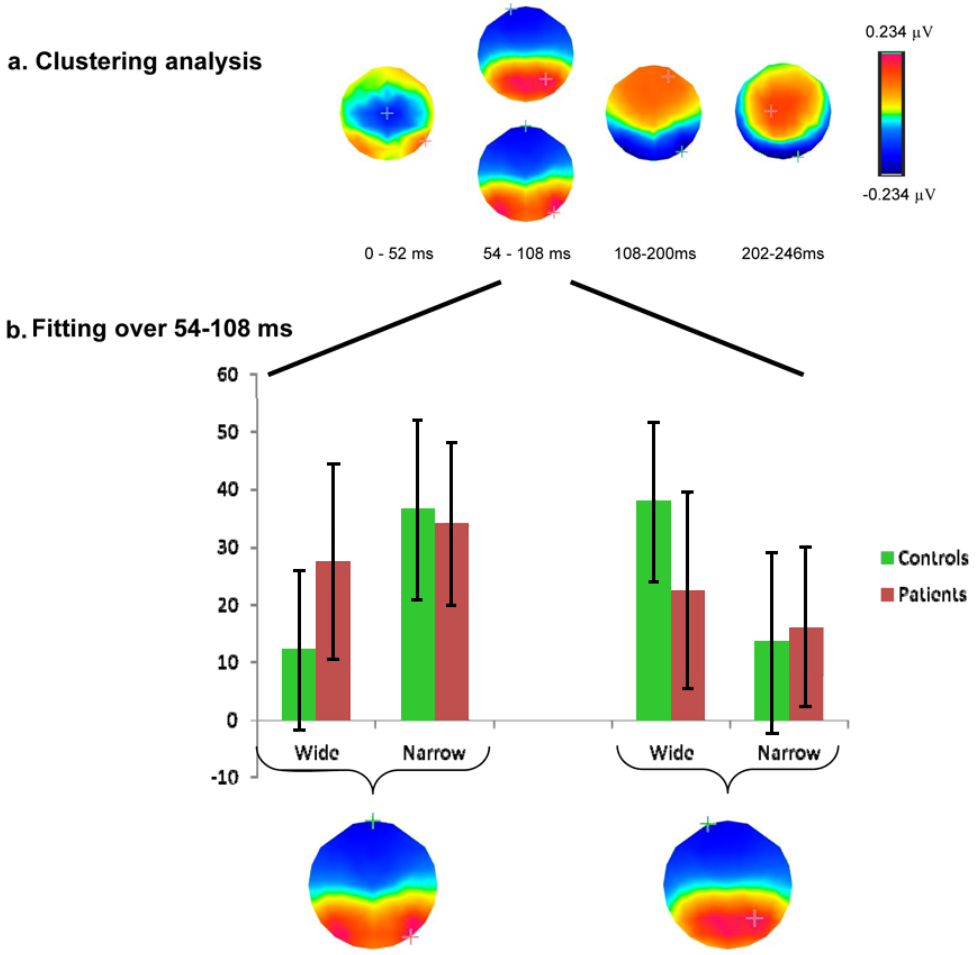

Figure 26 : Schizophrenia article ; Topographical segmentation and fitting results
Panel a displays the results of the topographic cluster analysis of the group-averaged VEPs from both patients and controls. Over the initial ~250ms post-stimulus period, 4 topographies were identified in the group-averaged dataset. Two of these were observed over the 54-108ms post-stimulus period and were in turn used for single-subject fitting (see Materials and Methods for details). Panel b displays the results of the single-subject fitting analysis wherein both of the two topographies identified over the 54-108ms was spatially correlated with the instantaneous VEP. The bar graph shows the mean amount of time (over the 54-108ms post-stimulus interval) labeled with each topography (s.d. indicated) as a function of each cohort, stimulus condition, and stimulus eccentricity.

Distributed source estimations were performed on single-subject data after first averaging the VEPs as a function of time over the 54-108ms post-stimulus interval. This period was selected based on the above topographic clustering analysis. For each node within the solution space we performed a 2X2X2 repeated measures non parametric F-test (clinical status X stimulus condition X stimulus eccentricity). We applied a $p<0.01$ threshold at the single-node level in conjunction with a 6-node spatial extent criterion. There was a significant clinical status X stimulus eccentricity interaction within two circumscribed brain regions (Figure 27). To label the location of these brain regions, we used a weighted mean across nodes (using 1-p-values)

and selected the node with the maximal value within each region. The clinical status X stimulus eccentricity interaction was observed within Brodmann Areas 7/31 (i.e. left precuneus and medial inferior parietal cortex) and Brodmann Area 3 (i.e. left post-central gyrus). The basis for this interaction within each region was due to wide vs. narrow modulations in healthy controls, but not in chronic patients (Figure 27)

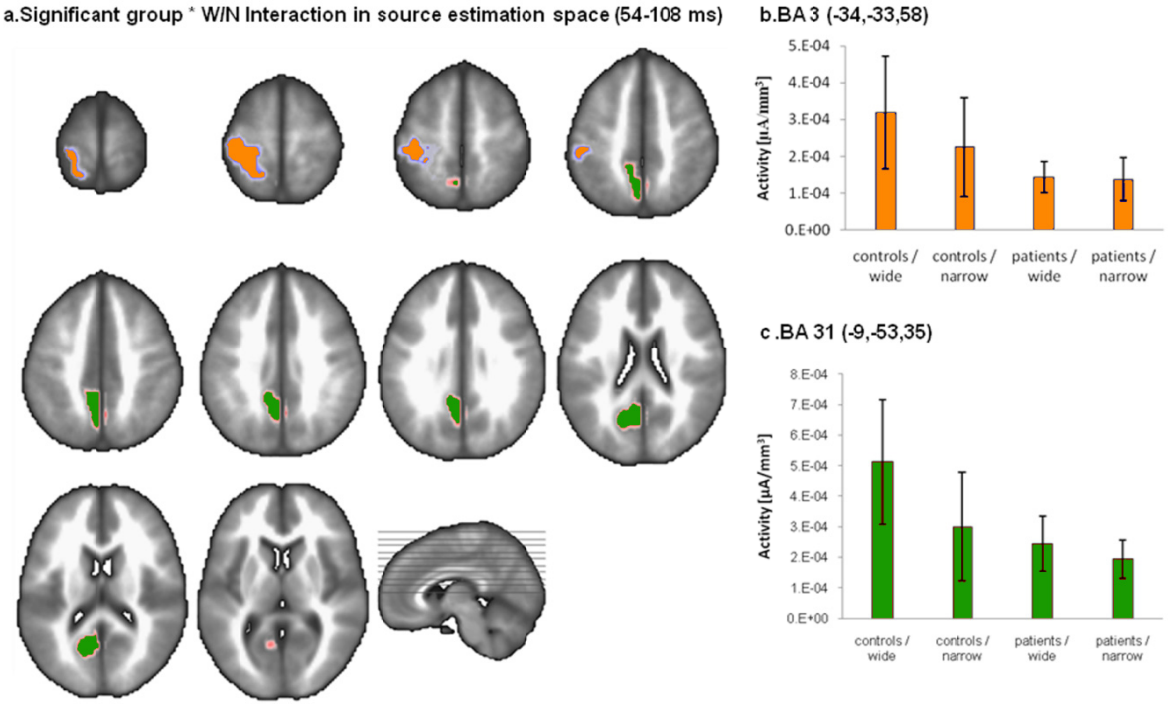

Figure 27 : Schizophrenia article ; Source estimation Results
Source estimation analyses. Panel a depicts the loci within the source estimation space that exhibited a significant group * stimulus eccentricity interaction (non-parametric F-test). This test was performed after first averaging the VEPs from each condition and group as a function of time (54-108ms) to obtain a single vector per participant and condition that was in turn submitted to the source estimation and statistically analyzed. Two clusters were identified, which for clarity are colored orange and green. Panels b and c display the mean (s.d. indicated) scalar values within the cluster and across subjects and stimulus conditions. In both clusters, controls exhibited a significant difference between wide and narrow stimulus eccentricities, whereas patients did not.

6.2.5 Discussion

The present findings deepen our understanding of early, low-level sensory processing impairments in patients with chronic schizophrenia. To date, general visual impairments have been documented without also assessing whether such diminished responses also exhibited intact modulations with stimulus or task parameters. Here, we showed that the P1 deficit is not simply due to attenuated responses in patients. Rather, there was an interaction between spatial features of the stimuli and clinical status, such that patients failed to exhibit a P1 modulation as a function of stimulus eccentricity while controls exhibited larger and topographically distinct

responses to widely distributed stimuli. Not only were P1 responses indistinguishable between wide and narrow stimulus eccentricities, but the VEP topography in patients was characterized by that accounting for responses to the narrow condition in healthy controls. That is, patients responded to both eccentricities as if they were "narrow". Source estimations further revealed that this impairment followed from diminished activity within parietal structures, consistent with models implicating magnocellular and/or dorsal visual stream processing impairments in schizophrenia. Importantly, the temporal resolution of VEP and electrical neuroimaging analyses revealed that patients did indeed exhibit sensitivity to spatial stimulus features at subsequent processing stages when control subjects also exhibited recursive treatment of this feature, ruling out explanations in terms of general insensitivity.

Prior studies have documented reduced P1 responses to visual stimuli not only in chronic patients (Foxe et al. 2001; Doniger et al. 2002; Foxe et al. 2005; Butler et al. 2007), but also in their first-degree relatives (Yeap et al. 2006). In the Yeap et al. 2006 study a substantial P1 reduction was demonstrated in response to isolated-check stimuli in both patients as well as their first-degree relatives compared to controls. These findings are suggestive of a potential endophenotype, though more recently Yeap et al. 2009 observed a similar impairment in patients with bipolar disorder. Thus, the specificity of the P1 reduction remains to be established. The present study, which we would emphasize is a more fine-grained analysis of a subset of the data in Foxe et al. (2005), highlights analytical methods that may assist in differentiating patient populations according to specific functional impairments and/or specific patterns of VEP modulations (e.g. topographic vs. strength) during the P1 component (or other periods) that in turn would reflect distinct neurophysiologic mechanisms and/or clinical states. Source estimations of effects in the present study revealed significant differences between healthy controls and chronic patients within the left precuneus and medial inferior parietal cortex as well as the left pre-central gyrus. On the one hand, the left-hemisphere laterality of this localization is also consistent with prior studies (Roemer et al., 1978; though see Butler et al., 2006). On the other hand, this localization is consistent with a deficit within the dorsal visual pathway (see also Sehatpour al., 2010).

While sensitivity to the spatial eccentricity of the inducers was impaired over the P1 component, intact processing of this feature by chronic patients was indeed observed at subsequent processing stages. That is, main effects of stimulus eccentricity were observed in both groups over the 100-150ms post-stimulus interval both at the level of individual scalp electrodes (Figure 24) and also at the level of Global Field Power (Figure 25). Thus, impaired sensitivity to the spatial eccentricity of stimuli would appear to be delimited to early time periods. At later latencies (i.e. ~250ms and thereafter), by contrast, there was evidence for main effects of

stimulus eccentricity in patients that were not evident in controls. One possibility is that such effects constitute a compensatory mechanism in patients for early spatial processing impairments. This possibility is particularly tempting in light of psychophysical evidence that patients are impaired in hierarchical processing of visual stimuli, favoring global over local percepts (e.g.Coleman et al. 2009). A speculative possibility is that compensatory mechanisms for early deficits that particularly effect sensitivity to wider spatial distributions result in a subsequent hyper-sensitivity to spatially distributed information.

Several aspects of our findings speak against an explanation in terms of generally diminished attention or arousal in patients vs. controls. First, performance by the patients on the discrimination of the presence vs. absence of illusory contour stimuli was indistinguishable from that of controls, suggesting that patients were adequately engaged in the task and did not find it more (or less) demanding than control subjects. Second, the wide/narrow difference was not requisite to the task of illusory contour presence discrimination. Such being said, sensitivity to the spatial position and orientation of the inducer stimuli was (likely) necessary for accurate performance. Finally, our analyses revealed that while sensitivity to the wide/narrow distribution of inducers was not observed over the P1 period, it was indeed observed at subsequent time periods preceding the initial sensitivity to the presence vs. absence of illusory contours. This would suggest that any deficit is not general, but rather likely specific to early stages of spatial processing; though fully resolving this will require additional investigations. Plus, it will be informative to examine to what extent and in what manner factors like spatial attention impact patients' sensitivity to the spatial features of the stimuli. For example, it may be the case that early-latency deficits like that reported here persist even when attention (viz. task demands) is directed to the spatial distribution of the stimuli. By contrast, subsequent stages, which in the present paradigm were intact, might well become susceptible to impairments when spatial attention is also at play, given previous demonstrations of impaired attention-related functions in patients with schizophrenia (e.g. Schwartz et al. 2001).

An alternative explanation for the VEP modulation seen in control subjects is that the differences are due to the position of the inducers (in terms of their polar angle) rather to their spatial eccentricity. That is, the inducers defining the circle (as well as its NC counterpart) are located along the horizontal and vertical meridians, whereas those defining the square (and its NC counterpart) are located along the diagonals. Any VEP differences would therefore reflect this polar angle difference in stimulus position, rather than their eccentricity per se. If this were indeed the case, then the deficit reported here for patients with schizophrenia would be indicative of impaired processing of specific retinotopic positions – something to our knowledge that has yet to be documented (cf. Martínez et al. 2008 for retinotopic mapping data in patients).

Nonetheless, we consider such an account unlikely because the present VEP modulations as a function of inducer eccentricity can be observed even when controlling for their position in terms of polar angle (Murray et al., 2002). Plus, the localization of the statistical differences in the source estimations observed in the present study within parietal structures provides a further argument against a purely retinotopic impairment in patients with schizophrenia.

6.2.6 Acknowledgements

We thank Gail Silipo for assistance with patient recruitment and for conducting clinical examinations. The Cartool software (http://brainmapping.unige.ch/Cartool.htm) has been programmed by Denis Brunet, from the Functional Brain Mapping Laboratory, Geneva, Switzerland, and is supported by the Center for Biomedical Imaging (CIBM) of Geneva and Lausanne. Funding for this study was provided by the Swiss National Science Foundation (grants 31003A_118419 and 320030_120579 to MMM), the Leenaards Foundation (2005 Prize for the Promotion of Scientific Research (to MMM), and National Institutes of Mental Health (grant R37 MH49334 to DCJ). None of the funding sources had any further role in study design; in the collection, analysis and interpretation of data; in the writing of the report; and in the decision to submit the paper for publication.

6.2.7 References

Brenner, C.A., Lysaker, P.H., Wilt, M.A., O'Donnell, B.F., 2002. Visual processing and neuropsychological function in schizophrenia and schizoaffective disorder. Psychiatry Res 111, 125-136.

Butler, P.D., Schechter, I., Zemon, V., Schwartz, S.G., Greenstein, V.C., Gordon, J., Schroeder, C.E., Javitt, D.C., 2001. Dysfunction of early-stage visual processing in schizophrenia. Am J Psychiatry 158, 1126-1133.

Butler, P.D., DeSanti, L.A., Maddox, J., Harkavy-Friedman, J.M., Amador, X.F., Goetz, R.R., Javitt, D.C., Gorman, J.M., 2003. Visual backward-masking deficits in schizophrenia: relationship to visual pathway function and symptomatology. Schizophr. Res 59, 199-209.

Butler, P.D., Hoptman, M.J., Nierenberg, J., Foxe, J.J., Javitt, D.C., Lim, K.O., 2006. Visual white matter integrity in schizophrenia. Am J Psychiatry 163, 2011-2013.

Butler, P.D., Javitt, D.C., 2005. Early-stage visual processing deficits in schizophrenia. Curr Opin Psychiatry 18, 151-157.

Butler, P.D., Martinez, A., Foxe, J.J., Kim, D., Zemon, V., Silipo, G., Mahoney, J., Shpaner, M., Jalbrzikowski, M., Javitt, D.C., 2007. Subcortical visual dysfunction in schizophrenia drives secondary cortical impairments. Brain 130, 417-430.

Cadenhead, K.S., Serper, Y., Braff, D.L., 1998. Transient versus sustained visual channels in the visual backward masking deficits of schizophrenia patients. Biol. Psychiatry 43, 132-138.

Coleman, M.J., Cestnick, L., Krastoshevsky, O., Krause, V., Huang, Z., Mendell, N.R., Levy, D.L., 2009. Schizophrenia patients show deficits in shifts of attention to different levels of global-local stimuli: evidence for magnocellular dysfunction. Schizophr Bull 35, 1108-1116.

Doniger, G.M., Foxe, J.J., Murray, M.M., Higgins, B.A., Javitt, D.C., 2002. Impaired Visual Object Recognition and Dorsal/Ventral Stream Interaction in Schizophrenia. Arch Gen Psychiatry 59, 1011-1020.

Foxe, J.J., Doniger, G.M., Javitt, D.C., 2001. Early visual processing deficits in schizophrenia: impaired P1 generation revealed by high-density electrical mapping. Neuroreport 12, 3815-3820.

Foxe, J.J., Murray, M.M., Javitt, D.C., 2005. Filling-in in Schizophrenia: a High-density Electrical Mapping and Source-analysis Investigation of Illusory Contour Processing. Cereb. Cortex 15, 1914-1927.

Goldberg TE, Gold JM, 1995. Neurocognitive functioning in patients with schizophrenia: an overview, in: Kupfer DJ (Éd.), Psychopharmacology, the fourth generation of progress. p. 1245-1257.

Goldman-Rakic, P.S., 1994. Working memory dysfunction in schizophrenia. J Neuropsychiatry Clin Neurosci 6, 348-357.

Gonzalez Andino, S.L., Michel, C.M., Thut, G., Landis, T., Grave de Peralta, R., 2005. Prediction of response speed by anticipatory high-frequency (gamma band) oscillations in the human brain. Hum Brain Mapp 24, 50-58.

Gonzalez Andino, S.L., Murray, M.M., Foxe, J.J., de Peralta Menendez, R.G., 2005. How single-trial electrical neuroimaging contributes to multisensory research. Exp Brain Res 166, 298-304.

Grave de Peralta Menendez, R., Gonzalez Andino, S., Lantz, G., Michel, C.M., Landis, T., 2001. Noninvasive localization of electromagnetic epileptic activity. I. Method descriptions and simulations. Brain Topogr 14, 131-137.

Grave de Peralta Menendez, R., Murray, M.M., Michel, C.M., Martuzzi, R., Gonzalez Andino, S.L., 2004. Electrical neuroimaging based on biophysical constraints. Neuroimage 21, 527-539.

Green, M.F., 1998. Schizophrenia from a neurocognitive perspective. Boston, MA: Allyn & Bacon.

Guthrie, D., Buchwald, J.S., 1991. Significance testing of difference potentials. Psychophysiology 28, 240–4.

Javitt, D.C., 2009. When doors of perception close: bottom-up models of disrupted cognition in schizophrenia. Annu Rev Clin Psychol 5, 249-275.

Kanizsa, G., 1976. Subjective contours. Sci. Am 234, 48-52.

Kiss, I., Fábián, A., Benedek, G., Kéri, S., 2010. When doors of perception open: visual contrast sensitivity in never-medicated, first-episode schizophrenia. J Abnorm Psychol 119, 586-593.

Koenig, T., Melie-Garcia, L., 2010. A method to determine the presence of averaged event-related fields using randomization tests. Brain Topogr 23, 233–242.

Lavoie, S., Murray, M.M., Deppen, P., Knyazeva, M.G., Berk, M., Boulat, O., Bovet, P., Bush, A.I., Conus, P., Copolov, D., Fornari, E., Meuli, R., Solida, A., Vianin, P., Cuénod, M., Buclin, T., Do, K.Q., 2008. Glutathione precursor, N-acetyl-cysteine, improves mismatch negativity in schizophrenia patients. Neuropsychopharmacology 33, 2187-2199.

Lehmann, D., 1987. Principles of spatial analysis. In: Gevins AS, Remond A, editors. Handbook of electroencephalography and clinical neurophysiology, vol. 1: methods of analysis of brain electrical and magnetic signals. Amsterdam: Elsevier, pp. 309–54.

Lehmann, D., Skrandies, W., 1980. Reference-free identification of components of checkerboard-evoked multichannel potential fields. Electroencephalogr Clin Neurophysiol 48, 609–621.

Martínez, A., Hillyard, S.A., Dias, E.C., Hagler, D.J., Butler, P.D., Guilfoyle, D.N., Jalbrzikowski, M., Silipo, G., Javitt, D.C., 2008. Magnocellular pathway impairment in schizophrenia: evidence from functional magnetic resonance imaging. J. Neurosci 28, 7492-7500.

Martuzzi, R., Murray, M.M., Meuli, R.A., Thiran, J., Maeder, P.P., Michel, C.M., Grave de Peralta Menendez, R., Gonzalez Andino, S.L., 2009. Methods for determining frequency- and region-dependent relationships between estimated LFPs and BOLD responses in humans. J. Neurophysiol 101, 491-502.

Michel, C.M., Murray, M.M., Lantz, G., Gonzalez, S., Spinelli, L., Grave de Peralta, R., 2004. EEG source imaging. Clin Neurophysiol 115, 2195-2222.

Murray MM, De Lucia M, Brunet D, Michel CM, 2009. Principles of Topographic Analyses for Electrical Neuroimaging. In : Brain Signal Analysis: Advances in Neuroelectric and Neuromagnetic Methods. MIT Press (Handy TC, Ed).

Murray, M.M., Brunet, D., Michel, C.M., 2008. Topographic ERP analyses: a step-by-step tutorial review. Brain Topogr 20, 249-264.

Murray, M.M., Wylie, G.R., Higgins, B.A., Javitt, D.C., Schroeder, C.E., Foxe, J.J., 2002. The spatiotemporal dynamics of illusory contour processing: combined high-density electrical mapping, source analysis, and functional magnetic resonance imaging. J. Neurosci 22, 5055-5073.

Perrin, F., Bertrand, O., Pernier, J., 1987. Scalp current density mapping: value and estimation from potential data. IEEE Trans Biomed Eng 34, 283-288.

Ringach, D.L., Shapley, R., 1996. Spatial and temporal properties of illusory contours and amodal boundary completion. Vision Res 36, 3037-3050.

Roemer, R.A., Shagass, C., Straumanis, J.J., Amadeo, M., 1978. Pattern evoked potential measurements suggesting lateralized hemispheric dysfunction in chronic schizophrenics. Biol. Psychiatry 13, 185-202.

Schwartz, B.D., Maron, B.A., Evans, W.J., Winstead, D.K., 1999. High velocity transient visual processing deficits diminish ability of patients with schizophrenia to recognize objects. Neuropsychiatry Neuropsychol Behav Neurol 12, 170-177.

Schwartz, B.D., Tomlin, H.R., Evans, W.J., Ross, K.V., 2001. Neurophysiologic mechanisms of attention: a selective review of early information processing in schizophrenics. Front. Biosci 6, D120-134.

Sehatpour, P., Dias, E.C., Butler, P.D., Revheim, N., Guilfoyle, D.N., Foxe, J.J., Javitt, D.C., 2010. Impaired visual object processing across an occipital-frontal-hippocampal brain network in schizophrenia: an integrated neuroimaging study. Arch. Gen. Psychiatry 67, 772-782.

Spinelli, L., Andino, S.G., Lantz, G., Seeck, M., Michel, C.M., 2000. Electromagnetic inverse solutions in anatomically constrained spherical head models. Brain Topogr 13, 115-125.

Spitzer, R.L., Williams, J.B., Gibbon, M., First, M.B., 1992. The Structured Clinical Interview for DSM-III-R (SCID). I: History, rationale, and description. Arch. Gen. Psychiatry 49, 624-629.

Talairach J, Tournoux P, 1988. Co-planar stereotaxic atlas of the human brain, Thieme. ed. New York.

Umbricht, D., Schmid, L., Koller, R., Vollenweider, F.X., Hell, D., Javitt, D.C., 2000. Ketamine-induced deficits in auditory and visual context-dependent processing in healthy volunteers: implications for models of cognitive deficits in schizophrenia. Arch. Gen. Psychiatry 57, 1139-1147.

Umbricht, D.S.G., Bates, J.A., Lieberman, J.A., Kane, J.M., Javitt, D.C., 2006. Electrophysiological indices of automatic and controlled auditory information processing in first-episode, recent-onset and chronic schizophrenia. Biol. Psychiatry 59, 762-772.

Weinberger, D.R., Gallhofer, B., 1997. Cognitive function in schizophrenia. Int Clin Psychopharmacol 12 Suppl 4, S29-36.

Yeap, S., Kelly, S.P., Reilly, R.B., Thakore, J.H., Foxe, J.J., 2009. Visual sensory processing deficits in patients with bipolar disorder revealed through high-density electrical mapping. J Psychiatry Neurosci 34, 459-464.

Yeap, S., Kelly, S.P., Sehatpour, P., Magno, E., Javitt, D.C., Garavan, H., Thakore, J.H., Foxe, J.J., 2006. Early visual sensory deficits as endophenotypes for schizophrenia: high-density electrical mapping in clinically unaffected first-degree relatives. Arch. Gen. Psychiatry 63, 1180-1188.

6.3 Towards a resolution of conflicting models of illusory contour processing in humans

Jean-François Knebel[1,2] and Micah M. Murray[1,2,3]

[1]Department of Clinical Neurosciences, [2]Radiology Department

Vaudois University Hospital Center and University of Lausanne, Switzerland

[3]EEG Brain Mapping Core, Center for Biomedical Imaging of Lausanne and Geneva, Switzerland

*Address correspondence to:

Micah M. Murray (micah.murray@chuv.ch)

6.3.1 Acknowledgements

This work has been supported by the Swiss National Science Foundation (grants 310030B_133136 and 320000_120579). Cartool software (http://brainmapping.unige.ch/Cartool.htm) has been programmed by Denis Brunet, from the Functional Brain Mapping Laboratory, Geneva, Switzerland, and is supported by the EEG Brain Mapping Core of the Center for Biomedical Imaging (www.cibm.ch) of Geneva and Lausanne. We thank Laurent Udry and Melanie Aeschlimann for their assistance during data collection.

6.3.2 Abstract

Despite numerous studies, the neurophysiologic mechanism mediating illusory contour (IC) sensitivity remains controversial. Three general models can be distinguished. One favors effects within lower-tier cortices, V1/V2, mediated by feed-forward inputs and/or long-range horizontal interactions. Another situates IC sensitivity within higher-tier cortices, principally lateral-occipital cortex (LOC), with feedback effects in V1/V2. Still others postulate that the LOC is sensitive to salient regions demarcated by the inducing stimuli, whereas effects within V1/V2 reflect specifically IC sensitivity. The present study resolved discordances between these models by using misaligned line gratings, oriented either horizontally or vertically, to induce ICs. These particular stimuli lack salient regions otherwise present in Kanizsa-type stimuli. Plus, varying line orientation one can assay early, low-level (V1/V2) modulations independently of IC

presence. Using this 2x2 within subject design, we recorded 160-channel visual evoked potentials (VEPs) from 15 healthy humans and disambiguated the relative timing and localization of IC sensitivity with respect to that for grating orientation (as well as any interactions between these features). Millisecond-by-millisecond analyses of VEPs, response strength, as well as of distributed source estimations revealed a main effect of grating orientation beginning at 65ms post-stimulus onset within the calcarine sulcus (and elsewhere) that was followed by a main effect of IC presence beginning at 85ms post-stimulus onset within the LOC and extending dorsally into inferior parietal cortices. There was no evidence for differential processing of ICs as a function of the orientation of the grating. The collective results support models wherein IC sensitivity occurs first within the LOC.

6.3.3 Introduction

Object recognition is possible despite degraded visual conditions and impediments that produce discontinuous or absent boundaries within or between objects. Experimentally, stimuli producing illusory contours (ICs) have been used to mimic these conditions (Figure 28). Despite extensive research in humans and animals, controversy persists regarding the neurophysiologic mechanisms of IC perception (Seghier and Vuilleumier, 2006).

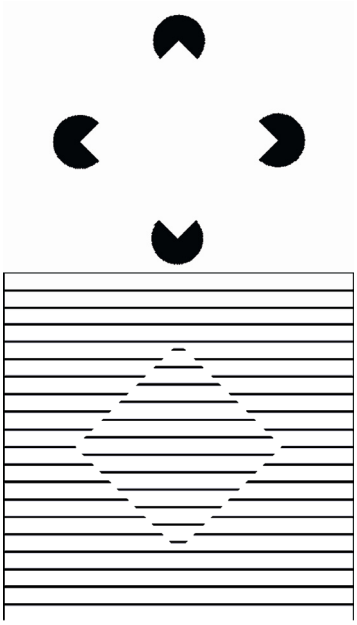

Figure 28: Examples of illusory contours
The upper panel illustrates a typical Kanizsa-type (Kanizsa, 1979) stimulus wherein pacmen inducers are oriented to generate the perception of a diamond. The lower panel illustrates a diamond induced by phase-shifting the linke gratings by 180°.

Three general models vary according to the region considered critical for discriminating illusory contours (Figure 29). One favors a predominant role of lower-tier cortices (V1/V2) through feed-forward and/or intrinsic long-range horizontal interactions (von der Heydt and Peterhans, 1989; Peterhans and von der Heydt, 1989; Grosof et al., 1993; Ffytche and Zeki, 1996; Sheth et al., 1996; Ramsden et al., 2001). Another favors higher-tier cortices, principally lateral-occipital cortex (LOC), as being the first to exhibit sensitivity to the presence of ICs(Mendola et al., 1999; Kruggel et al., 2001; Pegna et al., 2002; Murray et al., 2002, 2004, 2006; Halgren et al., 2003; Brighina et al., 2003; Foxe et al., 2005; de-Wit et al., 2009; alsoLee and Nguyen, 2001; Sáry et al., 2007, 2008). Still others postulate that the effects within LOC reflect sensitivity to salient regions demarcated by the inducing stimuli, whereas effects within V1/V2 reflect sensitivity to the illusory contour itself, though likely driven by feedback from LOC and/or other regions(Stanley and Rubin, 2003; Yoshino et al., 2006; through see Shpaner et al., 2009).

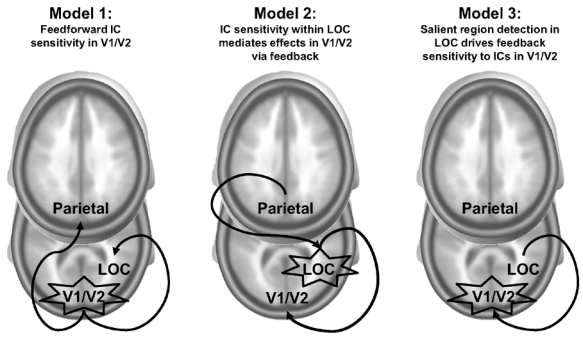

Figure 29: Schema of the three models of illusory contour differentiations
Model one supports a modulation "bottom-up" of high-level cortices to V1/V2 illusory contour differentiation. Model two supports an illusory differentiation in LOC and activities in other region are due to a "top-down" modulation. Model three supports a salient region differentiation in LOC and a illusory contour differentiation in V1/V2 "top-down" modulate by LOC.

Support for one or another of these models is contingent upon the recording method and choice of stimuli, particularly for studies in humans. Electroencephalographic (EEG) and magneto-encephalographic (MEG) recordings reliably demonstrate effects within LOC at ~100-150ms post-stimulus onset (Murray et al., 2002a, 2004a, 2006),but have failed to document early-latency effects within V1/V2; though embracing the null hypothesis is problematic. Late latency (presumably feedback) modulations have been reported based on MEG (Ohtani et al., 2002; Halgren et al., 2003).In the case of hemodynamic imaging, evidence for IC sensitivity within V1/V2 is similarly unreliable. Some report robust effects (Hirsch et al., 1995; Larsson et al., 1999; Seghier et al., 2000; Maertens and Pollmann, 2005; Montaser-Kouhsari et al., 2007), others

none (Kruggel et al., 2001; Murray et al., 2002b; Stanley and Rubin, 2003), and still others observed V1/V2 modulations with abutting gratings but not Kanizsa-type stimuli (Mendola et al., 1999).

Another contributing factor is therefore the choice of stimuli. Investigations in animals and humans suggest that misaligned gratings elicit larger response modulations than Kanizsa-type stimuli (Peterhans and von der Heydt, 1989; Mendola et al., 1999). Psychophysical data in humans likewise indicate there to be perceptual differences between these stimuli (Petry et al., 1983). Abutting gratings are advantageous insofar as line orientation reliably modulates low-level visual cortices in a bottom-up manner(Shapley, 2007). By applying electrical neuroimaging analyses of visual evoked potentials (VEPs; (Murray et al., 2008) in combination with a 2x2 within subject design that varied grating orientation and IC presence, we were able to determine the timing, locus, and independence of orientation sensitivity and IC sensitivity.

6.3.4 Materials and Methods

6.3.4.a Participants

A total of 18 individuals participated (9 males; 1 left-handed) in this study, aged 20-34 years at the time of EEG recording. No participant had a history of or current neurological or psychiatric illness. All had normal or corrected-to-normal vision. Data from 3 participants were excluded due to poor signal quality. The presented analyses are therefore based on a final population of 15 subjects (7 males; 1 left-handed), aged 20-34.

6.3.4.b Stimuli and Task

The stimuli were composed of vertical and horizontal line gratings of 3 different spatial frequencies (1, 2 and 3 cycles per degree) that appeared white on a black background (i.e. 100% contrast). These were the no contour (NC) stimuli. The IC stimuli were created by misaligning the gratings by half a cycle. There were 2 possible shapes – a circle and a diamond. There were thus a total of 18 distinct stimuli, and the presentation of an IC stimulus was twice as likely as that of an NC stimulus (we return to this when discussing the analyses of the VEPs). The spatial frequency and induced shape were varied to minimize adaptation effects across trials. Analyses were based on a 2x2 within subject design, involving factors of stimulus condition (IC vs. NC) and orientation of the gratings (horizontal vs. vertical).

The stimuli were presented within the context of an interposed auditory experiment that required participants to discriminate human vocalizations from other sound sources (Aeschlimann et al., in preparation). No task was required with the visual stimuli (note that prior

studies from our group have shown nearly identical effects with Kanizsa-type stimuli under active and passive conditions; Murray et al., 2002). Participants were instructed to fixate a centrally presented crosshair and to avoid blinking during stimulus presentations. Visual stimuli were presented for 200ms. The inter-stimulus interval (ISI) between the end of the sound (2s duration) and the visual stimuli (ISI1) varied from 500ms to 900ms. The ISI between the end of the visual stimuli (ISI2) and the next sound varied according to the equation (ISI2=1400ms – ISI1; ISI2 ϵ [500;900ms]). The order of visual stimuli within a block of trials stimuli was randomized, but each stimulus appeared 8 times within each block. Stimulus delivery and response recordings were controlled by E-Prime (Psychology Software Tools Inc., Pittsburgh, USA; www.pstnet.com/eprime). Stimuli were presented on a 21" CRT monitor at a viewing distance of 100cm from the participant.

6.3.4.c EEG acquisition and pre-processing

Continuous EEG was acquired at 1024Hz through a 160-channel Biosemi ActiveTwo AD-box (http://www.biosemi.com) referenced to the common mode sense (CMS; active electrode) and grounded to the driven right leg (DRL; passive electrode), which functions as a feedback loop driving the average potential across the electrode montage to the amplifier zero (full details, including a diagram of this circuitry, can be found at http://www.biosemi.com/faq/cms&drl.htm).

EEG epochs were time-locked to the presentation of visual stimuli and spanned 100ms pre-stimulus and 500ms post-stimulus. Epochs with amplitude deviations in excess of ±80μV at any channel, with the exception of those labeled as 'bad' due to poor electrode-skin contact or damage, were considered artifacts and were excluded. Likewise, trials with blinks or other transients were excluded off-line based on vertical and horizontal electrooculograms. Data from 'bad' channels were interpolated using 3D splines (Perrin et al. 1987). Prior to group-averaging VEPs, data were band-pass filtered (0.1-60Hz), re-calculated to an average reference, and baseline corrected using the pre-stimulus interval. For each participant, 6 VEPs were calculated that were each based on the acceptance of ~200 epochs (average across subject range 202 to 206; $F_{(5,70)}$=28.8, p=0.31). There were three stimulus varieties (NC, IC when forming a diamond, and IC when forming a circle) and two grating orientations (horizontal and vertical). Because preliminary VEP analyses failed to reveal differences between IC conditions that formed a diamond vs. circle, we collapsed these data in subsequent analyses by repeating the entry of the NC condition in the ANOVA. Analyses reported here are therefore based on a 2x2 within subjects design, including factors of stimulus condition (IC vs. NC) and stimulus orientation (horizontal vs. vertical gratings).

6.3.4.d EEG analyses

The analyses were performed using the Cartool software programmed by Denis Brunet (http://brainmapping.unige.ch/Cartool.htm). Effects were identified with an analysis procedure, referred to as electrical neuroimaging, which quantifies reference-independent global measures of the electric field at the scalp as well as distributed source estimations (Michel et al., 2004; Murray et al., 2008). Because our previous investigations have reliably demonstrated that IC sensitivity stems from modulations in response strength and not response topography (Murray et al., 2004b, 2006; Foxe et al., 2005; Shpaner et al., 2009), we focused our analyses of the electric field at the scalp on the quantification of global field power (GFP; Lehmann and Skrandies, 1980). GFP equals the spatial standard deviation across the electrode montage and yields larger values for stronger responses (Koenig and Melie-García, 2010). GFP values at each time point were compared with a repeated measures ANOVA. To account for temporal auto-correlation, only effects ($p<0.05$) persisting for at least 11 time frames (>10ms) were considered reliable (Guthrie and Buchwald, 1991).

In addition, we estimated the intracranial sources of the VEPs as a function of time using a distributed linear inverse solution (ELECTRA) and applying the local autoregressive average (LAURA) regularization approach to address the non-uniqueness of the inverse problem (Grave de Peralta Menendez et al., 2001, 2004; Michel et al., 2004). The inverse solution algorithm is based on biophysical principles derived from the quasi-static Maxwell's equations; most notably the fact that independent of the volume conductor model used to describe the head, only irrotational and not solenoidal currents contribute to the EEG (Grave de Peralta Menendez et al., 2001, 2004). As part of the regularization strategy, homogenous regression coefficients in all directions and within the whole solution space were used. LAURA uses a realistic head model, and the solution space included 3005 nodes, selected from a 6 × 6 × 6 mm grid equally distributed within the gray matter of the Montreal Neurological Institute's average brain (courtesy of Grave de Peralta Menendez and Gonzalez Andino; http://www.electrical-neuroimaging.ch/). The head model and lead field matrix were generated with the Spherical Model with Anatomical Constraints (SMAC;Spinelli et al., 2000). As an output, LAURA provides current density measures; the scalar values of which were evaluated at each node. Prior basic and clinical research has documented and discussed in detail the spatial accuracy of this inverse solution (e.g.Grave de Peralta Menendez et al., 2004; Michel et al., 2004; Gonzalez Andino, Michel, et al., 2005; Gonzalez Andino, Murray, et al., 2005; Martuzzi et al., 2009). The source estimations were calculated for each time point, subject and condition. These data matrices were then submitted to a repeated measures ANOVA as a function of time (see also Britz and Michel, 2010). To partially correct for multiple testing and temporal auto-correlation we applied an

significance threshold of $p<0.01$, a temporal criterion of 11 consecutive time-frames, and a spatial extent criterion of 15 contiguous solution points (see also De Lucia et al., 2010 for a similar approach).

6.3.5 Results

We would remind the reader that the subjects passively viewed the visual stimuli while centrally fixating (i.e. subjects were performing a task on intervening sounds). As such, there are no behavioral results to report, though prior work has shown near-ceiling performance on when discriminating the presence vs. absence of Kanizsa-type illusory contours and nearly identical VEP modulations for active vs. passive viewing conditions (e.g. Murray et al., 2002).

A first level of analysis of the VEP was performed using individual voltage waveforms, though we would remind the reader that our conclusions were based on reference-independent measures. VEPs from an occipital midline electrode (OZ) and a parieto-occipital electrode (PO6) are shown in Figure 30. Visual inspection of these waveforms was suggestive of two stages of differential responses: first an orientation differentiation (~60ms) followed by a modulation as a function of IC presence vs. absence (~100ms). These observations were statistically evaluated via a time-point by time-point 2x2 repeated measures ANOVA. There was a main effect of stimulus orientation (63-74ms at Oz and 74-112ms and 209-297ms at PO6). There was also a main effect of stimulus condition (228-291ms and 355-387ms for Oz and 107-143ms and 241-291ms for PO6). There was no evidence for an interaction at any latency.

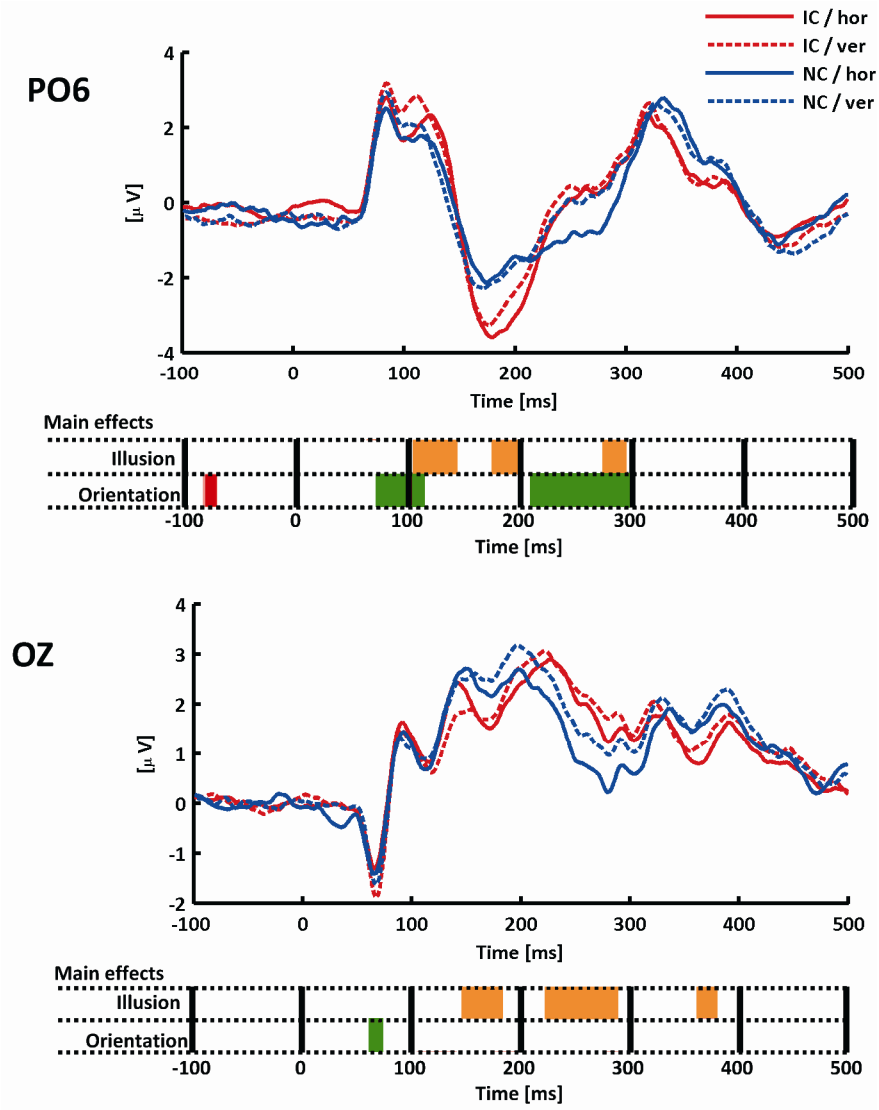

Figure 30 : misaligned gratings article waveform results
Exemplar group-average VEPs for parietal occipital electrodes PO6 and occipital electrodes OZ. In these plots the red lines represent the illusory contour (IC) stimulus condition and the blue lines the non-illusory contour (NC) stimulus condition. Solid lines refer to the horizontal stimulus condition and the dotted to the vertical stimulus condition. Below each electrode panel a statistical display shows the results of a time-point by time-point repeated measures ANOVA for each electrode (F(1,14); alpha ≤0.05; temporal criterion of at least 11 contiguous time-points).

As described in the Materials and Methods, the VEP data were analyzed using electrical neuroimaging methods; here principally in terms of reference-independent GFP waveforms. Group-averaged GFP waveforms from each condition are displayed in Figure 31. As above, Visual inspection of these waveforms suggests there to be differences as a function of stimulus orientation followed by effects of stimulus condition. These millisecond-wise 2x2 ANOVA on the GFP revealed a main effect of stimulus orientation over the 65-107ms, 128-175ms and 365-400ms post-stimulus intervals. Responses over the initial ~100ms were generally stronger responses to the 'vertical' than 'horizontal' condition (Maffei and Campbell, 1970). There was also a main effect of stimulus condition over the 85-102ms and 371-387ms post-stimulus

intervals, with generally stronger responses to IC than NC stimuli. There was no evidence for an interaction at any latency.

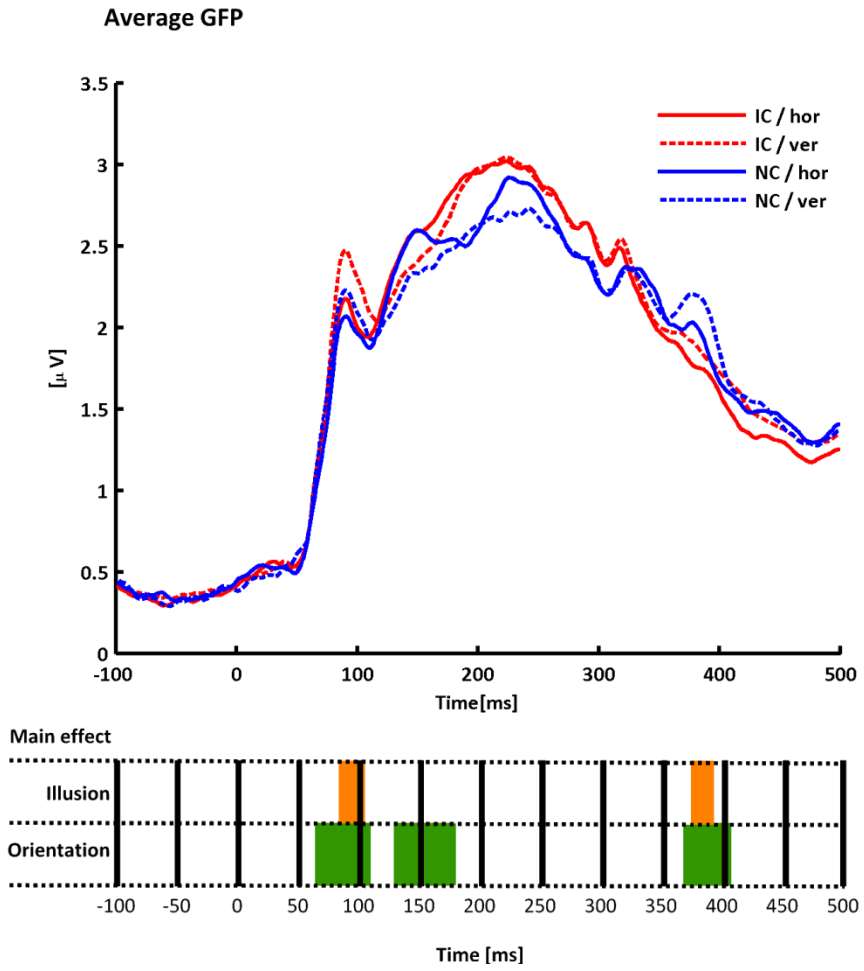

Figure 31: misaligned gratings article ; GFP results
Group-average global field power (GFP) waveforms conventions for the plots are identical to those in Figure 3. The bottom panel displays the results of a time-point by time-point repeated measures ANOVA on the GFP (F(1,14); alpha ≤0.05; temporal criterion of at least 11 contiguous time-points)

Given the above GFP results, the analyses of the source estimations focused on the initial 200ms post-stimulus interval. The repeated measures ANOVA revealed a main effect of stimulus orientation over the ~60-90ms post-stimulus period that was located in bilateral occipital and temporal regions, including the calcarine sulcus, with stronger responses to vertical than horizontal stimuli (Figure 32; red traces). A visualization of the distribution of this main effect is displayed at 66ms post-stimulus onset. There was a main effect of stimulus condition over the ~80-130ms post-stimulus period that was located first within left temporo-parietal regions (~80-110ms) and subsequently within right temporo-parietal regions (~100-130ms; Figure 32, blue traces). Source estimations were stronger for IC than NC stimuli. These regions extended

along a dorsal-ventral axis to include lateral occipital cortices (see e.g. Table 3 in Grill-Spector et al., 1998). Finally and in general agreement with evidence from MEG for IC sensitivity within the occipital pole (and presumably V1/V2) at relatively late post-stimulus latencies (Halgren et al., 2003), we also observed a main effect of stimulus condition over the ~280-340ms post-stimulus period that included effects within the calcarine sulcus as well as lateral and inferior occipito-temporal cortices (Figure 33).

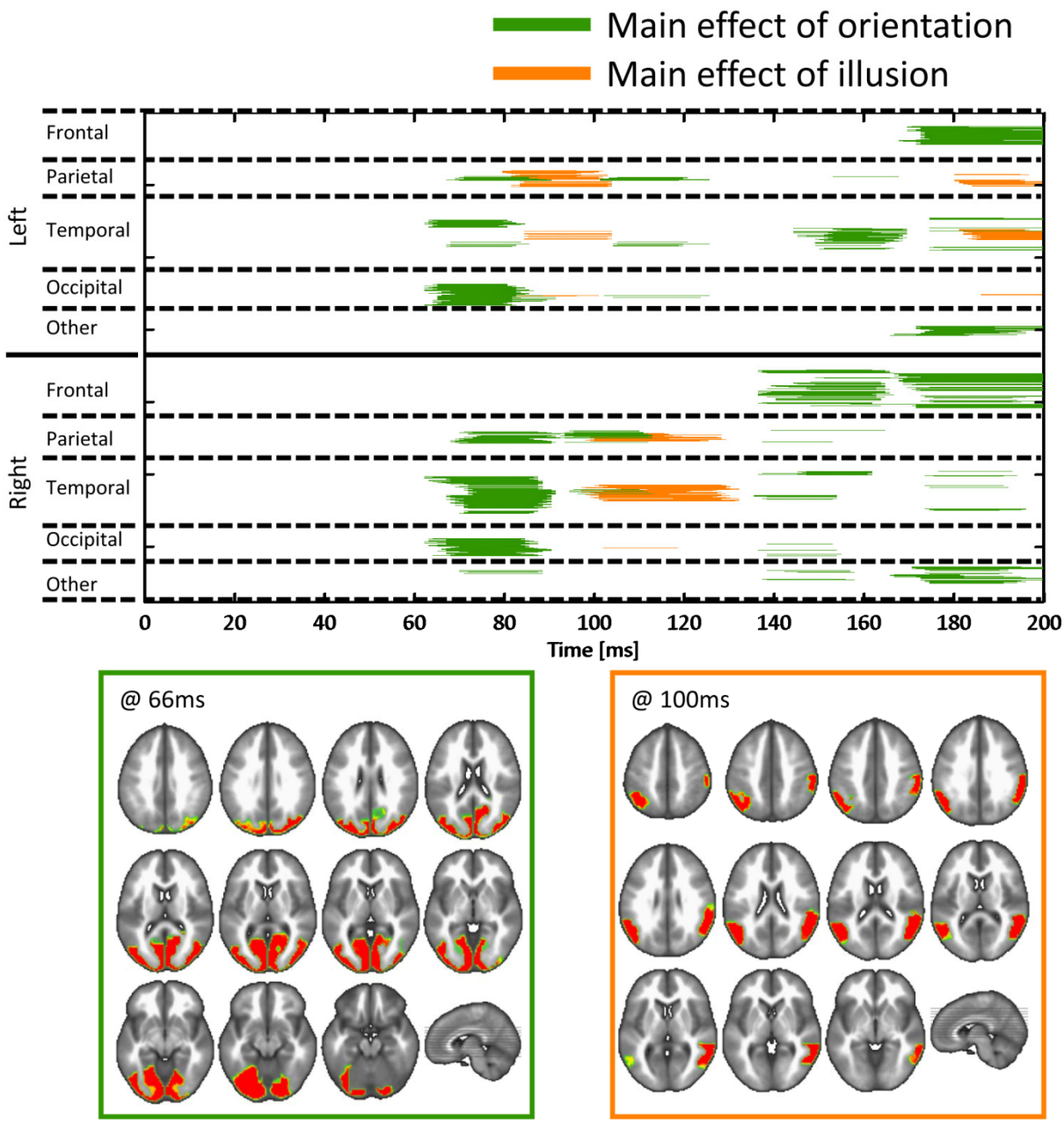

Figure 32: misaligned gratings article ; source estimation results over 0-200ms
Statistical analyses of source estimations over the initial 200ms post-stimulus interval. The upper panel displays a time-point by time-point repeated measures ANOVA on the source estimations (F(1,14); alpha ≤0.01; temporal criterion of at least 11 contiguous time-points and spatial extent criterion of 15 contiguous solution points). The red color represents the main effect of stimulus orientation and the blue color represents the main effect of stimulus condition. The bottom panel displays the distribution of significant effects at an exemplar instant (left and bottom panel: the main effect of stimulus orientation at 66ms; right and bottom panel: the main effect of stimulus condition at 100ms).

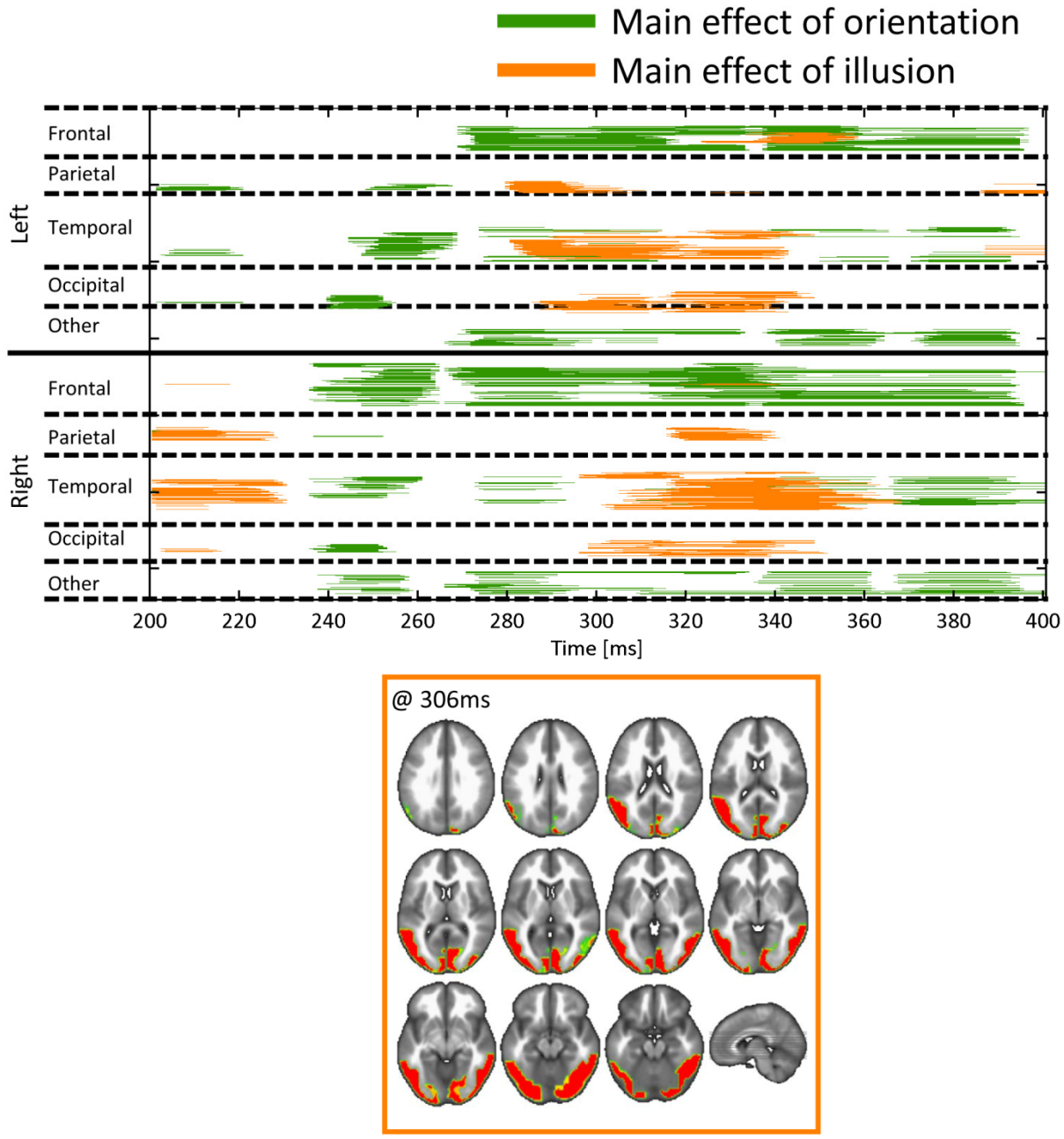

Figure 33 : misaligned gratings article ; source estimation results over 200-400ms
t Statistical analyses of source estimations over the 200-400ms post-stimulus interval. The upper panel displays a time-point by time-point repeated measures ANOVA on the source estimations (F(1,14); alpha ≤0.01; temporal criterion of at least 11 contiguous time-points and spatial extent criterion of 15 contiguous solution points). The red color represents the main effect of stimulus orientation and the blue color represents the main effect of stimulus condition. The bottom panel displays the distribution of significant effects at an exemplar instant (the main effect of stimulus condition at 306ms).

6.3.6 Discussion

The present study set out to resolve discordances across extant models of IC sensitivity. To do this, we recorded VEPs in response to misaligned line gratings that in turn induced the

perception of illusory contour shapes. Moreover, by varying the orientation of these gratings (both when inducing an IC and not), we could assay responsiveness of low-level visual cortices. The application of electrical neuroimaging analyses to these VEPs allowed us to determine both the temporal and spatial dynamics of IC sensitivity relative to that for grating orientation. We show that sensitivity to grating orientation transpires over the 60-90ms post-stimulus interval, principally within the calcarine sulcus, and prior to IC sensitivity over the 80-110ms post-stimulus interval, principally within the LOC (though later effects were observed within V1/V2). There was no evidence for interactions between the sensitivity to each of these features. As such, the collective data provide further support to models of IC sensitivity within the LOC that in turn mediates subsequent effects within V1/V2.

One major advance of the present study is that the line grating stimuli on the one hand allowed us to have a stimulus that reliably modulates responses within V1/V2 and on the other hand controlled for the presence of salient regions in the stimuli (this latter point is discussed in detail below). Analyses both at the level of surface VEPs and estimations of intracranial sources indicate that sensitivity to grating orientation occurred during the initial stages of visual processing (60-90ms) within regions within the calcarine sulcus and surrounding cortices. This effect coincides with the C1 component of the VEP, which is known to include prominent generators within V1/V2 (Clark et al., 1995; Foxe et al., 2008) (Foxe and Simpson, 2002). This effect of orientation sensitivity was followed by IC sensitivity (80-110ms) within the LOC and extended dorsally into parietal regions (though excluding modulations at this latency within the calcarine sulcus; Figure 32). Subsequent stages of IC sensitivity (~280-340ms), however, indeed demonstrated effects within the calcarine sulcus (and likely V1/V2). Additionally, the high temporal resolution of electrical neuroimaging allowed us to situate IC sensitivity in time and space with respect to these modulations within V1/V2. This collective pattern demonstrates the appropriateness of the stimuli as well as the sensitivity of our electrical neuroimaging methods to produce reliable effects within lower-tier visual cortices. However, we would acknowledge that despite using 160-channel VEPs and being able to detect modulations in GFP, we were unable to document topographic (and therefore generator configuration) differences between the horizontal and vertical orientations, which would constitute evidence for the sensitivity of surface-recorded VEPs to the differential activity of sub-populations of neurons (e.g. orientation columns) within lower-tier visual cortices. This sensitivity awaits further advances in EEG/MEG methods.

That IC sensitivity occurs first within the LOC is highly consistent with results using Kanizsa-type stimuli. In a series of studies by our group (Pegna et al. (2002); Murray et al.(2002, 2004, 2006); Foxe et al.(2005); Shpaner et al.(2009)) it was shown that IC sensitivity onsets

~90ms post-stimulus within LOC irrespective of contrast polarity, modal vs. amodal completion, active vs. passive viewing, and accuracy during IC curvature discrimination. In all cases, IC sensitivity manifested as a modulation in response strength (i.e. GFP) with no evidence for topographic differences relative to the NC condition. Parsimony thus favors a mechanism whereby a configuration of statistically indistinguishable intracranial generators responds more strongly to IC presence than absence, which was further confirmed by source estimations in these studies. This pattern is highly consistent with findings at the single-cell level in animals (Peterhans and von der Heydt, 1989; Lee and Nguyen, 2001; Sáry et al., 2007), as well as with MEG recordings (Halgren et al., 2003) and functional magnetic resonance imaging (fMRI) investigations in humans (Hirsch et al., 1995; Mendola et al., 1999; Kruggel et al., 2001).

The present findings extend this pattern to show that misaligned line gratings elicit qualitatively similar effects as Kanizsa-type stimuli in their timing, directionality, and localization. Using MEG, Ohtani et al. (2002) described IC sensitivity to misaligned line gratings over the 80-150ms post-stimulus period. However, effects were only reliable in just two of the four subjects. In their seminal fMRI study, Mendola et al. (1999) found larger effects of IC sensitivity induced by misaligned gratings than by Kanizsa-type stimuli (additional conditions included stereopsis-defined and luminance-defined shapes). It will therefore be of interest for future research or meta-analyses to establish a quantitative metric of IC sensitivity for different varieties of inducers based on EEG data. More recently, Montaser-Kouhsari et al. (2007) examined the impact of grating orientation on adaptation to ICs as measured with fMRI from four observers. While they observed orientation-sensitive adaptation effects throughout visual cortices, they were larger within higher-tier than lower-tier regions. This increase across regions was furthermore not readily explained by passive transmission of effects (perhaps in a bottom-up fashion) from lower-tier to higher-tier regions. Instead, they leave open the possibility that IC sensitivity and its adaption may originate within higher-tier regions, including LOC, and acknowledge the need for measurements with higher temporal resolution. The present electrical neuroimaging study provides this temporal information as well as a degree of spatial location. While we were not able to detect any interactions between IC sensitivity and orientation sensitivity here, applying an adatption paradigm similar to that in Montaser-Kouhsari et al. (2007) and/or other task parameters explicitly requiring attention to stimulus orientation may uncover finer levels of interaction between contour and orientation processes. Such notwithstanding, the present findings do provide indicate a degree of successive processing of orientation information first within lower-tier visual cortices and subsequently contour information within higher-tier visual cortices.

While the present data clearly support a model of IC sensitivity wherein effects within lower-tier visual cortices (V1/V2) are driven by feedback activity from the LOC (and perhaps also elsewhere), it could still be contended that it is salient regions of the stimuli rather than illusory contours per se that are being treated within the LOC and that sensitivity to the ICs themselves is a function specific to V1/V2 (see Model 3 in Figure 29). This model was initially put forward by Stanely and Rubin (2003) based on fMRI results showing equivalent depth of modulation within the LOC to Kanizsa-type ICs as well as rounded versions of these stimuli that lacked a perception of bound contours. It is worth noting, however, that while their model proposes a differential response within V1/V2 to ICs versus these rounded versions, their actual data provide no direct evidence for such. More recently, Shpaner et al. (2009) conducted an electrical neuroimaging study with similar stimuli to directly assess this model and its inherent temporal predictions. They found that initial responses within the LOC were significantly stronger for IC stimuli than to rounded versions of the stimuli and also differed topographically. Thus, initial responsiveness within the LOC cannot simply reflect the discrimination of salient regions within the visual scene. However, as neither they nor Stanley and Rubin (2003) reported evidence for IC sensitivity (early or late) within V1/V2, it is impossible from these data alone to completely dismiss other models proposing feedforward IC sensitivity within V1/V2 (cf. model 1 in Figure 29). Likewise, neither of these studies provided evidence for V1/V2 responsiveness to another stimulus parameter against which they could situate the timing (and/or magnitude in the case of fMRI) IC sensitivity. Instead, data from Mendola et al. (1999) speak to this issue by showing stronger IC effects within the LOC and other higher-tier visual cortices with stimuli with lower spatial frequencies (and by extension fewer line endings that could arguably be said to provide information concerning salient regions in the image; cf. their Figure 6).

In conclusion, the present study combined an optimized stimulus with state-of-the-art analyses of scalp-recorded VEPs to provide spatio-temporal information regarding mechanisms of illusory contour sensitivity in humans. As such, we were able to disambiguate competing models generated from a combination of evidence from humans and animals. First, the initial IC sensitivity we documented was subsequent to and spatially distinct from preceding effects of grating orientation. This allowed us to invalidate models based on early, feedforward sensitivity within V1/V2 (von der Heydt and Peterhans, 1989; Peterhans and von der Heydt, 1989; Ffytche and Zeki, 1996; Ramsden et al., 2001). Second, the consistency of the present effects using line gratings with our and others' previous observations using Kanizsa-type stimuli (Herrmann and Bosch, 2001; Murray et al., 2002, 2004, 2006) allowed us to invalidate models claiming that initial responsiveness within the LOC is due to the detection of salient regions that

in turn drive IC sensitivity within V1/V2. Instead, the collective results support models wherein IC sensitivity occurs first within the LOC.

6.3.7 References

Brighina, F., Ricci, R., Piazza, A., Scalia, S., Giglia, G., Fierro, B., 2003. Illusory contours and specific regions of human extrastriate cortex: evidence from rTMS. Eur. J. Neurosci 17, 2469-2474.

Britz, J., Michel, C.M., 2010. Errors can be related to pre-stimulus differences in ERP topography and their concomitant sources. Neuroimage 49, 2774-2782.

Clark, V., Fan, S., Hillyard, S., 1995. Identification of early visual evoked potential generators by retinotopic and topographic analyses. Human Brain Mapping 2, 170-187.

De Lucia, M., Clarke, S., Murray, M.M., 2010. A temporal hierarchy for conspecific vocalization discrimination in humans. J. Neurosci 30, 11210-11221.

de-Wit, L.H., Kentridge, R.W., Milner, A.D., 2009. Shape processing area LO and illusory contours. Perception 38, 1260-1263.

Ffytche, D.H., Zeki, S., 1996. Brain activity related to the perception of illusory contours. Neuroimage 3, 104-108.

Foxe, J.J., Strugstad, E.C., Sehatpour, P., Molholm, S., Pasieka, W., Schroeder, C.E., McCourt, M.E., 2008. Parvocellular and magnocellular contributions to the initial generators of the visual evoked potential: high-density electrical mapping of the "C1" component. Brain Topogr 21, 11-21.

Foxe, J.J., Murray, M.M., Javitt, D.C., 2005. Filling-in in Schizophrenia: a High-density Electrical Mapping and Source-analysis Investigation of Illusory Contour Processing. Cereb. Cortex 15, 1914-1927.

Gonzalez Andino, S.L., Michel, C.M., Thut, G., Landis, T., Grave de Peralta, R., 2005. Prediction of response speed by anticipatory high-frequency (gamma band) oscillations in the human brain. Hum Brain Mapp 24, 50-58.

Gonzalez Andino, S.L., Murray, M.M., Foxe, J.J., de Peralta Menendez, R.G., 2005. How single-trial electrical neuroimaging contributes to multisensory research. Exp Brain Res 166, 298-304.

Grave de Peralta Menendez, R., Gonzalez Andino, S., Lantz, G., Michel, C.M., Landis, T., 2001. Noninvasive localization of electromagnetic epileptic activity. I. Method descriptions and simulations. Brain Topogr 14, 131-137.

Grave de Peralta Menendez, R., Murray, M.M., Michel, C.M., Martuzzi, R., Gonzalez Andino, S.L., 2004. Electrical neuroimaging based on biophysical constraints. Neuroimage 21, 527-539.

Grill-Spector, K., Kushnir, T., Edelman, S., Itzchak, Y., Malach, R., 1998. Cue-invariant activation in object-related areas of the human occipital lobe. Neuron 21, 191-202.

Grosof, D.H., Shapley, R.M., Hawken, M.J., 1993. Macaque V1 neurons can signal 'illusory' contours. Nature 365, 550-552.

Guthrie, D., Buchwald, J.S., 1991. Significance testing of difference potentials. Psychophysiology 28, 240-244.

Halgren, E., Mendola, J., Chong, C.D.R., Dale, A.M., 2003. Cortical activation to illusory shapes as measured with magnetoencephalography. Neuroimage 18, 1001-1009.

Herrmann, C.S., Bosch, V., 2001. Gestalt perception modulates early visual processing. Neuroreport 12, 901-904.

von der Heydt, R., Peterhans, E., 1989. Mechanisms of contour perception in monkey visual cortex. I. Lines of pattern discontinuity. J. Neurosci 9, 1731-1748.

Hirsch, J., DeLaPaz, R.L., Relkin, N.R., Victor, J., Kim, K., Li, T., Borden, P., Rubin, N., Shapley, R., 1995. Illusory contours activate specific regions in human visual cortex: evidence from functional magnetic resonance imaging. Proceedings of the National Academy of Sciences of the United States of America 92, 6469 -6473.

Koenig, T., Melie-García, L., 2010. A method to determine the presence of averaged event-related fields using randomization tests. Brain Topogr 23, 233-242.

Kruggel, F., Herrmann, C.S., Wiggins, C.J., von Cramon, D.Y., 2001. Hemodynamic and electroencephalographic responses to illusory figures: recording of the evoked potentials during functional MRI. Neuroimage 14, 1327-1336.

Larsson, J., Amunts, K., Gulyás, B., Malikovic, A., Zilles, K., Roland, P.E., 1999. Neuronal correlates of real and illusory contour perception: functional anatomy with PET. Eur. J. Neurosci 11, 4024-4036.

Lee, T.S., Nguyen, M., 2001. Dynamics of subjective contour formation in the early visual cortex. Proceedings of the National Academy of Sciences of the United States of America 98, 1907 -1911.

Lehmann, D., Skrandies, W., 1980. Reference-free identification of components of checkerboard-evoked multichannel potential fields. Electroencephalogr Clin Neurophysiol 48, 609-621.

Maertens, M., Pollmann, S., 2005. fMRI reveals a common neural substrate of illusory and real contours in V1 after perceptual learning. J Cogn Neurosci 17, 1553-1564.

Martuzzi, R., Murray, M.M., Meuli, R.A., Thiran, J., Maeder, P.P., Michel, C.M., Grave de Peralta Menendez, R., Gonzalez Andino, S.L., 2009. Methods for determining frequency- and region-dependent relationships between estimated LFPs and BOLD responses in humans. J. Neurophysiol 101, 491-502.

Mendola, J.D., Dale, A.M., Fischl, B., Liu, A.K., Tootell, R.B., 1999. The representation of illusory and real contours in human cortical visual areas revealed by functional magnetic resonance imaging. J. Neurosci 19, 8560-8572.

Michel, C.M., Murray, M.M., Lantz, G., Gonzalez, S., Spinelli, L., Grave de Peralta, R., 2004. EEG source imaging. Clin Neurophysiol 115, 2195-2222.

Montaser-Kouhsari, L., Landy, M.S., Heeger, D.J., Larsson, J., 2007. Orientation-selective adaptation to illusory contours in human visual cortex. J. Neurosci 27, 2186-2195.

Murray, M.M., Brunet, D., Michel, C.M., 2008. Topographic ERP analyses: a step-by-step tutorial review. Brain Topogr 20, 249-264.

Murray, M.M., Foxe, D.M., Javitt, D.C., Foxe, J.J., 2004a. Setting boundaries: brain dynamics of

modal and amodal illusory shape completion in humans. J. Neurosci 24, 6898-6903.

Murray, M.M., Foxe, D.M., Javitt, D.C., Foxe, J.J., 2004b. Setting boundaries: brain dynamics of modal and amodal illusory shape completion in humans. J. Neurosci 24, 6898-6903.

Murray, M.M., Imber, M.L., Javitt, D.C., Foxe, J.J., 2006. Boundary completion is automatic and dissociable from shape discrimination. J. Neurosci 26, 12043-12054.

Murray, M.M., Wylie, G.R., Higgins, B.A., Javitt, D.C., Schroeder, C.E., Foxe, J.J., 2002a. The spatiotemporal dynamics of illusory contour processing: combined high-density electrical mapping, source analysis, and functional magnetic resonance imaging. J. Neurosci 22, 5055-5073.

Murray, M.M., Wylie, G.R., Higgins, B.A., Javitt, D.C., Schroeder, C.E., Foxe, J.J., 2002b. The spatiotemporal dynamics of illusory contour processing: combined high-density electrical mapping, source analysis, and functional magnetic resonance imaging. J. Neurosci 22, 5055-5073.

Ohtani, Y., Okamura, S., Shibasaki, T., Arakawa, A., Yoshida, Y., Toyama, K., Ejima, Y., 2002. Magnetic responses of human visual cortex to illusory contours. Neurosci. Lett 321, 173-176.

Pegna, A.J., Khateb, A., Murray, M.M., Landis, T., Michel, C.M., 2002. Neural processing of illusory and real contours revealed by high-density ERP mapping. Neuroreport 13, 965-968.

Peterhans, E., von der Heydt, R., 1989. Mechanisms of contour perception in monkey visual cortex. II. Contours bridging gaps. J. Neurosci 9, 1749-1763.

Petry, S., Harbeck, A., Conway, J., Levey, J., 1983. Stimulus determinants of brightness and distinctness of subjective contours. Percept Psychophys 34, 169-174.

Ramsden, B.M., Hung, C.P., Roe, A.W., 2001. Real and illusory contour processing in area V1 of the primate: a cortical balancing act. Cereb. Cortex 11, 648-665.

Sáry, G., Chadaide, Z., Tompa, T., Köteles, K., Kovács, G., Benedek, G., 2007. Illusory shape representation in the monkey inferior temporal cortex. Eur. J. Neurosci 25, 2558-2564.

Sáry, G., Köteles, K., Kaposvári, P., Lenti, L., Csifcsák, G., Frankó, E., Benedek, G., Tompa, T., 2008. The representation of Kanizsa illusory contours in the monkey inferior temporal cortex. Eur. J. Neurosci 28, 2137-2146.

Seghier, M.L., Vuilleumier, P., 2006. Functional neuroimaging findings on the human perception of illusory contours. Neurosci Biobehav Rev 30, 595-612.

Seghier, M., Dojat, M., Delon-Martin, C., Rubin, C., Warnking, J., Segebarth, C., Bullier, J., 2000. Moving Illusory Contours Activate Primary Visual Cortex: an fMRI Study. Cerebral Cortex 10, 663 -670.

Shapley, R., 2007. Early vision is early in time. Neuron 56, 755-756.

Sheth, B.R., Sharma, J., Rao, S.C., Sur, M., 1996. Orientation maps of subjective contours in visual cortex. Science 274, 2110-2115.

Shpaner, M., Murray, M.M., Foxe, J.J., 2009. Early processing in the human lateral occipital complex is highly responsive to illusory contours but not to salient regions. Eur. J. Neurosci 30, 2018-2028.

Spinelli, L., Andino, S.G., Lantz, G., Seeck, M., Michel, C.M., 2000. Electromagnetic inverse solutions

in anatomically constrained spherical head models. Brain Topogr 13, 115-125.

Stanley, D.A., Rubin, N., 2003. fMRI activation in response to illusory contours and salient regions in the human lateral occipital complex. Neuron 37, 323-331.

Yoshino, A., Kawamoto, M., Yoshida, T., Kobayashi, N., Shigemura, J., Takahashi, Y., Nomura, S., 2006. Activation time course of responses to illusory contours and salient region: a high-density electrical mapping comparison. Brain Res 1071, 137-144.